

**Structural investigations on the large-pore
aluminophosphate molecular sieve VPI-5**

A dissertation submitted to the
SWISS FEDERAL INSTITUTE OF TECHNOLOGY ZURICH
for the degree of
Doctor of Natural Sciences

presented by
Javier Enrique de Oñate Martínez
Dipl. Phys., Dresden University of Technology
born on June 4, 1962
citizen of Cuba

accepted on the recommendation of

Prof. Dr. R. Nesper	examiner
Prof. Dr. W. Steurer	co-examiner
Dr. Ch. Bärlocher	co-examiner

Zürich 1997

Abstract

VPI-5 is a microporous crystalline aluminophosphate molecular sieve with a three-dimensional framework containing a one-dimensional channel system circumscribed by 18-rings. The interest in this material is mainly due to its large pores of ca. 12Å free diameter and its conceivable applications in catalysis, separation of large molecules, adsorption and, more recently, in the construction of advanced optical and electronic devices.

The application of VPI-5, however, is limited by its thermal stability and by its facile conversion to $\text{AlPO}_4\text{-8}$. Thus, there has been an obvious interest in understanding the factors affecting the framework stability of VPI-5, and the mechanism of the transformation to $\text{AlPO}_4\text{-8}$. Although many procedures have been published, the synthesis of VPI-5 is not straightforward and not always reproducible. Furthermore, small changes in the synthesis parameters can have severe consequences for the thermal properties of the final product.

In this work the synthesis procedure of E. Jahn, based on the use of polyphosphoric acid as the source of P, was adapted for the preparation of a VPI-5 material with a very high crystallinity and good thermal properties. This method was also optimized for the synthesis of relatively large single crystals ($250 \times 25 \times 25 \mu\text{m}^3$) of this aluminophosphate molecular sieve.

To investigate the crystal structure and the thermal stability of different VPI-5 and $\text{AlPO}_4\text{-8}$ materials, powder diffraction, nuclear magnetic resonance and thermogravimetric techniques were applied.

VPI-5 at 90°C in a closed system: ^{31}P MAS NMR experiments indicated that VPI-5 adopts a higher symmetry when heated to 90°C in a closed system. Rietveld refinement confirmed that the symmetry of VPI-5 changes from $P6_3$ in the as-synthesized form to $P6_3cm$ at 90°C. The Al

atom located between the fused 4-rings remains octahedrally coordinated, but the well-ordered water structure observed in the as-synthesized form at RT has been destroyed. The removal of the constraints imposed by the well defined water structure in as-synthesized VPI-5, may explain the slight elongation of the a (0.1%) and contraction of the c (0.6%) lattice parameters upon heating.

At 90°C, the NMR parameters of both Al2 ($\delta = 41.8$ ppm, QCC = 1.6 MHz, $\eta = 0.7$) and P2 ($\delta = -26.1$ ppm) located at the connection of 4- and 6-rings, are closer to those of the original Al2 ($\delta = 41.9$ ppm, QCC = 1.4 MHz, $\eta = 0.6$) and P2 ($\delta = -27.1$ ppm), than to those of the original Al3 ($\delta = 44.5$ ppm, QCC = 2.7 MHz, $\eta = 0.2$) and P3 ($\delta = -23.2$ ppm), which are symmetrically inequivalent in the RT structure. The NMR results suggest also that after the 'symmetrization' of the structure at 90°C, the VPI-5 framework is less distorted than in the as-synthesized form.

Dehydrated VPI-5: a series of thermogravimetric studies were carried out to investigate the thermal stability of VPI-5 samples prepared using different procedures, and to establish the conditions necessary for their dehydration while avoiding the transformation to $\text{AlPO}_4\cdot 8$. It was observed, that once the samples had been evacuated at room temperature, they could be heated up to at least 650°C at practically any heating rate without conversion to $\text{AlPO}_4\cdot 8$ or loss of structural integrity. However, the duration of the outgassing is dependent on the sample. Although samples prepared with organic quaternary ions showed, in general, a higher thermal stability than those synthesized using di-*n*-propylamine as an additive, it was found that samples prepared with this amine but using polyphosphoric acid as the source of P are less likely to transform to $\text{AlPO}_4\cdot 8$.

The structures of two dehydrated samples (A and E) prepared using different methods were investigated. Rietveld refinements carried out on both samples showed that it is possible to obtain a totally anhydrous phase, which retains the VFI topology. The structure, however, contains some

unusually small P-O-Al angles (ranging from 122° to 154°). These are all located in the 18-ring at the fused 4-rings. The existence of these very small angles was also indicated by the ^{31}P NMR experiments. The structure could not longer be described in the space group $P6_3$ (used for the as-synthesized form), and the symmetry had to be reduced to monoclinic. The refinements were carried out in the space group Cm , but with a pseudo ortho hexagonal metric (sample A: $a = 18.4680(5) \text{ \AA}$, $b = 31.9703(4) \text{ \AA}$, $c = 16.6759(2) \text{ \AA}$, $\beta = 90.0^\circ$, $R_F = 0.054$, $R_{wp} = 0.110$, $R_{exp} = 0.067$; sample E: $a = 18.5218(1) \text{ \AA}$, $b = 32.1247(2) \text{ \AA}$, $c = 8.40026(2) \text{ \AA}$, $\beta = 90.0^\circ$, $R_F = 0.062$, $R_{wp} = 0.098$, $R_{exp} = 0.047$). In the structure of sample A, the central chain in the triple crankshaft chain building unit is distorted in such a manner that the unit cell is doubled in the c direction. Such a distortion was not observed in the structure of sample E. In the powder pattern of this sample, however, two minor peaks remained unindexed even after the cell was doubled. It may be that the dehydration process of VPI-5 leads to a modulation of the structure that results in a simple doubling of the unit cell in the c direction for sample A, but that is incommensurate for sample E.

Dehydrated $\text{AlPO}_4\text{-8}$: a good quality $\text{AlPO}_4\text{-8}$ powder was obtained by solid-state transformation of a well crystallized VPI-5 sample. The synchrotron powder diffraction pattern of the former indicates the existence of large domains of coherent scattering. Its diffraction pattern, however, could not be indexed either in the published orthorhombic unit cell, or in any other derived from it. Since the **VFI** and **AET** topologies contain the same building unit, it is speculated that a modulation similar to that observed in dehydrated VPI-5, might also be present in $\text{AlPO}_4\text{-8}$.

Zusammenfassung

VPI-5 ist ein kristallines mikroporöses Aluminiumphosphat, dessen Struktur sich als dreidimensionales Gerüst mit einem eindimensionalen Kanalsystem beschreiben lässt. Die Ringe, die den Kanal umschliessen, enthalten 18 T-Atome. Dieses Material ist vor allem wegen der relativ grossen Poren mit einem maximalen freien Durchmesser von 12\AA interessant. Deswegen könnte es eine Anwendung in der Katalyse, bei der Trennung von Molekülen und bei Adsorptionsprozessen finden. Weiter wäre die Herstellung optischer und elektronischer Bauelemente denkbar. Diese Möglichkeiten sind allerdings durch den spontanen Phasenübergang zu $\text{AlPO}_4\text{-8}$ bei höheren Temperaturen begrenzt.

Obwohl es viele Veröffentlichungen über die Synthese von VPI-5 gibt, ist diese nicht immer reproduzierbar. Kleine Änderungen in den Syntheseparametern können die thermische Eigenschaften des Endproduktes stark beeinflussen.

In dieser Arbeit wurde die Synthesevorschrift von E. Jahn (basierend auf der Verwendung von Polyphosphorsäure als Phosphor Quelle) für die Herstellung gut kristalliner und thermisch stabiler VPI-5 Proben angepasst. Weiter wurde diese Methode für die Herstellung relativ grosser ($250 \times 25 \times 25 \mu\text{m}^3$) Einkristalle dieses Aluminiumphosphates optimiert.

Um die Kristallstruktur und die thermische Stabilität der verschiedenen VPI-5 und $\text{AlPO}_4\text{-8}$ Proben zu untersuchen, wurden Pulverdiffraktometrie, Thermogravimetrie und Kernresonanzspektroskopie angewandt.

VPI-5 bei 90°C in einem geschlossenen System: Die Rietveld Verfeinerung hat gezeigt, dass sich die Symmetrie von VPI-5 durch Erhitzen in einem geschlossenen System von $P6_3$ zu $P6_3cm$ verändert. Während das Aluminiumatom in der Mitte der Doppelviererringe oktaedrisch

koordiniert bleibt, existiert die in der Raumtemperaturphase auftretende Ordnung der Wassermoleküle bei 90°C nicht mehr. Der Verlust dieser Ordnung bei 90°C könnte die leichte Elongation der *a*- (0.1%) und die Kontraktion der *c*-Gitterkonstante (0.6%) beim Aufheizen erklären.

Bei 90°C entsprechen die NMR Parameter der neuen 4- und 6-Ring verknüpfenden Al₂-Atome ($\delta = 41.8$ ppm, QCC = 1.6 MHz, $\eta = 0.7$) und P2 ($\delta = -26.1$ ppm) Atome eher denen der alten Al₂ ($\delta = 41.9$ ppm, QCC = 1.4 MHz, $\eta = 0.6$) und P2 ($\delta = -27.1$ ppm) als denen der Al₃-Atome ($\delta = 44.5$ ppm, QCC = 2.7 MHz, $\eta = 0.2$) bzw. P3 ($\delta = -23.2$ ppm). Weiterhin zeigen die NMR Daten, dass die höher symmetrische Struktur der Hochtemperaturphase weniger verzerrt ist als die der Tieftemperaturphase.

Dehydratisiertes VPI-5: Es wurden eine Reihe thermogravimetrischer Untersuchungen durchgeführt, um die thermische Stabilität der mit verschiedenen organischen Additiven synthetisierten VPI-5 Proben und die Bedingungen für eine Dehydratisierung ohne Phasenumwandlung zu AlPO₄-8 zu untersuchen. Es wurde festgestellt, dass die Proben nach einer Evakuierung bei Raumtemperatur bei beliebigen Heizraten bis zu mindestens 650°C aufgeheizt werden konnten, ohne dass es zur Phasenumwandlung kam oder die Kristallinität vermindert wurde. Die Länge der Evakuierung ist allerdings probenabhängig. Die mit quaternären Ionen synthetisierten Proben sind im allgemeinen stabiler als die mit di-*n*-Propylamin hergestellten. Trotzdem zeigte sich, dass die mit diesem Amin und Polyphosphorsäure hergestellten Proben eine höhere thermische Stabilität haben.

Es wurden die Strukturen zweier unterschiedlich hergestellter dehydratisierter Proben untersucht (A und E). Wie die Rietveld-Verfeinerung gezeigt hat, ist es möglich, eine total wasserfreie Phase mit VFI Topologie zu erhalten. Diese Struktur enthält allerdings ungewöhnlich kleine P-O-Al-Winkel (der mittlere Winkel um P20 in der Struktur der Probe A ist z.B. 129°) in den Doppelviererringen. Das

Auftreten dieser extrem kleinen Bindungswinkel wurde durch ^{31}P MAS-NMR-Experimente bestätigt. Auf Grund dieser Verzerrung erniedrigt sich die Symmetrie von $P6_3$ zu monoklin. Die Verfeinerungen wurden mit pseudo-hexagonaler Metrik in der Raumgruppe Cm durchgeführt ($a = 18.4680(5) \text{ \AA}$, $b = 31.9703(4) \text{ \AA}$, $c = 16.6759(2) \text{ \AA}$, $\beta = 90.0^\circ$, $R_F = 0.054$, $R_{wp} = 0.110$, $R_{exp} = 0.067$, für Probe A; $a = 18.5218(1) \text{ \AA}$, $b = 32.1247(2) \text{ \AA}$, $c = 8.40026(2) \text{ \AA}$, $\beta = 90.0^\circ$, $R_F = 0.062$, $R_{wp} = 0.098$, $R_{exp} = 0.047$, für Probe E). Während für die Struktur der Probe A eine Verzerrung der zentralen Kette in der 'triple crankshaft chain' Baueinheit beobachtet wurde, die zu einer Verdopplung der c -Gitterkonstante führt, konnte dieses für die Struktur der Probe E nicht gefunden werden. Im Pulverdiffraktogramm der Probe E konnten allerdings zwei kleine Peaks nicht indiziert werden, auch nicht durch eine Verdopplung der Elementarzelle. Es wird vermutet, dass der Dehydratisierungsvorgang des VPI-5 zu einer modulierten Struktur führt, welche sich im Fall der Probe A in einer einfachen Verdopplung in c -Richtung äussert, während sie im Fall der Probe E möglicherweise inkommensurabler Natur ist.

Dehydratisiertes $\text{AlPO}_4\text{-8}$: Eine $\text{AlPO}_4\text{-8}$ -Probe hoher Qualität konnte durch die Festkörperumwandlung einer gut kristallisierten VPI-5-Probe erhalten werden. Die schmalen Linien im Synchrotronpulverdiffraktogramm weisen auf die Existenz grosser kohärent streuender Domänen hin. Trotzdem gelang keine vollständige Indizierung, weder in der bekannten orthorhombischen Zelle, noch mit einer damit verwandten Metrik. Da sowohl das **VFI**- als auch das **AET**-Gerüst aus gleichen Baueinheiten aufgebaut sind, kann vermutet werden, dass die bereits erwähnte Modulation der dehydratisierten VPI-5 Struktur auch in der dehydratisierten $\text{AlPO}_4\text{-8}$ Struktur auftritt.

Table of contents

1. Introduction	1
2. Literature survey on VPI-5	4
2.1. Large pore molecular sieves	4
2.2. Synthesis	5
2.2.1. Synthesis with organic additives	5
2.2.2. Synthesis in the absence of organic additives	7
2.2.3. Synthesis of element-substituted VPI-5	7
2.3. Structure	8
2.3.1. Structure of as-synthesized VPI-5	8
2.3.2. Structure of dehydrated VPI-5	13
2.3.3. Structure of VPI-5 as a function of temperature	16
2.4. Thermal stability	17
2.5. Other physico-chemical properties	18
2.5.1. Adsorption	18
2.5.2. Diffusion	19
2.5.3. Catalysis	19
2.6. Advanced materials applications	20
3. Experimental characterization techniques	21
3.1. Powder diffraction	21
3.1.1. General considerations	21
3.1.2. Crystal structure refinement from powder data: the Rietveld method	22
3.1.3. Use of polycrystalline diffraction techniques on zeolites	26
3.2. Solid-State nuclear magnetic resonance (NMR) spectroscopy	27
3.3. Instrumentation	29
3.3.1. Powder diffraction	29
3.3.2. Solid-state NMR spectroscopy	30
3.3.3. Thermogravimetric analysis	31
3.3.4. Scanning electron microscopy	31
3.3.5. Others	31

4. Synthesis optimization	32
4.1. Synthesis procedure of E. Jahn	33
4.2. Materials	34
4.3. Synthesis optimization	35
4.4. Summary of results and discussion	44
4.5. Conclusions	49
 5. Structural investigation of VPI-5 at 90°C under closed conditions	 52
5.1. Sample preparation and data collection	52
5.2. Results	53
5.2.1. Solid state NMR	53
5.2.2. Rietveld refinement	59
5.3. Discussion	65
 6. Structural investigations of dehydrated VPI-5	 68
6.1. Samples investigated	68
6.2. Dehydration experiments	71
6.2.1. Experimental conditions	71
6.2.2. Results and discussion	71
6.3. Structural investigations	81
6.3.1. Solid-state NMR	81
6.3.2. Rietveld refinement	85
6.3.2.1. Data collection	85
6.3.2.2. X-ray Rietveld refinement of sample A	87
6.3.2.3. Synchrotron Rietveld refinement of sample E	93
6.3.3. Discussion	97
 7. Structural investigations on AlPO₄-8	 102
7.1. Brief literature overview	102
7.2. Structural investigations	103
7.2.1. Sample preparation and data collection	103
7.2.2. Solid-state NMR	105
7.2.3. Synchrotron powder diffraction	106

<i>8. Conclusions</i>	110
<i>9. References</i>	114
<i>10. Appendix</i>	121
<i>List of abbreviations and symbols</i>	124
<i>Acknowledgments</i>	126
<i>Curriculum Vitae</i>	128

1. Introduction

Zeolites are open-framework aluminosilicates constructed from TO_4 tetrahedra (where T is a tetrahedrally coordinated atom such as Si or Al), with each oxygen atom shared with an adjacent tetrahedron. Strictly speaking, molecular sieves with framework atoms other than silicon, aluminum and oxygen are not termed zeolites.

An important related class of microporous materials are the aluminophosphate molecular sieves, originally reported by d'Yvoire [1] and then studied more extensively by Wilson and co-workers [2]. This last group designated their materials as $\text{AlPO}_4\text{-}n$ (the number n denoting a particular material). These neutral frameworks contain equal numbers of Al and P in the T-sites ($\text{Al/P} = 1$), and the Al and P atoms alternate throughout the framework. Additional elements (e.g. Si, Mg, Fe, Ti, Co, Zn, Mn, Ga, Ge, Be, etc.) can be incorporated into the AlPO_4 frameworks, to create a vast number of element-substituted aluminophosphate-based molecular sieves [2].

Zeolites and aluminophosphate-based materials constitute a broad class of molecular sieves that have a wide variety of physico-chemical properties, including variations in pore size (from about 4 to 20Å), pore shape (circular, elliptical, etc.), dimensionality of the pore system (one-, two or three-dimensional), presence or absence of cages, surface properties (hydrophilic or hydrophobic), void volume (up to 50%), and framework composition.

Because of their unique properties, these materials have found widespread use as adsorbents, ion exchangers, catalysts and/or catalytic supports, etc. The field of molecular sieve science continues to expand at a rapid pace, and has also filtered into other areas of materials science such as ceramics, electronic materials, and drug release agents.

Many of the above mentioned applications of zeolites and zeolite-like materials are governed by their framework structures. The topology of a given framework, which describes the connectivity of the T-atoms, is called a structure type. A three letter code is assigned by the Structure Commission of the International Zeolite Association to each confirmed structure type. 108 structure type codes have been assigned to date, 98 of which appear in the 4th. edition of the Atlas of Zeolite Structure Types [4]

VPI-5 (Virginia Polytechnic Institute number 5) is a microporous crystalline aluminophosphate molecular sieve with a three-dimensional framework (**VFI** topology) containing a one-dimensional channel system circumscribed by 18-rings [5]. The interest in this material is due mainly to its large pores of ca. 12Å free diameter and its conceivable applications in catalysis, separation of large molecules, adsorption and, more recently, in the construction of advanced optical and electronic devices.

The application of VPI-5, however, is limited by its thermal stability, which is dependent on synthesis and post-synthesis treatment conditions, and by its facile conversion to $\text{AlPO}_4\text{-8}$, another large-pore aluminophosphate molecular sieve (**AET** topology) with an one-dimensional 14-ring channel system [6,7]. Thus, there has been an obvious interest in understanding the factors affecting the framework stability of VPI-5, and the mechanism of the transformation to $\text{AlPO}_4\text{-8}$. To gain this understanding, structural analysis is essential.

Among the analytical techniques that have been applied to study the atomic ordering in molecular sieves, diffraction and solid-state nuclear magnetic resonance (NMR) methods occupy a central position. The combination of NMR and diffraction techniques is particularly appropriate since the former is sensitive to short-range order (local environment) and the latter to long-range order. Thus, the use of NMR and diffraction methods together provides a more complete understanding of structure and bonding.

Although many procedures have been published, the synthesis of VPI-5 is not straightforward. The procedures themselves are easy to follow, but there are a number of important details that affect the reproducibility. Small changes in the synthesis parameters can have severe consequences on the thermal properties of the final product.

To get a better and more complete picture of the structure and thermal behavior of VPI-5, thermogravimetric, diffraction and NMR techniques were applied to a variety of VPI-5 materials. Since synthesis conditions proved to play an important role in the thermal stability of the material, a synthesis study, to investigate this aspect of the problem and to generate a reproducible source of highly crystalline and stable material, was undertaken.

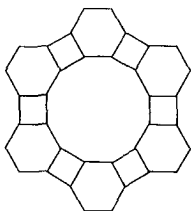
2. Literature survey on VPI-5

2.1. Large pore molecular sieves

Since the discovery of the first zeolite by Cronsted in 1756 [9], many natural and synthetic zeolites have been reported. However, for quite a while, the largest pore openings in these materials were 12 T-atoms (12-ring), e.g. Linde L (LTL), faujasite (FAU), EMC-2 (EMT), mordenite (MOR), $\text{AlPO}_4\text{-5}$ (AFI), etc. [4]. More recently, a few materials containing rings of more than 12 T-atoms have been reported, e.g. $\text{AlPO}_4\text{-8}$ (AET) and Cloverite (-CLO) with 14- and 20-rings, respectively [4]. Producing thermally stable molecular sieves with large pores remains an objective of molecular sieve synthesis.

Hypothetical molecular sieve topologies with 18- or 24-ring one-dimensional channels were first proposed by Barrer and Villiger in 1969 [10]. Other such large pore framework topologies were later discussed by Smith and Dytrych [11], who generated the net 81(1) by inserting 4-rings into the net 81 (the AFI topology) so that pairs of 4-rings separate the 6-rings (see Fig. 1). In 1986 Meier evaluated previous predictions and suggested that net 81(1) was most likely to be stereochemically feasible and stable [12]. He also pointed out that novel very large pore molecular sieve frameworks would probably consist of one-dimensional channel systems only.

a)



b)

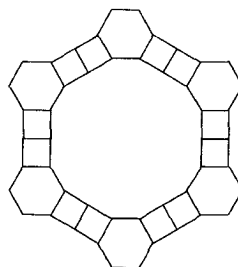


Fig. 1: Schematic representations of (a) the $\text{AlPO}_4\text{-5}$ (AFI topology, net 81) and (b) the VPI-5 (VFI topology, net 81(1)) nets

Two years later Davis et al. [5,13] reported the successful synthesis of an aluminophosphate which was thought to have this topology. It was called VPI-5 (Virginia Polytechnic Institute number 5). Subsequent X-ray analysis confirmed this assumption, and it was given the IUPAC code **VFI** [4].

2.2. Synthesis

2.2.1. Synthesis with organic additives

Since the synthesis report by Davis et al., a large number of different preparative procedures have been published [8,14-23]. The optimal conditions reported differ considerably in terms of gel composition (e.g. nature and quantity of organic species, water content), source of P or Al, and preparation (with or without aging, aging time, time and temperature regimes for the crystallization). Small changes in the synthesis procedure can affect both the type and level of impurities and the thermal stability of the final product. There has also been some question regarding the reproducibility of the published procedures [23,24].

VPI-5 can be synthesized from a reactive aluminophosphate gel containing organic species [14], but these species are not (or only to a very limited extent) incorporated into the channel system. Instead, water molecules fill the void space and account for ca. 25 wt% of the sample [25,26].

The synthesis procedure, originally reported by Davis et al. [14,26] and frequently modified by other groups, involves the following main steps: (i) pseudoboehmite alumina is slurried in water, (ii) phosphoric acid (85%) is diluted in water and added to the alumina slurry, (iii) the mixture is aged at ambient temperature, (iv) an organic compound is added to the precursor mixture, (v) the mixture is aged under ambient conditions with rapid agitation to form the final gel, (vi) the gel is charged into PTFE-lined

autoclaves and heated at temperatures between 130 and 150°C for 20 hours.

Typically, pseudoboehmite alumina and phosphoric acid (85%) are used as sources for Al and P, respectively, but aluminum-isopropoxide [15] and polyphosphoric acid [8] have also been employed with success.

Organic species can be either secondary or tertiary amines or quaternary ammonium ions, e.g. di-n-propylamine [8,14,18,19,21-23,27], di-n-pentylamine [19], di-n-butylamine [16], triethanolamine [28], triisopropanolamine, cyclopentylamine and cyclohexylamine [28], tetrabutylammonium hydroxide [14,26], or mixtures thereof, such as tri-n-butyl- and di-n-pentylamine [19], or tetramethylammonium hydroxide and triisopropanolamine [28]. Since VPI-5 can be synthesized using a wide variety of organic species, it has been suggested that they do not act as templates or structure-directing agents for the crystallization, but that they may serve as effective pH moderators during the synthesis [14].

Perez et al. reported the synthesis of an aluminophosphate with an X-ray diffraction pattern similar to VPI-5, but showing compositional and structural differences [19]. In their series of papers, VPI-5 is used to describe a phase which is thermally stable and has an Al to P ratio very close to 1, while H1 is used to describe a thermally unstable material with an Al to P ratio greater than 1. The latter converts readily to $\text{AlPO}_4\cdot 8$ at elevated temperatures [19]. The name H1 was chosen because of the similarity of its X-ray pattern to that of a material first prepared by d'Yvoire in 1961 [1] from an inorganic aluminophosphate gel. He used the designation H1 to describe a minor component of a mixture of phases. To avoid confusion regarding these two phases, i.e., the organic-free product reported by d'Yvoire (see next section) and the aluminophosphate referred as to H1 by Perez et al., the latter will be given the acronym 'dis-VPI-5' (Al-rich material with a disordered structure) here.

2.2.2. Synthesis in the absence of organic additives

In 1961, d'Yvoire reported the synthesis of several aluminophosphate hydrates, H1, H2, H3 and H4 [1]. These materials were prepared from dilute aqueous solutions of alumina and phosphoric acid with a P_2O_5 : Al_2O_3 ratio of 2.7. However, d'Yvoire's synthesis never resulted in pure single phases.

Duncan et al. [17] optimized the organic-free synthesis of H1 of d'Yvoire to produce an aluminophosphate material with the same X-ray pattern and thermal behavior as VPI-5. The authors concluded that VPI-5 and H1 do not differ. Their synthesis was achieved by blending a reactive aluminum hydroxide with phosphoric acid, and adding hydrochloric acid to the gel [17].

Li and Davis [29] crystallized VPI-5 from a wholly inorganic system following Duncan's procedure, but also from an acidic inorganic medium prepared with pseudoboehmite alumina instead of aluminum hydroxide. The synthesis products have X-ray patterns similar to those of samples prepared with organic agents. However, they found that the sample synthesized following Duncan's procedure contained a considerable number of hydroxyl groups (P-OH), which may cause its thermal instability [29].

The fact that VPI-5 can be synthesized in an organic-free system is a further indication that, at least in this case, organic species do not function as templates.

2.2.3. Synthesis of element-substituted VPI-5

Since the VPI-5 framework is electrically neutral, there has been an obvious interest in synthesizing silica-based molecular sieves with pore sizes similar to this aluminophosphate, or introducing acid sites by the incorporation of heteroatoms into the framework of this material, e.g. Si

[15,21,26,30-32], Co [26,33] and Fe [34]. Partial substitution of heteroatoms would create a negatively charged framework that could be protonated to form acid sites [35]

The crystallization of VPI-5 with partial substitution of heteroatoms like Si has proven to be a rather challenging task. The framework concentration of silicon obtained so far is very low, compared to those of other silicon-substituted aluminophosphate molecular sieves [29,30,31]. Furthermore, the ^{29}Si NMR data for Si-VPI-5 do not support the substitution mechanisms proposed by Flanigen et al. [29,35] that normally occur in SAPO- n molecular sieves.

2.3. Structure

The structures of as-synthesized and dehydrated VPI-5, as well as its structure as a function of temperature have been studied by various groups. In this section, the relevant results of these crystallographic and NMR investigations are summarized.

2.3.1. Structure of as-synthesized VPI-5

A model for the framework structure of VPI-5 was first proposed by Crowder et al. based on X-ray powder diffraction and modelling methods [36]. Although no Rietveld refinement of the structure could be performed at that time, the proposed framework topology eventually proved to be correct.

Rudolf and Crowder later conducted a Rietveld refinement in the space group $P6_3cm$, using X-ray powder diffraction data collected on the as-synthesized material [37]. They located the water molecules in the 18-ring channels, and suggested that they form weakly associated layers within the pore in a manner not unlike that of liquid water [37]. However, their final Rietveld plot shows large differences between the observed and

calculated profiles, which were attributed to the presence of a second VPI-5 phase that was slightly dehydrated.

The most complete structure refinement to date was carried out by McCusker et al. using synchrotron powder diffraction data collected on the fully hydrated material [38]. It was accomplished by reducing the symmetry from $P6_3cm$ (topochemical symmetry[†]) to $P6_3$, so that there are three crystallographically distinct Al (and P) sites in the framework: two of them located at the connection of 6- and 4-rings, and the third between the fused 4-rings. The Al atoms at the center of the fused 4-rings are octahedrally coordinated to two water molecules in addition to four framework oxygens, while the Al in the 6-rings are tetrahedral.

Fig. 2a illustrates the [001] projection of the structure of as-synthesized VPI-5. The positions of the octahedral Al atoms have been marked. The framework structure can be constructed exclusively from the triple crankshaft chain [40] depicted in Fig. 2b.

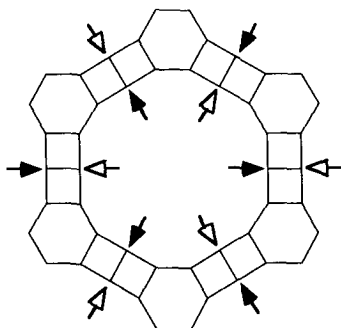


Fig. 2a: [001] projection of the structure of VPI-5. Marks represent two water molecules bonded to Al in different layers (at z and $z+1/2$)

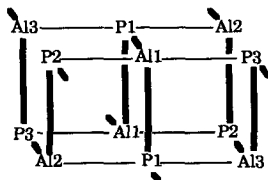


Fig. 2b: The hydrated triple crankshaft chain building unit of which VPI-5 can be constructed

[†] The topochemical symmetry describes the symmetry of an idealized framework when the chemical occupancy of the tetrahedral nodes is considered [39].

Two water molecules bond to the Al1 atom in the center chain. Such a building unit has also been observed in the structure of $\text{AlPO}_4\text{-H}_2$ [40]. In both structures, the fused 4-rings are in a *trans* conformation (Fig. 3a), which has never been observed in an aluminosilicate or pure-silica framework [40]. However, it has been suggested that the octahedral coordination of the Al atoms might reduce the geometric strain inherent to this conformation and stabilize the aluminophosphate triple-chain building unit [38,40].

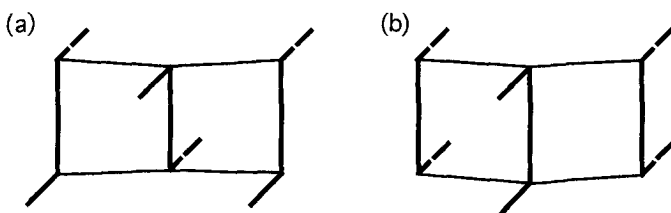


Fig. 3: Fused 4-rings with (a) the *trans*, and (b) the *cis* conformation

Unlike other hydrated aluminophosphate molecular sieves, the water molecules in VPI-5 were found to be ordered. They follow the framework symmetry and form a triple helix inside the 18-ring channels. This water structure is presumed to be stabilized by hydrogen bonding [38].

The location of the octahedral Al in the fused 4-rings was also found by Perez et al. in both their thermally stable and thermally unstable phases [19]. In both cases, the refinement of the structure was carried out in the space group $P6_3cm$, but the 6-rings in the latter phase were found to contain disordered phosphate groups. Two partially occupied models were required to describe the structure, and their relative populations were found to vary from one preparation to another [42].

Cheetham and Harding recorded single crystal synchrotron diffraction data on a very small VPI-5 crystal ($70 \times 10 \times 10 \mu\text{m}^3$) taken from the sample used by McCusker et al. [43]. Although their data were weak and not of the highest quality (due in part to experimental aspects of the data

collection procedure, and in part because the crystal was twinned [43]), their structure refinement fully confirmed the $P6_3$ symmetry, the framework positions and the two water molecules of the octahedrally coordinated Al in the model of McCusker et al. Six additional water molecule positions, which cannot all be simultaneously occupied, were identified. They line the wall of the channel and are at distances suitable for hydrogen bonding to a framework oxygen position or to other water molecules [43]. Thus, this model for the water structure differs from that of the triple helix model. However, the powder pattern calculated using these parameters does not fit the low angle part of the observed powder diffraction pattern, which is particularly sensitive to species in the channels.

The structure model in $P6_3$ is in full agreement with the findings of ^{27}Al - and ^{31}P solid-state NMR studies, which show that the as-synthesized form has three crystallographically distinct Al and P sites, respectively.

The ^{27}Al MAS NMR spectrum contains an asymmetric line at ca. 40 ppm and a broad peak at ca. -18 ppm (relative to $\text{Al}(\text{NO}_3)_3$), with an intensity ratio of 2:1. These have been assigned to tetrahedrally and octahedrally coordinated framework Al, respectively [16,25]. Using ^{27}Al double-rotation (DOR) NMR, Wu et al. [44] have shown that the line at 40 ppm is actually composed of two overlapping resonances from 4-coordinated Al in a 1:1 intensity ratio (see Fig. 4). Furthermore, ^{27}Al nutation MAS NMR reveals that these two signals from tetrahedral Al have slightly different quadrupole interaction parameters [45], allowing their differentiation in the MAS spectrum at a lower magnetic field strength [46].

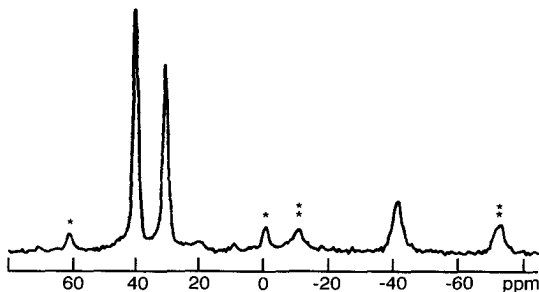


Fig. 4: ^{27}Al DOR NMR spectrum of as-synthesized VPI-5 at a field strength of 4.7 T (from ref. 46). Spinning sidebands are labeled with asterisks

The ^{31}P spectrum of hydrated VPI-5 (Fig. 5) also displays three resonances with approximate chemical shifts of -23, -27 and -33 ppm (relative to a 85% solution of H_3PO_4), and an approximate 1:1:1 ratio for the peak areas [25]. The existence of three signals in the ^{31}P spectrum also confirms the presence of three crystallographically distinct P positions in the framework. The overall features of the ^{31}P spectrum are thus well understood. However, numerous interpretations, in part contradictory, dealing with the detailed assignment of the distinct resonances to the specific crystallographic P sites have been published [16,45-51]. The complete understanding of the ^{31}P spectrum of as synthesized VPI-5 will require further investigation.

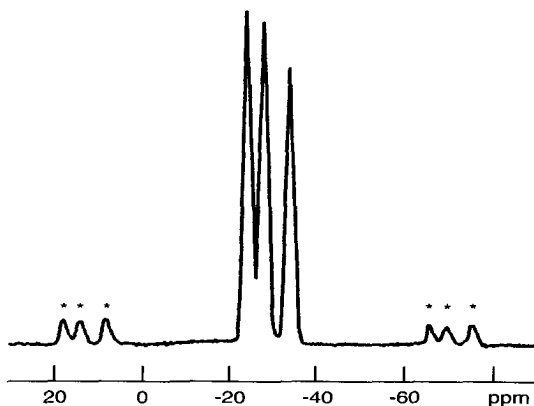


Fig. 5: ^{31}P spectrum of as-synthesized VPI-5 (from ref. 26). Spinning sidebands are labeled with asterisks

The results of other experimental solid-state NMR experiments involving newer techniques like 2D-heteronuclear ^{27}Al - ^{31}P correlation [50], 1D-cross-polarization (CP) and transferred-echo double-resonance (TEDOR) [51], further corroborate the proposed structure of VPI-5 [38].

The dynamic properties of water within the channels of VPI-5 has been studied by ^2H MAS NMR spectroscopy [52,53]. Two types of water molecules were found: the first corresponds to water molecules undergoing fast isotropic reorientation within the channels, and the second to water molecules bound to the framework Al. Exchange between the two types of water was observed, accompanied by a 3-fold jump, which is indicative of a relatively high degree of water ordering within the VPI-5 channels [52]. This model was later improved by assuming internal rotational motions of the bound water molecules about the Al-OH₂ bond, and by allowing the relative populations of the bound and free sites to vary with temperature [53].

2.3.2. Structure of dehydrated VPI-5

Richardson et al. made the first attempt to refine the structure of the anhydrous form of VPI-5 using neutron time-of-flight data [54]. A Rietveld refinement assuming disordered Al/P in the space group $P6_3/mcm$ converged, but very high uncertainties in distances and angles were observed in their final model. Refinement assuming strict alternation of Al and P in the space group $P6_3cm$ was unsuccessful, because of the strong pseudosymmetry [54].

The crystal structures of the dehydrated phases of VPI-5 and the aluminophosphate denoted 'dis-VPI-5' in this work, were also refined by Poojary et al. using X-ray powder data [55]. The structure of the anhydrous form of 'dis-VPI-5' is similar to that of dehydrated VPI-5, but the atoms in the 6-rings of the channel wall were found to be disordered, requiring two partially occupied structures to define the atomic positions. One structure is the regular VPI-5 framework, the other structure requires a rotation of

the 6-ring phosphate groups to produce 4-, 6- and 10-rings in the channel wall.

The ^{27}Al MAS NMR spectrum of dehydrated VPI-5 is shown in Fig. 6a. It displays only one resonance line with a chemical shift of ca. 35 ppm, relative to $\text{Al}(\text{NO}_3)_3$, indicating that all Al atoms are in a tetrahedral environment [56,57]. The ^{27}Al NMR spectrum taken under double-rotation conditions (Fig. 6b) shows that there are actually two peaks at ca. 33 and 36 ppm, representing tetrahedrally coordinated Al [44,58], with an intensity ratio of 1:2, respectively.

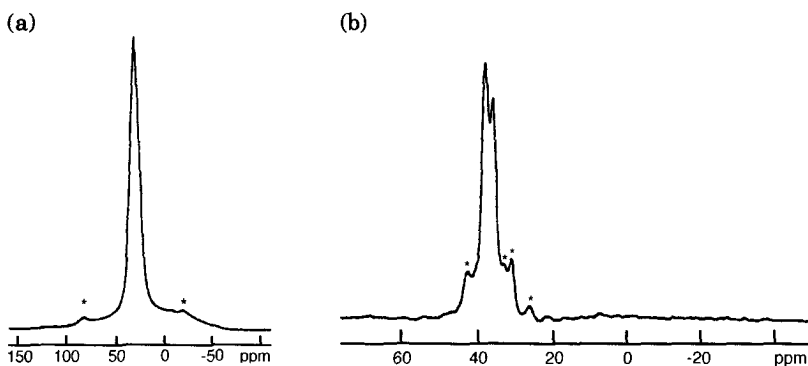


Fig. 6: (a) ^{27}Al MAS- and (b) ^{27}Al -DOR NMR spectra of dehydrated VPI-5 (from ref. 20,58). Spinning sidebands are labeled with asterisks

The ^{31}P MAS NMR spectrum of dehydrated VPI-5 is more complicated. The spectrum as measured by Martens et al. [56] is shown in Fig. 7. Instead of three peaks with equal intensities (fully hydrated form), three resonance maxima are present at ca. -32, -27 and -17 ppm, with relative intensities 3:5:1, respectively [56]. This is not consistent with the $P6_3cm$ symmetry assumed for the refinement of the structure from X-ray data, where two resonances in a 2:1 ratio would be expected. Thus, the ^{31}P MAS spectrum suggests that the anhydrous phase has a lower symmetry than $P6_3cm$. Further, since the resonance at -32 ppm has been assigned to P located between the fused 4-rings, the ^{31}P spectrum also suggests that one-sixth of the P sites located at the connection of 6- and 4-rings are different

from the others, giving rise for a signal with an extreme chemical shift of -17 ppm, which is indicative of a reduction of the average P-O-Al angle [56].

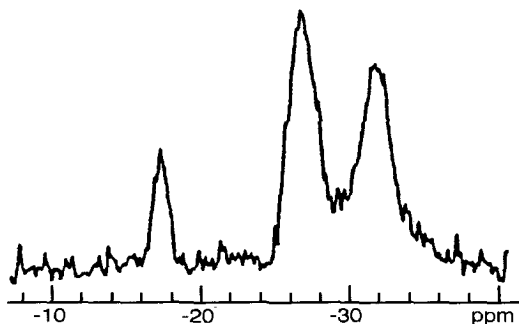


Fig. 7: ^{31}P MAS NMR spectrum of dehydrated VPI-5 as measured by Martens et al. (from ref. 56)

Perez et al. carried out an MAS NMR study on two samples (VPI-5 and 'dis-VPI-5') as a function of hydration level [57]. Their ^{31}P spectra (Fig. 8) contain six well resolved resonances, but they assumed that only the three with chemical shifts of ca. -31, -27 and -17 ppm, represent the fully dehydrated structure, and that the other three were caused by a small amount of water that was still present in the channels [57]. They also suggested that, in the dry state, the P-O-Al bond in every other 4-ring is broken to produce a P=O site and three-coordinated Al, to explain the resonance at -17 ppm [57].

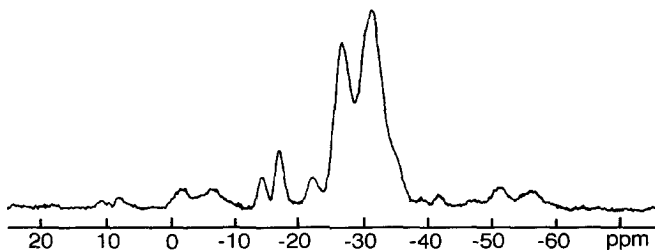


Fig. 8: ^{31}P MAS NMR spectrum of dehydrated VPI-5 as measured by Perez et al. (from ref. 57)

2.3.3. Structure of VPI-5 as a function of temperature

Using variable-temperature (VT) solid-state ^{31}P NMR, van Braam Houckgeest et al. have shown that fully hydrated VPI-5 undergoes a reversible phase transformation at ca. 80°C in a closed system [47]. The room-temperature spectrum containing three resonances with intensity ratios 1:1:1 transforms to a spectrum having only two signals and peak intensities in the ratio 2:1. Rocha et al. recorded spectra of as synthesized VPI-5 using an even wider range of temperatures (from -82 to 97°C) and confirmed the above described transition [45]. No substantial changes were observed below RT, where all the ^{31}P NMR spectra contain three resonances in a 1:1:1 intensity ratio with only minor differences in chemical shifts and peak widths. Very recently, the transformation at ca. 80°C was also observed with the newly developed two-dimensional (2D) triple-quantum (3Q) ^{27}Al MAS NMR technique [59].

Rocha et al. [45] also conducted ^1H - ^{31}P and ^1H - ^{27}Al cross-polarization (CP) NMR experiments at various temperatures and found a significant decrease in the efficiency of the ^1H - ^{31}P and ^1H - ^{27}Al CP/MAS signals with increasing temperature. This is indicative of an increased mobility of the water molecules.

The ^{31}P NMR results suggest that above 80°C the VPI-5 framework assumes the higher symmetry space group $P6_3cm$.

Interestingly, a similar reversible symmetry change has also been observed in ^{31}P MAS NMR experiments on a partially dehydrated sample of VPI-5. Even though all water molecules except those coordinated to Al had been removed from the VPI-5 sample, the ^{31}P NMR spectra showed three peaks at room temperature and two at ca. 80°C. This fact indicates that the breakdown of the hydrogen-bonded water structure inside the pores probably does not provoke the symmetry change [60].

2.4. Thermal stability

The limiting factor for all the potential applications of VPI-5 has been its thermal instability and facile conversion to $\text{AlPO}_4\text{-8}$. The obvious interest in understanding the factors affecting the framework stability of this aluminophosphate molecular sieve and the mechanisms of such a transformation, has led to a large number of studies (primarily XRD and NMR), which, to some extent, present conflicting evidence for the prerequisite conditions for a stable sample.

As stated before, under relatively mild conditions, VPI-5 undergoes an irreversible, topotactic phase transformation to $\text{AlPO}_4\text{-8}$ (**AET**) [61-63], another large-pore aluminophosphate molecular sieve with a one-dimensional 14-ring channel system [6,7]. This transformation from the hexagonal VPI-5 to the orthorhombic $\text{AlPO}_4\text{-8}$ (see Fig. 9) can occur in three directions, and this leads to stacking disorder along the channel direction, which reduces the effective pore diameter and severely limits its function as a molecular sieve [7]. The similarity of the structures of these two materials is evident from Fig. 9. If the suggested instability of the *trans* conformation of the fused 4-rings for tetrahedral frameworks is correct [41], the solid state conversion to $\text{AlPO}_4\text{-8}$ is not difficult to envisage.

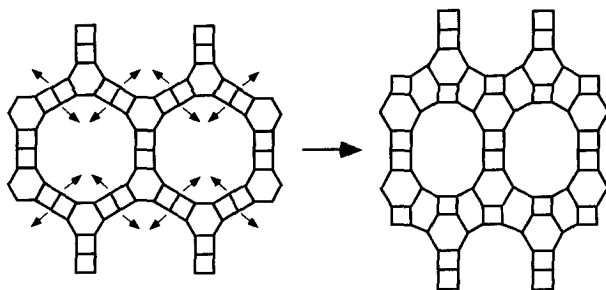


Fig. 9: Schematic representation of the **AFI** and **AET** topologies

Investigations indicate that the VPI-5 structure is particularly susceptible to this transformation at a level of dehydration between the monohydrated and dehydrated forms, i.e., after approximately 95% of the total water content has been removed [56].

However, when the 18-ring channels of VPI-5 are blocked by large guest molecules, such as C_{60} [65], the transformation cannot occur because there is insufficient space for the structural rearrangement leading to $AlPO_4-8$. The incorporation of smaller organic molecules, such as formamide, dimethylformamide, ethylformamide, formylmorpholine, etc., also has a stabilizing effect and causes an increase in the temperature at which the conversion occurs [66].

Apparently, the thermal stability of VPI-5 strongly depends on many factors, such as the method of preparation of the precursor [48], the nature of the organic additive used in the crystallization [19,25,64,67], washing of the synthesis product [40,68,69], and the type of solvent used in the washing [48], etc. The stability of the samples has often been associated with a low concentration of structural defects (i.e., P-OH groups) and the absence of impurity phases [19,27,40,61,69,70]. A further characteristic believed to be important for stable VPI-5 is the P/Al ratio being close to the ideal value of 1 [19,71,72].

2.5. Other physico-chemical properties

In the following, some adsorption, diffusion and catalysis results are summarized. They are given to complete the picture on VPI-5 and are by no means exhaustive.

2.5.1. Adsorption

The adsorption of molecules with different kinetic diameters, such as O_2 , N_2 , n-hexane, cyclohexane, neopentane, triisopropylbenzene and perfluorotributylamine into VPI-5, as well as high resolution isotherms

over a wide range of pressures using gas (e.g. argon, nitrogen) adsorption techniques, have been reported [5,13,56,73-76]. Based on these studies, the effective pore size of VPI-5 was calculated to be 12-13Å [5,13].

Adsorption of water vapor into VPI-5 has also been studied [77,78]. The results suggested that a three-dimensional array of water molecules can form in the large pores of this aluminophosphate molecular sieve.

2.5.2. Diffusion

Molecular diffusion of methane and tetrafluoromethane in VPI-5 has been studied by pulsed field gradient nuclear magnetic resonance (PFG NMR) and NMR exchange experiments [79]. The translational mobility of both molecules in this microporous material was found to be at least two orders of magnitude smaller than in ZSM-5 [79]. This is surprising since the channels in the aluminophosphate are about twice as wide as those in ZSM-5. It was speculated that this small translational mobility could be correlated with the fact that VPI-5 has only a 1-dimensional channel system, while ZSM-5 has a 3-dimensional one. A 1-dimensional channel system may lead to a reduced mobility as a consequence of single-file diffusion [79]. Furthermore, it was stated that molecular propagation over length scales of the order of the crystallite dimensions (i.e. in the micrometer range) must be determined by the laws of ordinary diffusion [79].

2.5.3. Catalysis

As stated before (compare 2.2.3), it is not likely that Si will substitute for Al and/or P in the framework of VPI-5 and, therefore, no Brønsted acid sites can be generated. Thus, although many attempts have been made to use the extra-large pores of this molecular sieve, VPI-5 has not found any industrial application as a catalyst. There are, however, some examples of catalytic reactions studied over VPI-5, such as the hydrogenation of 1-octene and *cis*-cyclooctene (with Rh supported on VPI-5) [25], the oxidation

of n-octane (on iron-phthalocyanines loaded into VPI-5) [80], and the aromatization of n-hexane (on Pt loaded into VPI-5) [81]. VPI-5 has also been used for the stereoselective alkylation of a racemic 2-phenyl-propionaldehyde [82].

2.6. Advanced materials applications

Anderson et al. reported the incorporation of buckminsterfullerene, C_{60} , into the one-dimensional channels of VPI-5 [65]. Apparently, the C_{60} molecule interacts weakly with the wall of the aluminophosphate framework, provoking an emission of white light. The form of this 'white light' spectrum is weighted much more towards the higher frequencies than a black body spectrum, making it interesting for visible-light emission [83].

3. Experimental characterization techniques

3.1. Powder diffraction

3.1.1. General considerations

Powder diffraction has experienced a steady development since the early part of this century and constitutes, undoubtedly, one of the most versatile, powerful and widely used analytical techniques available to scientists in the fields of solid-state physics and chemistry and materials science.

Powder diffraction has become a standard technique for the detection and identification of crystalline phases, the quantitative analysis of samples containing a mixture of phases, the determination of accurate unit cell dimensions, the analysis of structural imperfections, the investigation of bulk and microscopic strain, and the characterization of microstructure and texture. Besides these 'traditional' applications, powder methods have been used extensively in the refinement of crystal structures, and, more recently, in their determination *ab initio*, which has long been the exclusive domain of single crystal techniques.

Although powder diffraction has experienced substantial progress both instrumentally and methodologically during the last decades, the power of the method is hindered by the fact that the three-dimensional diffraction data are effectively reduced to one dimension. Due to this inherent projection, individual peaks are systematically or accidentally superimposed in the powder experiment, making it difficult, if not impossible, to ascertain the intensities of the individual components. This results in a loss of valuable information that is essential if the classical methods of structure solving (e.g. direct methods) are to be employed. However, the development of high resolution laboratory instruments and the advent of synchrotron radiation as an accessible and reliable source of high-intensity, highly collimated radiation, has led to a dramatic reduction in the incidence of peak overlap and the solving of structures,

although not straightforward, is now possible. The impact is even more remarkable if the quality (crystallinity) of the sample is high, i.e., when the broadening of the diffraction lines due to microstrain, stress or crystallite size is minimal.

3.1.2. Crystal structure refinement from powder diffraction data: the Rietveld method

Structure refinement from powder data can in principle be performed in a way analogous to conventional single crystal methods, using integrated intensities extracted from the diffraction pattern by means of a pattern decomposition method [84]. In a second step, the *pseudo* single crystal data set thus derived is used as input for a subsequent least-squares structure refinement [84]. This so-called two stage procedure, proved to be satisfactory for simple structures, but not for more complex ones with large unit cells such as zeolites [85]. As the number of reflections increases, the pattern becomes more and more difficult to decompose. Furthermore, if peaks overlap completely, either accidentally or exactly (e.g. for high lattice symmetries), they cannot be separated.

An alternative structure refinement procedure that circumvents the reflection overlap problem was introduced by Rietveld in 1967 [86,87]. Instead of comparing the observed and calculated intensities of individual reflections (or groups of reflections), it compares each step of the observed and calculated powder patterns. Thus, no effort is made to allocate observed intensity to particular Bragg reflections or to resolve overlapped reflections. In the Rietveld, or whole-profile fitting, method, the entire powder diffraction pattern is calculated and that is fitted to the experimental profile.

The Rietveld method which was initially developed for neutron diffraction data, has now been extended to the analysis of X-ray data, and represents the most widely used procedure for the refinement of crystal structures from powder diffraction data.

In the Rietveld method the following residual function is minimized:

$$S_y = \sum_i w_i (y_i - y_{ci})^2 \quad (1)$$

where

w_i : weight assigned to the individual intensity y_i , normally $w_i = \sqrt{\frac{1}{y_i}}$
 y_i : observed intensity at the i th step of the diffraction pattern,
 y_{ci} : calculated intensity at the i th step of the diffraction pattern,
 and the sum runs over all data points.

Typically, many Bragg reflections contribute to the intensity, y_p , observed at any arbitrarily chosen point, i , in the pattern. The calculated intensities y_{ci} are determined from the $|F_{hkl}|^2$ values calculated from the structural model by summing the calculated contributions from neighboring (overlapping) Bragg reflections plus the background:

$$y_{ci} = b_i + s \sum_{hkl} L_{hkl} M_{hkl} O_{hkl} |F_{hkl}|^2 P_{hkl}(2\theta_i - 2\theta_{hkl}) A \quad (2)$$

where

b_i : background count at the i th step,
 s : scale factor,
 L_{hkl} : Lorentz-polarization factor,
 M_{hkl} : multiplicity factor of the hkl reflection,
 O_{hkl} : preferred orientation correction function,
 $|F_{hkl}|$: structure factor,
 P_{hkl} : peak profile function (dependent on half width, peak asymmetry and shape parameters),
 A : absorption correction.

The summation is over all reflections (hkl) contributing to a given step i .

As stated before, the total intensity of a reflection is determined from the $|F_{hkl}|^2$ values derived from the structural model, but the shape of the

Bragg reflection depends on the instrumental and sample parameters, which are approximated by the peak profile function. In the Rietveld method, all these structural and profile parameters are refined simultaneously until the best fit between the observed and calculated patterns is obtained. A key feature, not present in other methods of structure refinement, is the feedback during refinement which allows the allocation of the observed intensity to partially overlapping Bragg reflections to be improved [88].

It is obvious that an accurate description of the shape of the peaks in the powder diffraction pattern is critical to the success of the Rietveld refinement. A function used to model an individual diffraction peak must clearly approximate the observed distribution of intensity. If interpretation in terms of physical quantities (e.g. information on microstructural properties) is also required, the function should also be deconvolvable [84].

In contrast to the generally symmetric (Gaussian) nature of neutron diffraction lines, X-ray diffraction profiles are asymmetric and non-Gaussian, and difficult to model properly. There are numerous approaches to the modeling of X-ray diffraction lines, both analytical and non-analytical [e.g. 89-94]. However, the fact remains that in many current refinements, a major portion of the least-squares residual is determined by the profile mismatch between the model and observed data rather than being determined by the fit of the structural parameters [95].

Since the residual function, S_r (see equation 1), being minimized in the Rietveld method is non-linear, the solution must be found with an iterative procedure in which, in each iteration, a linear approximation to the model is used to construct an approximate normal equations ($m \times m$) matrix (where m is the number of parameters being refined). This is then inverted to compute a new, hopefully improved estimate for the values of the parameters. Because of this non-linearity of the residual function, the starting model should be close to the correct one. Otherwise, the non-

linear least-squares procedure will not lead to the global minimum [88,96]. It will either diverge or lead to a false minimum.

A pure geometric distance least squares (DLS) refinement [93] can also be used to get a geometrically idealized structure model for the refinement. If the structural model is poor or incomplete, the introduction of restraints (see below) and the selection of different least-squares algorithms (e.g. Gauss-Newton or Variable Metric) at different stages of the refinement may help to avoid false minima in some cases. An alternative solution to this problem is the introduction of damping factors that reduce the size of the parameter shifts, but this does not guarantee stability [96].

There are some indicators and criteria for following the progress of a Rietveld refinement and judging the agreement between the observed and the calculated intensity distributions. The most informative criterion is the visual inspection of a plot of the intensity *versus* 2θ of the entire observed, calculated and difference patterns [97,98]. However, as in single crystal analysis, discrepancy factors (R-factors) have also been defined [89,99].

To test for serial correlation between adjacent steps in a power diffraction profile, a statistic-based indicator, the Durbin-Watson statistic factor d_{dw} [100], is used. If serial correlation is present, then the estimated standard deviations (e.s.d.'s) associated with the parameters being refined are not a valid measure of uncertainty [101], and wrong conclusions regarding the adequacy of a given model and/or the global minimum can be drawn.

Rietveld refinement relies heavily on the starting model, which should contain enough well-placed atoms to phase the powder data. If only a partial model is available, difference Fourier techniques can be applied to produce a three-dimensional difference electron density map and yield the positions of the missing atoms. However, because both the partitioning of the overlapping reflections and the phases (or the signs in the centrosymmetric case) of the F_{hkl} are calculated from the partial model, such an

electron density map will be biased towards the model. Maps calculated from powder data are, in general, more diffuse than those calculated from single crystal data [85,98]. This explains why normally more than one Fourier cycle is needed to locate all missing atoms [98].

3.1.3. Use of polycrystalline diffraction techniques on zeolites

Among the many standard analytical techniques that have been applied to the physical and chemical characterization of zeolites and zeolite-like molecular sieves, diffraction methods have proved to be very versatile and useful. Many interesting and important properties of these materials, such as the ion-exchange and molecular sieve properties, the catalytic behavior, sorption capacity and shape selectivity, are governed by their structure. Unfortunately, single crystals suitable for a structure analysis are not always available, especially in the case of synthetic zeolites, so polycrystalline diffraction techniques have to be applied.

Generally, zeolite topologies have relatively high symmetries, but in most cases the real structures are more complex [102]. The number of structural parameters needed to describe them is correspondingly high, so that a poor observation-to-parameter ratio for powder data and zeolitic materials is often observed [98]. This not only affects the convergence of a Rietveld refinement, but also leads to false minima, so incorrect conclusions regarding the structure of the material being studied can be drawn.

To enhance the convergence of a Rietveld refinement, geometric information in form of interatomic distances and angles, which are well established for zeolitic frameworks (e.g. P-O and Al-O distances, O-P-O, O-Al-O and P-O-Al angles in the case of aluminophosphate molecular sieves), can be incorporated as additional 'observations' to the powder data set [103]. These so called geometric restraints not only increase the number of observations allowing more parameters to be refined, but also keep the structure chemically sensible. This is especially important in the

early stages of refinement, when the structure model might be incomplete.

Another form of geometric restriction that effectively reduces the number of variables to be refined, the so called hard constraints, is a group refinement, where a group of atoms (e.g. a sorbed organic molecule) is refined together and only the position and the orientation of the whole group is refined [98].

Besides the critical observation-to-parameter ratio in polycrystalline diffraction data, zeolite crystallography is confronted with a number of additional difficulties. Cations or sorbed molecules can cause subtle distortions of the ideal framework symmetry and this can lead to dramatic pseudosymmetry problems [102,105], that seriously hinder a structure refinement. Non-framework species can also require partial occupancies, which not only complicates the interpretation of the electron density maps, but also the structure refinement [102]. Other common difficulties present in zeolite structure analysis are stacking faults and intergrowths [102,105].

3.2. Solid-state nuclear magnetic resonance spectroscopy

High-resolution solid-state nuclear magnetic resonance (NMR) spectroscopy is a well established technique for the characterization of zeolites and other porous materials. It has been used to examine local structure, pore architecture, catalytic behavior and diffusion properties of adsorbed molecules. The combination of NMR and X-ray diffraction techniques is particularly appropriate as the former is most sensitive to short-range order and geometries (local environment), while the latter is influenced by long-range order and periodicities. Thus, the use of NMR and diffraction methods together provides a more complete understanding of structure and bonding.

^{31}P magic-angle spinning (MAS) NMR spectroscopy is considered to be the most sensitive technique for extracting information on the local structure in aluminophosphate molecular sieves [106]. In the case of these highly ordered solids, ^{31}P MAS NMR can provide *direct* evidence of the numbers and relative occupancies of crystallographically inequivalent P sites in the unit cell of the framework [107].

In principle, ^{27}Al is also a very favorable nucleus for NMR: it has a 100% natural abundance with a large chemical shift range [104] and short relaxation times [106]. However, ^{27}Al MAS NMR has had limited utility in the study of framework ordering in aluminophosphate molecular sieves. ^{27}Al nuclei (nuclear spin $I=5/2$) have a nuclear quadrupole moment which interacts not only with the magnetic field in which the sample is placed but also with the electric field gradient. Both, line broadening/distortion and chemical shift changes can arise from those quadrupolar interactions, rendering interpretation of NMR spectra difficult [58,106-108]. Although these interactions decrease with increasing magnetic field strength, they can only be partly reduced by MAS [106].

The development of new techniques such as dynamic angle spinning (DAS) [109,110] and double orientation rotation (DOR) [44,111] NMR, represents a major advance in the study of quadrupolar nuclei by solid-state NMR, since they remove not only first-order broadening effects such as chemical shift anisotropy, but also second-order quadrupolar interactions. Thus better resolved spectra, which yield greater insight into the local structural arrangements of Al and other quadrupolar nuclei, can be produced.

^{27}Al DOR NMR has been employed effectively to study the distribution of Al in the crystalline framework of several aluminophosphate molecular sieves, including VPI-5 [44,46,107].

Solid-state ^1H NMR has been shown to be a viable method for obtaining information about H-containing species in zeolitic materials. Whether an

OH group is terminal or bridging can be discerned, and the environments of hydrogen containing probe molecules can be determined [106].

^2H NMR spectroscopy is a useful method for studying the dynamic properties of adsorbates [112], and has been successfully applied to the investigation of the motion of small molecules within the pores of zeolites [113,114]. The analysis is performed by simulating ^2H NMR line shapes for different models of the molecular motion until reasonable agreement with experiment is obtained [53]. This provides information on the distribution of the species, the nature of the bridging site, and the characteristics of the motion of the sorbed molecules [52].

There are some other NMR techniques, some of which have been developed very recently, which have been applied with success to investigate aluminophosphate molecular sieves. Cross polarization MAS, which allows an intensity enhancement and a reduction of the recycle time between experiments [106], provides information on the magnitude of dipolar interactions and, thus, on the distance between the nuclei. Double-resonance NMR connectivity involving quadrupolar nuclei [51] directly maps connectivities between sites with resolved NMR resonances. Two-dimensional heteronuclear ^{27}Al - ^{31}P correlation [50] provides an alternative for establishing connectivities between the different P and Al sites in an aluminophosphate framework.

3.3. Instrumentation

3.3.1. Powder diffraction

Film methods:

Guinier - de Wolff: Enraf - Nonius camera equipped with a quartz monochromator. $\text{CuK}\alpha$ radiation was used.

Guinier - Lenné: Huber high-temperature camera equipped with a quartz monochromator. CuK α radiation was used.

Diffractometers:

PAD-X powder diffractometer: Scintag $\theta - \theta$ diffractometer with Bragg-Brentano geometry, equipped with a solid-state detector and a vacuum oven. The sample is mounted in a rotating flat plate holder. No monochromator was used. CuK α radiation (45mA, 45kV) was selected using the solid-stated detector. A silicon sample (NBS Standard Reference Material 640a) was used as an external standard.

STOE powder diffractometer: STOE STADI diffractometer in transmission mode. The diffractometer is equipped with a Ge primary beam monochromator, a linear position sensitive detector (PSD) and a high-temperature attachment for capillaries. For data collection for structure refinements, the samples were sealed in glass capillaries of 0.3mm diameter. For the high-temperature experiments, the samples were sealed in quartz capillaries of 0.5mm diameter. CuK α_1 radiation (45mA, 45kV) was used.

Synchrotron powder diffraction: High resolution data were collected on the Swiss Norwegian Beam Line (SNBL) at the European Synchrotron Radiation Facility (ESRF) in Grenoble using Debye-Scherrer geometry. For the dehydrated sample E (see chapter 6) data were collected on the ESRF beamline BM 16, which is equipped with a multi-analyzer detector system.

3.3.2. Solid-state NMR spectroscopy

NMR spectra were recorded on a Bruker AMX 400 spectrometer equipped with a wide-bore magnet ($B_0 = 9.4$ T) and a High-Speed Double-Bearing MAS head. The variable-temperature (VT) ^{31}P -, ^{27}Al - and ^1H - MAS NMR

spectra were recorded at 162.0, 104.3 and 400.1 MHz, respectively, on a Bruker MSL-400 spectrometer in the temperature range 30 - 108°C. The VPI-5 powder was filled in rotors of 4 mm diameter, which were tightly closed with boron nitride caps and spun at 10 kHz. The ^{31}P , ^{27}Al and ^1H spectra were measured relative to 85wt% H_3PO_4 , $\text{Al}(\text{H}_2\text{O})_6^{3+}$ in an aqueous $\text{Al}(\text{NO}_3)_3$ solution, and tetramethylsilane, respectively. Spectra simulations were carried out with the PC program Bruker WINFIT.

3.3.3. Thermogravimetric analysis

Thermogravimetric (TG) and differential thermogravimetric (DTG) curves were measured with the Mettler Thermoanalysis System, composed of a TA processor, a Mettler M3 microbalance and an oven which is controlled by the processor. Dynamic and isothermic experiments were carried out under different atmospheres and using different temperature and time regimes.

3.3.4. Scanning electron microscopy

Scanning electron micrographs were taken on a JEOL JSM 6400 electron microscope with an accelerating voltage of 20 kV.

3.3.5. Others

-Laboratory centrifugal ball mill (Retch) with agate grinding bowl and balls.

-Ultrasonic baths ELMA (Transsonic digital, working frequency 35kHz) and Esterline Angus.

4. VPI-5 synthesis optimization

A large number of procedures have been reported for the synthesis of VPI-5, but the reproducibility of those preparations is not always guaranteed. Although the procedures themselves seem to be easy to follow, there are a number of details that make the synthesis of this aluminophosphate not so straightforward. It appears that the thermal stability of VPI-5 depends heavily on these details.

The structural investigations described here were initiated with two samples provided by Piet Grobet (KU Leuven, Belgium) and one from E. Jahn, all of which showed markedly different behaviors upon dehydration. To avoid this strong sample dependence, a synthesis study to produce highly crystalline VPI-5 was undertaken. The procedure first reported by Jahn et al. [8], which seemed to yield a relatively stable and highly crystalline material, was used as starting point for the optimization.

Large single crystals of zeolites and zeolite-like molecular sieves are useful not only for structural investigations, but also for advanced optical and electronic material applications. However, the synthesis of such crystals by conventional hydrothermal methods is not straightforward. It is generally assumed that the crystallization of a molecular sieve is a solution-mediated process, in which the gel phase supplies the framework building species through continuous dissolution until a supersaturation of the solution phase is reached [115]. The high degree of supersaturation causes high nucleation rates, and results in the formation of many small crystallites. Only in a few cases has careful control of the synthesis parameters led to the production of large single crystals, e.g. Linde type A (LTA) [116], faujasite (FAU) [117], ZSM-39 (MTN) [118], silicon-rich, Al-, B- and (Al+B) ZSM-5 (MFI), ferrierite (FER), ZSM-23 (MTT), ZSM-39 (MTN), theta-1 (TON) [119], AlPO₄-5 (AFI), dodecasil-1 (DOH), deca-dodecasil 3R (DDR), ZSM-11 (MEL) [120]. Large crystals of silica-based zeolites (ZSM-39, ferrierite, silicalite-1, etc.) have also been obtained from systems in which

pyridine is used as the solvent and water only in reagent quantities [121]. Microwave heating has also been applied successfully to the synthesis of large crystals of the aluminophosphate molecular sieve $\text{AlPO}_4\text{-5}$ [122].

Aluminophosphate-based molecular sieves seem to crystallize more easily than do their silicate-based counterparts. This can be seen in the large number of AlPO_4 structures that have been elucidated or refined from single crystal diffraction data. It is not yet clear whether this is a result of the differences in the gel chemistry, the synthesis conditions or the inherent ability of an AlPO_4 structure to accommodate different framework cations, in both tetrahedral and octahedral sites, better than the silicate structure does.

Of the aluminophosphate molecular sieves, VPI-5 with its one-dimensional 12-13 Å pores, is perhaps the most promising and versatile candidate for advanced material applications. Unfortunately, large single crystals of this particular structure type have not yet been reported. If large crystals of VPI-5 could be synthesized, perhaps further details of its unusual structure could be learned, and its application in the advanced material area be considered more seriously. Thus, an attempt to optimize the synthesis conditions for the production of large single crystals was also undertaken.

4.1. Synthesis procedure of E. Jahn

The standard preparation is based on a mixture with the molar composition: $\text{Al}_2\text{O}_3 : \text{P}_2\text{O}_5 : \text{DPA} : n\text{H}_2\text{O}$, where pseudoboehmite is used as the source of Al, di-n-propylamine (DPA) as the organic additive, and polyphosphoric acid as the source of P. The latter is the most unusual aspect of this synthesis procedure.

For defining the quantities of Al_2O_3 , P_2O_5 , and H_2O , the water content of both pseudoboehmite and ortho-phosphoric acid has to be taken into account.

There are five main preparative steps:

(1) *Preparation of the gel*: a stoichiometric mixture of pseudoboehmite, polyphosphoric acid and distilled water is milled for 60 minutes in an agate ball mill. This step is essential for the homogenization of the initial gel and for obtaining the desired gel viscosity.

(2) *Ultrasonic treatment*: the resulting gel is charged into a plastic beaker and placed into an ultrasonic water bath for a preselected time.

(3) *Dilution of the gel*: the organic additive (DPA) is added and the mixture further diluted with the appropriate amount of water.

(4) *Stirring*: the resulting hydrogel is stirred for 30 minutes at room temperature.

(5) *Crystallization*: the diluted hydrogel is poured into 25ml Teflon-lined autoclaves. The autoclaves are then put into a forced air oven at the set temperature for a preselected time.

The crystallization process is stopped by quenching the autoclave to room temperature in cold water. The product slurry from the autoclave is then filtered and washed with distilled water 3-4 times to remove all traces of mother liquor and then dried at room temperature in air.

4.2. Materials

The starting materials used (all reagent grade chemicals) were: pseudoboehmite alumina (Pural SB, 25.8 wt% H_2O , CONDEA Chemie; Catapal SB, 27.2 wt% H_2O , Conoco Chemicals), P_2O_5 (Merck), ortho-phosphoric acid (85.0wt% aqueous H_3PO_4 , Fluka), di-n-propylamine (Fluka), distilled water.

Polyphosphoric acid, with the approximate formula $H_{10}P_8O_{26}$, was freshly prepared by dissolving 71g of dry P_2O_5 in 39g of H_3PO_4 . Since the reaction is very exothermic, the ortho-phosphoric acid was first cooled in ice. P_2O_5 was then added in small amounts under continuous stirring, allowing ample time for cooling between additions. After all the P_2O_5 had been added, the solution was stirred for an additional 90 minutes to enhance the homogeneity.

4.3. Synthesis optimization

Many factors influence the formation of VPI-5. The range of parameters examined is summarized in Table 1. Given the very large number of variables involved, sometimes a simplified approach was adopted. The influence of a particular parameter when varied singly was studied, and then the other significant parameters were adjusted to achieve optimal results for each batch composition. For instance, increasing the P_2O_5/Al_2O_3 molar ratio had to be accompanied by an increase in the DPA/Al_2O_3 molar ratio to counteract the pH depressing effects of the extra polyphosphoric acid.

Table 1: Parameter variation in the synthesis optimization

Parameter	Values investigated
P_2O_5/Al_2O_3	0.67, 0.77, 0.9, 1.0, 1.1, 1.3, 1.5, 1.7
H_2O/Al_2O_3 (gel preparation)	25, 30, 35, 40
H_2O/Al_2O_3 (total amount), n [mol]	40, 50, 60, 70, 80, 90, 120, 150
DPA/Al_2O_3	0.9, 1.0, 1.1, 1.3, 1.5, 1.7
Milling time, t_m [min]	0, 60, 90, 720
Ultrasonic bath time, t_{US} [min]	0, 8, 15, 20, 22, 25, 30, 45, 90
Stirring time, t_s [min]	30, 45, 60, 90
Reaction time, t_c [h]	12, 16, 24, 36, 48, 64, 72, 90
Reaction temperature, T_c [°C]	120, 122, 124, 125, 127, 130, 135

The results of optimization experiments carried out using Pural SB as the source for Al and the ultrasonic bath *ELMA* (working frequency 35 kHz) are presented in Tables 2-9. For the results of other investigations using Catapal SB and the ultrasonic bath *Esterline Angus* see Appendix A.

The tables are organized as follows: in Tables 2 - 8, the results of the experiments carried out with a fixed gel composition (only the total amount of water was varied) are summarized. For these experiments, the milling and stirring times were kept fixed at 60 and 30 minutes, respectively. For the experiments summarized in Tables 2 - 4, 25 moles from the total amount of water were used for the gel preparation, while for those described in Tables 5 - 7, 30 moles were used. The tables are organized according to the crystallization temperature: 125, 130 or 135°C. Table 8 summarizes experiments carried out at different temperatures, while Table 9 shows the results of experiments with variable gel composition.

In the tables, t_m , t_{US} and t_s denote the milling, ultrasonic and stirring times, respectively; T_c and t_c are the crystallization temperature and time, and n denotes the total amount of water used in the synthesis. The final pH value for each experiment is also reported. In the *Results* column, the products of the reaction are reported in order of yield as determined by optical microscopy and XRD (Guinier-Camera). A + or - superscript means a large quantity or traces of a given phase, respectively (e.g. H3⁺ means traces of H3). *Bundles* describes the wheat sheaf morphology of the VPI-5 polycrystals, as shown in Fig. 10a. This is the most common growth form for VPI-5. *Needles* (Fig. 10b) indicates that isolated crystallites were obtained. VFI and AEL stand for VPI-5 and AlPO₄-11, respectively.

Table 2: Optimization experiments at 125°C, using 25 moles of H₂O for the gel preparation**Batch composition:** Al₂O₃ : P₂O₅ : nH₂O : DPA, t_g: 60 min, t_c: 30 min, T_c: 125°C

t _g [min]	n [mol]	t _c [h]	pH	Results
8	60	16	7	H3, gel
		24	7	H3 ⁺ , gel
		36	7	H3 ⁺ , gel
	70	16	7	H3, gel
		24	7	H3 ⁺ , gel
		36	7	H3 ⁺ , gel
15	50	16	6	H3, gel
		24	7	H3 ⁺ , gel
		48	7	H3 ⁺ , gel
	60	16	6	VFI (small bundles, thin needles), H3, gel
		24	7	VFI (small bundles, thin needles), H3 ⁺ , gel
		48	7	VFI (small bundles, thin needles), H3 ⁺ , gel
	70	16	5	VFI (small bundles, thin needles), gel
		24	6	VFI (small bundles, thin needles), H3 ⁺ , gel
		48	7	VFI (small bundles, thin needles), H3 ⁺ , gel
	80	16	5	VFI (small bundles, thin needles), gel
		24	6	VFI (small bundles, thin needles), H3 ⁺ , gel
		48	7	VFI (small bundles, thin needles), H3 ⁺ , gel
30	50	16	6	VFI (small bundles), H3 ⁺ , gel
		24	7	VFI (small bundles), H3, gel
		48	7	VFI (small bundles), H3, gel
	60	16	6	VFI (small bundles), H3 ⁺ , gel
		24	6-7	VFI (small bundles), H3, gel
	70	16	5	VFI (small bundles, thin needles), H3, gel
		24	6	VFI (small bundles, thin needles), H3, gel
	80	16	5	VFI (small bundles, thin needles), H3, gel
45	40	16	7	VFI (small bundles), gel
		24	7	VFI (small bundles), H3 ⁺ , gel
		48	7	VFI (as above, but some degradation), H3 ⁺ , gel
	50	16	6	VFI (small bundles), gel
		24	7	VFI (small bundles), H3, gel
		48	7	VFI (as above, but some degradation), H3 ⁺ , gel
	60	16	5	VFI (small bundles, thin needles), H3, gel
		24	6	VFI (small bundles, thin needles), H3, gel
		48	7	VFI (as above, but some degradation), H3 ⁺ , gel

Table 3: Optimization experiments at 130°C, using 25 moles of H₂O for the gel preparation**Batch composition:** Al₂O₃ : P₂O₅ : nH₂O : DPA, t_m: 60 min, t_c: 30 min, T_c: 130°C

t _{is} [min]	n [mol]	t _c [h]	pH	Results
15	50	16	7	VFI (bundles), gel
		36	7	VFI (bundles), AEL, gel
	60	16	7	VFI (bundles), gel
		36	7	VFI (bundles), AEL, gel
	70	16	6	VFI (bundles), AEL, gel
		36	6	VFI (bundles), AEL, gel
	80	16	6	VFI (bundles, thin needles), AEL, gel
		36	6	VFI (bundles, thin needles), AEL, gel
30	50	16	6-7	VFI (bundles), gel
		36	7	VFI (bundles), AEL, gel
	60	16	6-7	VFI (bundles), gel
		36	7	VFI (bundles), AEL, gel
	70	16	6-7	VFI (bundles, some thin needles), gel
		36	7	VFI (bundles, some thin needles), AEL, gel
	80	16	6	VFI (bundles, some thin needles), gel
		36	6	VFI (bundles, some thin needles), AEL, gel
45	50	16	6-7	VFI (bundles), gel
		36	7	VFI (bundles), AEL, gel
	60	16	6-7	VFI (bundles), gel
		36	7	VFI (bundles), AEL, gel
	70	16	6	VFI (bundles, some thin needles), gel
		36	6-7	VFI (bundles, some thin needles), AEL, gel
	80	16	6	VFI (bundles, some thin needles), gel
		36	6-7	VFI (bundles, some thin needles), AEL, gel

Table 4: Optimization experiments at 135°C, using 25 moles of H₂O for the gel preparation**Batch composition:** Al₂O₃ : P₂O₅ : nH₂O : DPA, t_m: 60 min, t_c: 30 min, T_c: 135°C

t _{is} [min]	n [mol]	t _c [h]	pH	Results
8	60	16	7	VFI (bundles), gel
		24	7	VFI (bundles), AEL
		36	7-8	VFI (bundles), AEL
	70	16	7	VFI (bundles), gel
		24	7	VFI (bundles), AEL
		36	7-8	VFI (bundles), AEL
15	50	16	7-8	VFI (bundles), gel
		24	7-8	VFI (bundles), AEL
		36	8	VFI (bundles), AEL
	60	16	7-8	VFI (bundles), gel
		24	7-8	VFI (bundles), AEL
		36	8	VFI (bundles), AEL
	70	16	7	VFI (bundles), gel
		24	7	VFI (bundles), AEL
		36	7	VFI (bundles), AEL
30	60	16	7	VFI (bundles), AEL, gel
		24	7	VFI (bundles), AEL
		36	7	VFI (bundles), AEL
	70	16	7	VFI (bundles), AEL, gel
		24	7	VFI (bundles), AEL
		36	7	VFI (bundles), AEL

Table 5: Optimization experiments at 125°C, using 30 moles of H₂O for the gel preparation**Batch composition:** Al₂O₃ : P₂O₅ : nH₂O : DPA, t_m: 60 min, t_c: 30 min, T_c: 125°C

t _{cs} [min]	n [mol]	t _c [h]	pH	Results
30	60	16	5-6	VFI (small bundles, some needles), H3, gel
		24	6	VFI (small bundles, some needles), H3, gel
		36	6	VFI (small bundles, some needles), H3 ⁺ , gel
	70	16	5-6	VFI (small bundles, needles ~250x20x20μm ³), H3, gel
		24	6	VFI (small bundles, needles), H3, gel
		36	6	VFI (small bundles, needles), H3 ⁺ , gel
	80	16	5	VFI (small bundles, needles), H3, gel
		24	5-6	VFI (small bundles, needles ~ 250x25x25μm ³), H3, gel
		36	6	VFI (small bundles, needles ~ 250x25x25μm ³), H3 ⁺ , gel
	90	16	5	VFI (small bundles, needles ~ 250x25x25μm ³), H3 ⁺ , gel
		24	5	VFI (small bundles, needles ~ 250x25x25μm ³), H3 ⁺ , gel
		36	5-6	VFI (small bundles, needles ~ 250x25x25μm ³), H3 ⁺ , gel
45	40	16	6	VFI (small bundles), H3, gel
		24	6-7	VFI (small bundles), H3 ⁺ , gel
	50	16	6	VFI (small bundles), H3, gel
		24	6-7	VFI (small bundles), H3 ⁺ , gel
	60	16	6	VFI (small bundles, some thin needles), H3, gel
		24	6-7	VFI (small bundles, some thin needles), H3 ⁺ , gel
	70	16	6	VFI (small bundles, needles), H3, gel
		24	6-7	VFI (small bundles, needles ~ 250x20x20μm ³), H3 ⁺ , gel
		36	6-7	VFI (as above, but degraded), H3 ⁺ , gel
	80	16	6-7	VFI (small bundles, needles), H3, gel
		24	6-7	VFI (small bundles, needles ~ 250x20x20μm ³), H3 ⁺ , gel

Table 6: Optimization experiments at 130°C, using 30 moles of H₂O for the gel preparation**Batch composition:** Al₂O₃ : P₂O₅ : nH₂O : DPA, t_m: 60 min, t_{cs}: 30 min, t_c: 30 min, T_c: 130°C

n [mol]	t _c [h]	pH	Results
50	12	7	VFI(bundles), AEL, gel
	24	7	VFI(bundles), AEL, gel
60	24	6-7	VFI(bundles), AEL, gel
	36	7	VFI(bundles), AEL ⁺
70	24	6-7	VFI(bundles), AEL ⁺ , gel
	36	7	VFI(bundles, some needles), AEL ⁺
80	12	6	VFI(as above, but more needles), AEL, gel
	24	6	VFI(as above), AEL ⁺

Table 7: Optimization experiments at 135°C, using 30 moles of H₂O for the gel preparation**Batch composition:** Al₂O₃ : P₂O₅ : nH₂O : DPA, t_m : 60 min, t_r : 30 min, T_c : 135°C

t_{CS} [min]	n [mol]	t_c [h]	pH	Results
30	60	16	7	VFI(bundles), AEL, gel
		24	7	VFI(bundles), AEL
		36	7	VFI(bundles), AEL ⁺
	70	16	7	VFI(bundles), AEL, gel
		24	7	VFI(bundles), AEL
		36	7	VFI(bundles), AEL ⁺
	80	16	6 - 7	VFI(bundles), AEL ⁺ , gel
		24	7	VFI(bundles), AEL ⁺
	90	16	6	VFI(bundles), AEL ⁺ , gel
		24	7	VFI(bundles), AEL ⁺
45	70	16	7	VFI(bundles), AEL ⁺ , gel
		24	7	VFI(bundles), AEL ⁺
	80	16	7	VFI(bundles), AEL ⁺ , gel
		24	7	VFI(bundles), AEL ⁺

Table 8: Optimization experiments carried out at different temperatures, using 30 moles of H₂O for the gel preparation**Batch composition:** Al₂O₃ : P₂O₅ : nH₂O : DPA, t_m : 60 min, t_{CS} : 45 min, t_r : 30 min

T_c [°C]	n [mol]	t_c [h]	pH	Results
120	50	16	7	amorphous
		24	7	amorphous
	60	16	7	amorphous
		24	7	amorphous
122	50	16	7	VFI(needles ~190x13x13μm ³), gel ⁺
		24	7	VFI(some bundles, needles ~190x13x13μm ³), H3, gel ⁺
	60	16	6 - 7	VFI(some bundles, needles ~190x13x13μm ³), gel ⁺
		24	7	VFI(some bundles, needles ~190x13x13μm ³), H3, gel ⁺
124	50	16	6	VFI(some bundles, needles ~ 210x15x15μm ³), gel ⁺
		24	7	VFI(some bundles, needles ~ 210x15x15μm ³), H3, gel
	60	16	7	VFI(some bundles, needles ~ 210x20x20μm ³), H3, gel ⁺
		24	7	VFI(some bundles, needles ~ 210x20x20μm ³), H3, gel
127	50	16	7	VFI(more bundles, less needles), H3, gel
		24	7	VFI(as above), H3, gel
	60	16	6 - 7	VFI(as above), H3, gel
		24	6 - 7	VFI(as above), H3, gel

Table 9: Optimization experiments carried out with variable gel composition

gel composition [mol]		dilution [mol]		t_m	t_{gs}	t_g	T_c	t_c	pH	Results
Al_2O_3	P_2O_5	H_2O	H_2O^*	DPA	min	min	$^{\circ}C$	h		
1	1	30	50	1.2	60	30	120	24	7	amorphous
			60					36	7	amorphous
								24	7	amorphous
								36	7	amorphous
1	1.1	25	50	1.3	60	15	125	16	7	gel
								24	7	amorphous
			60					16	6-7	gel
								24	6-7	amorphous
			70					16	5	VFI (a few very thing needles), gel
								24	6-7	VFI (as above + some bundles)
			80					16	5	VFI (a few very thing needles), gel
								24	6-7	VFI (as above + some bundles)
1	1.3	25	50	1	60	20	125	16	6-7	VFI (spherical aggregates of needles), gel
								24	7	VFI (spherical aggregates of needles)
			60					16	6-7	VFI (spherical aggregates of needles), gel
								24	7	VFI (spherical aggregates of needles)
			70					16	5	VFI (spherical agg. of needles, single needles), gel
								24	5-6	VFI (spherical agg. of needles, single needles)
1	1.5	25	60	1.5	60	25	125	16	5-6	VFI (spherical aggregates of needles), gel
								24	7	VFI (sph. agg. needles, single needles~170x15x15 μm^3), gel
			70					16	5	VFI (as above, but more needles), gel
								24	6	VFI (sph. agg. needles, single needles~170x15x15 μm^3), gel
1	1.7	25	50	1.7	60	25	125	16	5-6	VFI (spherical aggregates of needles), gel
								24	6	VFI (spherical aggregates of needles), gel
			70					16	5	VFI (spherical aggregates of needles), gel
								24	6	VFI (spherical aggregates of needles), gel
1	1.5	25	50	2	60	25	125	16	7	H3, gel
								24	7	H3 ⁺ , gel
			70					16	5	H3, gel
								24	6	H3, gel

Table 9: continued

gel composition [mol]		dilution [mol]		t_w	t_{ts}	t_c	T_c	t_c	pH	Results
Al_2O_3	P_2O_5	H_2O	H_2O^*	min	min	min	°C	h		
1	2	25	50	2	60	25	125	16	3	unreacted gel
								24	3	unreacted gel
			60					16	3	unreacted gel
								24	3	unreacted gel
1.1	1.5	25	60	1.5	60	30	125	24	7	VFI(spherical aggregate of needles), gel
								72	7	VFI (sph. agg. needles, single needles ~170x15x15 μm^3), gel
			70					24	7	VFI(spherical aggregate of needles), gel
								24	7	VFI (sph. agg. needles, single needles ~170x15x15 μm^3), gel
1	1.5	25	60	1.5	60	45	125	24	6	VFI(spherical aggregate of needles), H3, gel
								72	7	VFI(spherical aggregate of needles), H3 ⁺ , gel
			70					24	6	VFI(spherical aggregate of needles), H3, gel
								72	7	VFI(spherical aggregate of needles), H3 ⁺ , gel
1	1.5	25	50	1.5	60	90	125	24	7	VFI (thin needles), H3 ⁺ , gel
								90	7	VFI (thin needles), H3 ⁺ , gel
			50					24	6	VFI(small bundles, thin needles), gel
								48	7	VFI(small bundles, thin needles), gel
			70					24	6	VFI(small bundles, thin needles), gel
								48	7	VFI(small bundles, thin needles), gel
			50			720		24	6-7	amorphous
			70					24	6-7	amorphous
1	1	35	50	1	60	30	125	16	6	VFI(small bundles), H3, gel
								24	7	VFI(small bundles), H3, gel
			70					16	6	VFI(small bundles), H3, gel
								24	7	VFI(small bundles, thin needles), H3, gel
1	1	40	50	1	60	30	125	16	6	VFI(small bundles), H3, gel
								24	6-7	VFI(small bundles), H3, gel
			70					16	6	VFI(small bundles), H3, gel
								24	6-7	VFI(small bundles), H3, gel

* represents the total amount of water

4.4. Summary of results and discussion

From the results presented in Tables 2 - 9, it is evident that there is an ample range of the parameters with which VPI-5 of good quality crystallizes. In almost all of the experiments, VPI-5 was obtained as a synthesis product. The main differences between the experiments lie in the efficiency of the reaction, judged from the amount of unreacted gel and the level of impurities, and the morphology of the VPI-5 crystals (needles, wheat sheaves, spherical aggregates). Unfortunately, it was not possible to obtain VPI-5 as a pure phase within the range of the variables investigated. In all cases, either $\text{AlPO}_4\text{-11}$ or H3 co-crystallized.

Effect of the single parameters

Milling time (t_m): for the preparation of the gel, a milling process was applied to enhance the homogeneity of the starting mixture. Increasing the milling time up to 90 minutes did not affect the nature of the synthesis product. However, increasing it to 720 minutes caused an amorphous solid to be produced.

Ultrasonic treatment time (t_{us}): an ultrasonic treatment of the gel proved to be essential, but slight variations in the treatment time did not have a noticeable effect on the composition or on the morphology of the final product. However, deviations of ± 15 minutes or more did provoke changes in the morphology and/or resulted in higher impurity levels ($\text{AlPO}_4\text{-H3}$ or $\text{AlPO}_4\text{-11}$, depending on the reaction temperature) and a higher amount of unreacted gel. The working frequency of the ultrasonic bath seems to be an important factor. Experiments carried out using a different ultrasonic bath (see Appendix) led to slightly different results.

Stirring time (t_s): prolonged stirring of the gel, up to 60 minutes, did not alter the synthesis results significantly, but much longer stirring times appeared to be conducive to the crystallization of impurities and to increasing the amount of unreacted gel.

Crystallization time (t_c): the optimal crystallization time was found to be ca. 24 hours. Actually, the first VPI-5 crystals form a few hours after the autoclave has reached the set temperature, depending on the gel composition and the reaction temperature itself. Shorter crystallization times produce a large amount of unreacted gel and small crystals with needle-like morphology aggregated into bundles. Longer times, up to 36 hours, did not produce larger crystals or improve the crystallinity of the synthesis product. Even longer crystallization times simply increase the level of impurity phases and may even induce a degradation of the VPI-5 crystals since they are not stable in the mother liquor.

Crystallization temperature (T_c): the crystallization temperature proved to be a critical synthesis parameter, which must be adjusted depending on the gel composition and the aim of the synthesis process, (i.e., the production of single crystals or of a polycrystalline material). In general, crystallization is faster at higher temperatures. At temperatures below 125°C, which is the optimal temperature for the synthesis of single crystals, a large amount of unreacted gel and $\text{AlPO}_4\text{-H3}$ is obtained. Higher temperatures seem to induce nucleation and thereby produce a large number of tiny VPI-5 crystallites and $\text{AlPO}_4\text{-11}$.

DPA/ Al_2O_3 molar ratio: DPA stabilizes the initial pH of the reactive hydrogel and therefore has to be changed whenever the $\text{P}_2\text{O}_5/\text{Al}_2\text{O}_3$ or the $\text{H}_2\text{O}/\text{Al}_2\text{O}_3$ molar ratios are changed. When changed singly, lower DPA/ Al_2O_3 molar ratios produce higher levels of $\text{AlPO}_4\text{-H3}$ and increasing the DPA/ Al_2O_3 molar ratio lowers efficiency and eventually produces an amorphous solid phase.

$\text{H}_2\text{O}/\text{Al}_2\text{O}_3$ molar ratio: the amount of water used for the gel preparation (step 1) does not have a dominant influence on the synthesis, within the range examined, but the total amount of water does. In general, increasing the $\text{H}_2\text{O}/\text{Al}_2\text{O}_3$ molar ratio (together with the crystallization time) improves the yield of VPI-5 crystals. However, too high a ratio (over

90), produced tiny VPI-5 needles and $\text{AlPO}_4\text{-H3}$. Lowering the ratio produces small bundles, unreacted gel and higher levels of impurities.

$\text{P}_2\text{O}_5/\text{Al}_2\text{O}_3$ molar ratio: it was changed in the hope that the impurity levels ($\text{AlPO}_4\text{-H3}$ and/or $\text{AlPO}_4\text{-11}$) could be reduced and thicker single crystals obtained. However, the optimal molar ratio was found to be 1. An excess of Al_2O_3 induced the crystallization of $\text{AlPO}_4\text{-H3}$ and yielded a large amount of unreacted gel, while an excess of P_2O_5 produced large highly intergrown VPI-5 spherical aggregates.

The composition of the gel, together with the crystallization temperature, are the prime parameters in the synthesis process and have to be varied in a concerted manner.

Optimal synthesis conditions

The optimal conditions for the synthesis of a polycrystalline material with high crystallinity and good thermal properties, and for the synthesis of single crystals of $250 \times 25 \times 25 \mu\text{m}^3$ are reported in Table 10. In the case of the polycrystalline material, a small amount of $\text{AlPO}_4\text{-11}$ is also obtained. The single crystals are produced together with smaller VPI-5 crystals with needlelike morphology aggregated into bundles, and a significant amount of $\text{AlPO}_4\text{-H3}$ and/or $\text{AlPO}_4\text{-11}$. Pertinent scanning electron micrographs of the polycrystalline material and the single crystals prepared with the optimal conditions reported in Table 10, are shown in Fig. 10a and 10b, respectively. Fig. 11 shows the X-ray diffraction pattern of the powder sample.

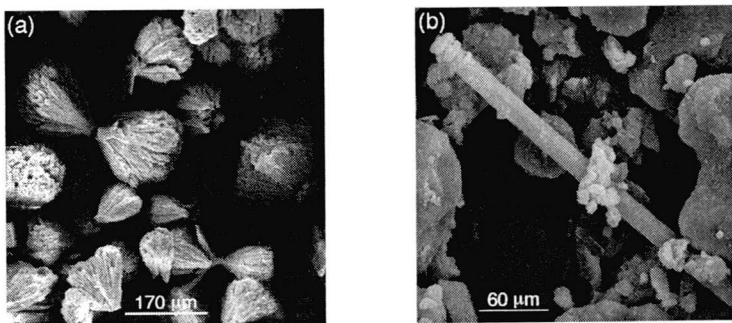


Fig. 10: Scanning electron micrographs showing the typical morphology of the polycrystals (a) and single crystals (b) obtained with the optimal conditions reported in Table 10

Table 10: Optimal conditions for the synthesis of (1) highly crystalline powder and (2) large single crystals of VPI-5

Parameter	polycrystalline material	single crystals
Gel composition	$\text{Al}_2\text{O}_3 : \text{P}_2\text{O}_5 : 60 \text{ H}_2\text{O} : \text{DPA}^{\text{a}}$	$\text{Al}_2\text{O}_3 : \text{P}_2\text{O}_5 : 80 \text{ H}_2\text{O} : \text{DPA}^{\text{b}}$
Milling time	60 min	60 min
US treatment time	15 min	30 min
Stirring time	30 min	30 min
Crystallization temperature	135°C	125°C
Reaction time:	24 h	24 h

^a 25 of the 60 moles of water were used for the gel preparation (step 1), and the rest was added with the amine during the dilution of the gel (step 3)

^b 30 of the 80 moles of water were used for the gel preparation (step 1), and the rest was added with the amine during the dilution of the gel (step 3)

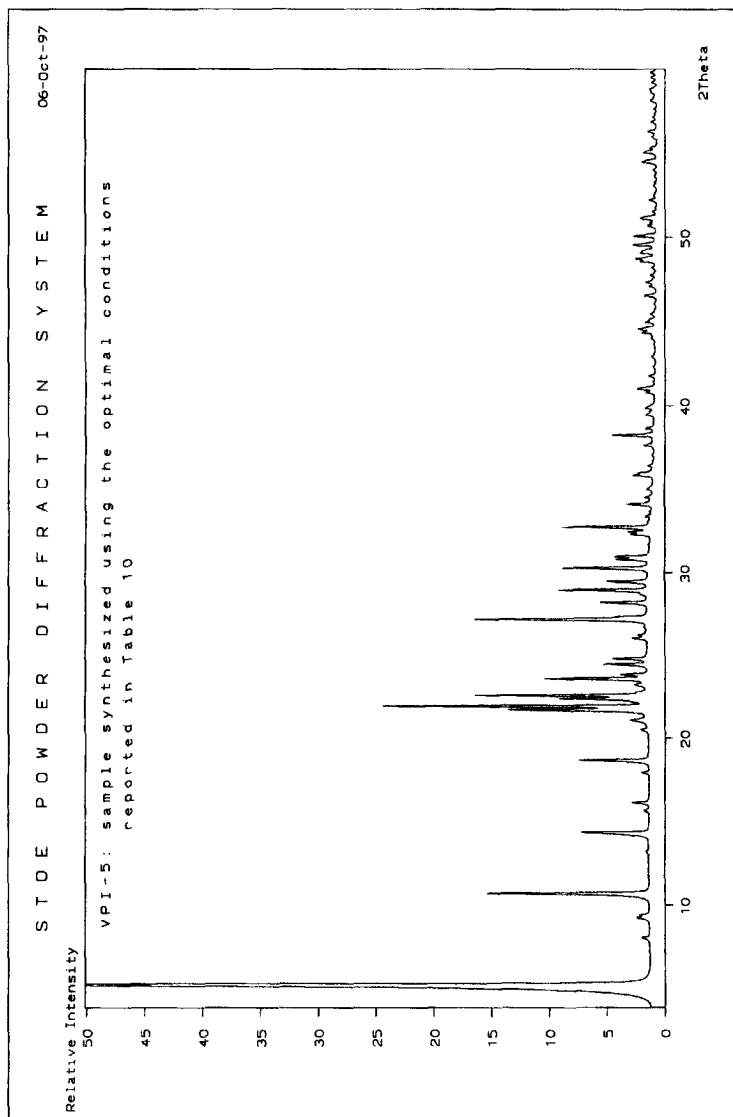


Fig. 11: X-ray powder diffraction pattern of VPI-5 synthesized using the optimal conditions given in Table 10

4.5. Conclusions

The procedure first reported by Jahn et al. [8] has been optimized to produce a VPI-5 material with very high crystallinity and good thermal stability (see chapter 6) reproducibly. Further, modification of the synthesis conditions allowed relatively large single crystals ($250 \times 25 \times 25 \mu\text{m}^3$) of this aluminophosphate molecular sieve to be prepared.

A comparison of the optimal conditions given in Table 10 shows that the main differences between the two procedures are the time of the ultrasonic treatment, the amount of water and the crystallization temperature.

For the production of single crystals, the gel was subjected to ultrasonic treatment for twice as long as for the synthesis of the polycrystalline material. Although small changes of ± 5 minutes in the treatment time do not have a significant effect on the synthesis product, the frequency of the ultrasonic equipment does. Experiments conducted under similar conditions but using different equipment yielded very different results. This seems to be an important factor that needs to be investigated in more detail, e.g. by means of NMR spectroscopy.

Single crystals are obtained from a more diluted gel and at a lower crystallization temperature. A more diluted gel and a lower temperature seem to allow thicker and more perfect single crystals to be formed. Water definitely plays a crucial role in the synthesis process, but, in view of the results presented in chapter 5, it may not have a templating effect.

The organic additives (di-*n*-propylamine in this work) do not assume this role either. They appear to serve as pH moderators. However, they affect not only the physico-chemical properties of the final product, but also their morphologies. This was demonstrated very recently in the synthesis of VPI-5 in the presence of selected transition metal-phthalocyanines, such as CuPc, CoPc and FePc [123]. While Cu-phthalocyanine leads to the formation of bundles of needles, Fe-phthalocyanine seems to favor the

formation of isolated needles. Such changes in the morphology of the products provoked by the use of different organic additives are not well understood yet, but are of considerable interest for the synthesis of single crystals of VPI-5.

As stated previously, this method relies on the use of polyphosphoric acid with an average P chain length (n_{av}) of 8 as the source of P, and di-n-propylamine as the structure directing agent. Experiments that have been carried out using ortho-phosphoric acid or polyphosphoric acid with a shorter P chain length ($n_{av}=4$) [120], lead to poorer results. In both cases, the synthesis product consisted of smaller VPI-5 aggregates with a severe intergrowth of the single crystals. A possible explanation for this fact could be the following:

The general morphology of the aggregates consists of a central core on which a large number of crystals grow. The small size of these aggregates indicates that once nucleation has begun, there is a rapid formation of tiny particles, all of which are competing for the available chemical nutrients. This behavior is typical for systems with a relatively high level of supersaturation in the liquid phase. Because of this high supersaturation, the outer surfaces of the initial nuclei are probably not very uniform, so there are many points on the nucleus surface on which additional crystals can grow. Furthermore, since the supersaturation is high, crystals will grow rapidly and with defects. These defects may act as secondary nuclei on which other crystals may grow. The net result is the observed morphology with highly intergrown, thin crystals. Crystal size could probably be influenced by experimental factors which reduce the supersaturation.

For the production of the VPI-5 precursor species in the liquid phase, the polyphosphate chains must undergo a depolymerization reaction. The longer the chains, the slower the reaction, so, the concentration of the precursor species in the liquid phase can be reduced by using a polyphosphoric acid with a longer chain. In this way, supersaturation

levels, and therefore the rate of nucleation and crystal growth, are lowered, so a smaller number of viable nuclei with a more uniform outer surface are produced. This is conducive to the growth of large single crystals. Using polyphosphoric acids with average chain lengths larger than 8, might allow even longer and thicker single crystals to be obtained.

Some AlPO_4 -based materials have been prepared in the presence of fluoride [125]. Although the pH conditions were close to those that would be used in its absence, it has been observed that crystals synthesized using HF as a mineralizer are usually larger and better formed. It may be assumed that the presence of fluoride ions favors the production of fewer nuclei. Thus, it would be interesting to study the combined effect of using polyphosphoric acids with larger average chain lengths and fluoride for the synthesis of large single crystals of VPI-5.

5. Structure investigation of VPI-5 at 90°C under sealed conditions

NMR experiments suggest that the VPI-5 structure assumes the higher symmetry space group $P6_3cm$ above 80°C (see chapter 2). To verify this change from $P6_3$ and to examine the structural basis for it, synchrotron powder diffraction data were collected at 90°C and a Rietveld refinement of the structure undertaken.

5.1. Sample preparation and data collection

The polycrystalline VPI-5 sample was synthesized according to the procedure given in Table 10, chapter 4.

The variable-temperature (VT) ^{31}P -, ^{27}Al - and ^1H - MAS NMR spectra were recorded on a Bruker MSL-400 spectrometer in the temperature range 30 - 108°C, with the conditions described in chapter 3.

For the synchrotron data collection, the hydrated sample was sealed in a 0.5 mm quartz capillary and heated up to 90°C in a continuous stream of warm nitrogen blown along the capillary. Since the capillary was sealed, water could not escape from it. This approximates the conditions used in the NMR experiments, which were carried out in sealed rotors. Data were then collected on the Swiss Norwegian Beam Line (SNBL) at the European Synchrotron Radiation Facility (ESRF) in Grenoble using Debye-Scherrer geometry and a simple slit system. The wavelength was calibrated with a standard silicon powder sample to be 1.1520Å. Further details of the experimental conditions for data collection are summarized in Table 11.

Table 11: Experimental conditions for the synchrotron data collection on hydrated VPI-5 at 90°C

Wavelength	1.1520Å	
Range	3.0 - 65.0° 2 θ	
Step size	0.01° 2 θ	
Measuring time	3.0 - 24.0° 2 θ	3s/step
	24.0 - 45.0° 2 θ	5s/step
	45.0 - 65.0° 2 θ	7s/step

5.2. Results

5.2.1. Solid state NMR

These experiments were performed to see if the sample used for this study showed the same NMR behavior as has been reported in the literature.

At RT the ^{31}P MAS spectrum consists of three resonances at -23.3, -27.2 and -33.1ppm with a 1:1:1 ratio for the peak areas (see Fig. 12). As the temperature is increased, the two leftmost peaks coalesce to yield spectra with only two peaks and a 2:1 intensity ratio. This process, which is indicative of a change in symmetry, appears to be complete at 81°C. The spectrum obtained after cooling to 30°C is virtually identical to the initial one, suggesting that the changes are reversible.

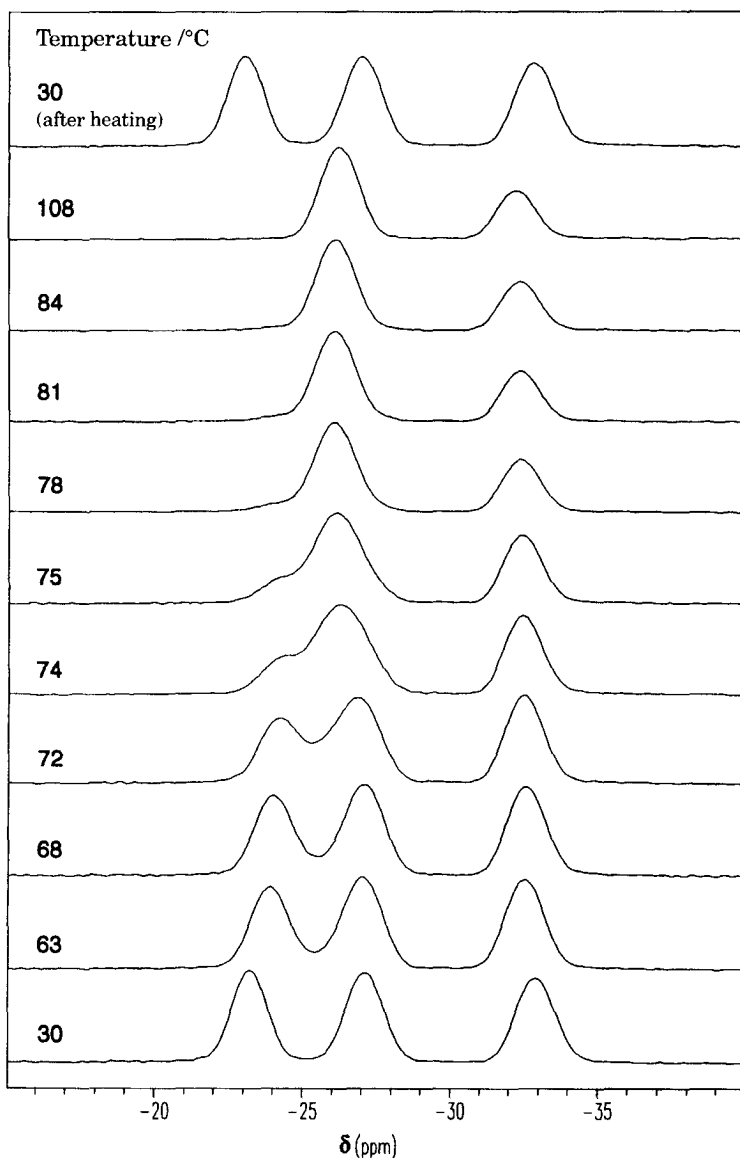


Fig. 12: VT- ^{31}P MAS NMR spectrum of as synthesized VPI-5

The significant changes observed in the VT ^{31}P MAS NMR spectra of VPI-5 are not immediately evident in the analogous VT ^{27}Al MAS NMR

experiments (see Fig. 13a). At all temperatures, two peaks with a 2:1 intensity ratio are observed. The sharper peak at ca. 40 ppm is indicative of tetrahedral Al, and the broad resonance at ca. -20ppm of octahedral Al. However, careful inspection of the signal from tetrahedral Al reveals characteristic changes of the line shape with increasing temperature.

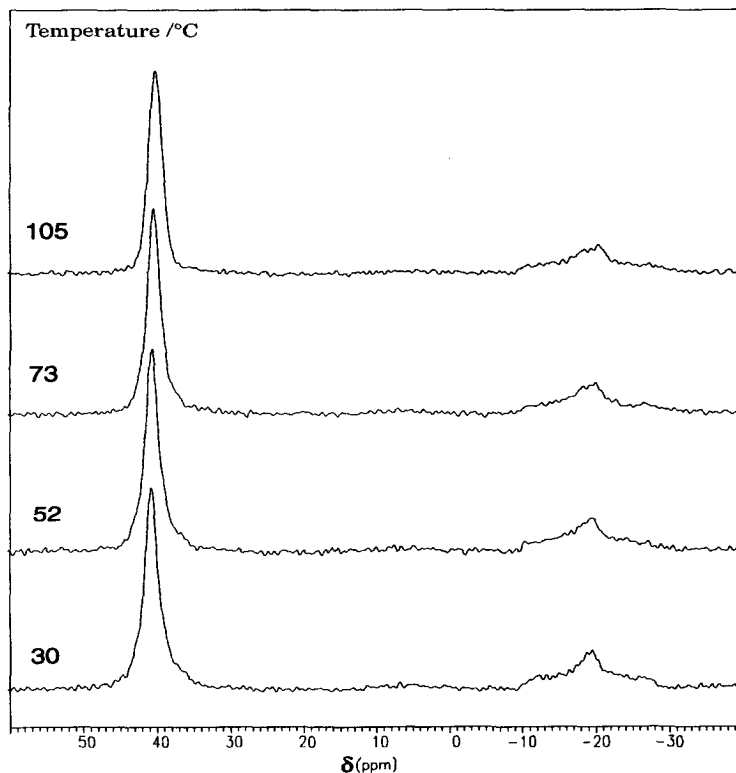


Fig.13a: VT- ^{27}Al MAS NMR spectrum of as synthesized VPI-5

The simulation of the ^{27}Al MAS NMR spectra shown in Fig. 13b, indicates that at 30 $^{\circ}\text{C}$ this signal actually consists of two quadrupolar patterns with an intensity ratio of 1:1, which coalesce to a single pattern at 105 $^{\circ}\text{C}$. This observation agrees with the results of the ^{27}Al MQ MAS NMR experiments of Rocha et al. [59], and confirms the crystallographic equivalence of the tetrahedral Al atoms in the high-temperature form of hydrated VPI-5. In contrast to the tetrahedral Al peak, the resonance of octahedral Al is only

slightly affected by temperature (see Table 12). In the whole range of temperatures studied, this resonance line could be simulated by a single quadrupolar pattern (not shown) with the chemical shift $\delta_{\text{iso}} = -9.5 \pm 0.3$ ppm, the quadrupole coupling constant $\text{QCC} = 3.7 \pm 0.2$ MHz, and the asymmetry parameter of the electric field gradient $\eta = 0.8 \pm 0.1$.

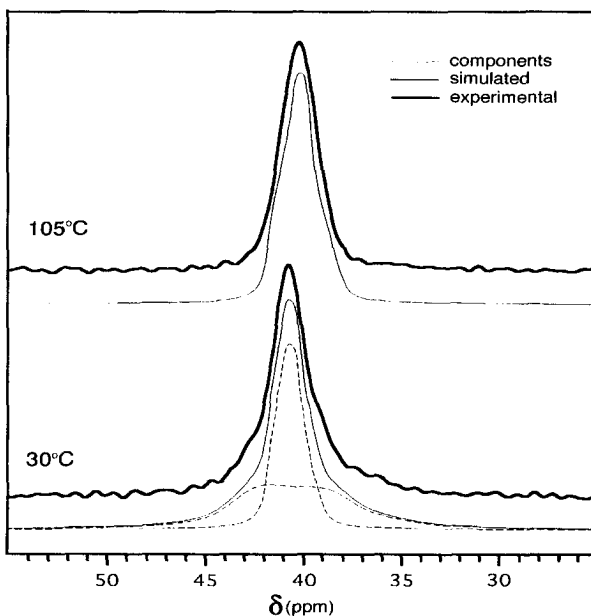


Fig. 13b: Simulation of the tetrahedral Al peaks at 30°C and 105°C. Simulation parameters are reported in Table 12

It should be noted that the specific NMR parameters obtained from the simulation of the ^{27}Al MAS NMR spectra and presented in Table 12 are in accord with the data of Rocha et al., and furthermore, yield an estimate of η . The latter parameter could not be derived from the MQ MAS NMR, or from previous DOR NMR [46] experiments, since QCC and η can not be determined separately by these techniques.

Table 12: ^{31}P and ^{27}Al isotropic chemical shifts (δ in ppm), and ^{27}Al quadrupole coupling constants (QCC in MHz) and asymmetry parameters (η) of as synthesized VPI-5^{a)}

	30°C			100°C		
	δ	QCC	η	δ	QCC	η
P1	-32.9	-	-	-32.3	-	-
P2	-27.1	-	-	-26.1	-	-
P3	-23.2	-	-	-	-	-
Al1 ^{oct}	-9.7	3.6	0.9	-9.2	3.8	0.9
Al2 ^{tet}	41.9	1.4	0.6	41.8	1.6	0.7
Al3 ^{tet}	44.5	2.7	0.2	-	-	-

^{a)} The assignment of the peaks to the specific crystallographic sites in the VFI framework, corresponds to the assignment proposed by G. Engelhardt [49]

Fig. 14 shows the ^1H MAS NMR spectra of VPI-5 taken at different temperatures. Above 30°C, a narrowing of the resonance line is observed, and this could be explained by an increased mobility of the water molecules at higher temperatures.

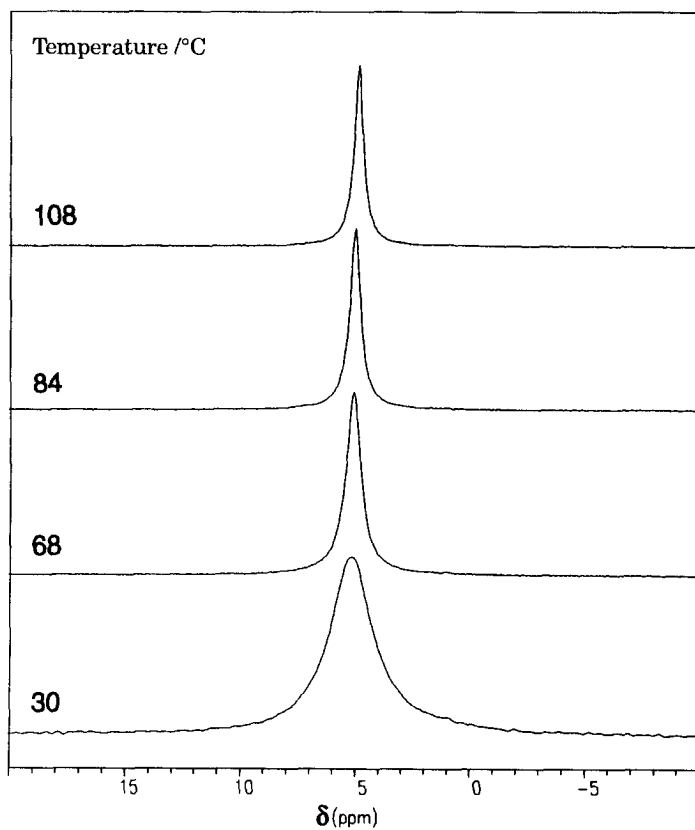


Fig. 14: VT- ^1H MAS NMR spectra of as synthesized VPI-5

In summary, it can be concluded that the results of our solid-state VT NMR experiments are similar to those reported previously, and that therefore the sample used does correspond to the samples described in the literature.

5.2.2. Rietveld refinement

Rietveld Refinement using the XRS-82 package of programs [126] was carried out in the space group $P6_3cm$, taking the transformed positional parameters reported for the framework atoms in the as synthesized form [38] as a starting model. The data were scaled, the background estimated and subtracted, and the 2 theta zero correction (determined during the wavelength calibration) applied. The contribution from the $AlPO_4$ -11 impurity was calculated using the positional parameters reported for $MnAPO_4$ -11 [127] and subtracted.

An experimental peak shape function was calculated using the single peak at $8.05^\circ 2\theta$, and the whole pattern was analyzed for changes in peak width and asymmetry as a function of 2θ . A second peak shape function was used to describe the first, very intense peak. In a 'Le Bail-type' refinement, the unit cell and peak width parameters were adjusted and a satisfactory agreement between the positions of the peaks in the observed and calculated patterns was obtained.

The positional parameters of the framework atoms were then refined using the data in the range $18 - 65^\circ 2\theta$, which is less sensitive to the absence of water in the initial structural model. Strong geometric restraints on the bond distances and angles were used to keep the framework geometry chemically sensible [103]. A difference Fourier map using all the diffraction data was then calculated using the Xtal System of programs [128]. Two non-framework atom positions within bonding distance of Al1 were immediately apparent and these were included in the model as water molecules with an occupancy factor of 1.0.

Subsequent difference Fourier maps revealed a diffuse cloud of electron density within the VPI-5 channels. This was modeled by selecting positions of high density and including them in the structural model as water molecules with relatively high displacement factors ($U = 0.13 \text{ \AA}^2$)

and reduced occupancy parameters. Since the water molecules are quite mobile at 90°C, the positions of the non-framework atoms should not be overinterpreted. They simply provide an approximate model of the electron density of the more-or-less liquid water in the channel.

After the electron density within the channel had been reasonably described with this model, the refinement in the whole 2 θ range progressed satisfactorily, even after the weight of the geometric restraints with respect to the X-ray data was reduced to 1. To keep the number of variables as low as possible, only one displacement factor for each type of atom was refined. The displacement factors of the 'free' water molecules were fixed at $U = 0.13\text{\AA}^2$. For the calculations, neutral atomic scattering factors were used for all atoms. Water positions were refined as oxygens. To estimate the standard deviations of the structural parameters, only every sixth step of the profile was used in the final cycle of the refinement (Durbin-Watson d -statistic of 1.90 [100]).

Further details of the refinement are given in Table 13, final positional, displacement and occupancy parameters in Table 14 and interatomic distances and angles in Table 15. The observed, calculated and difference profiles are presented in Fig. 15. Fig. 16 shows a portion of the structure with the labeling scheme.

Table 13: Crystallographic data for hydrated VPI-5 at 90°C**Unit Cell**

Space group:	$P6_3cm$
a	18.9468 (1) Å
c	8.15239 (5) Å

Refinement

Standard peak for peak shape function		
(1)	(200)	8.050° 2 θ
(2)	(100)	4.022° 2 θ
Peak range (number of FWHM)		13
No. of observations (N)		5273
No. of contributing reflections		406
No. of geometric 'observations'		41
No. of structural parameters (P1)		61
No. of profile parameters (P2)		8
$R_{\text{exp}} = [(N-P1-P2)/\sum w y^2(\text{obs})]^{1/2}$		0.065
$R_{\text{wp}} = \{\sum w [y(\text{obs}) - y(\text{cal})]^2 / \sum w y^2(\text{obs})\}^{1/2}$		0.098
$R_F = \sum F(\text{obs}) - F(\text{cal}) / \sum F(\text{obs})$		0.060
Durbin-Watson d -statistic (step size 0.06° 2 θ)		1.90

Table 14: Final positional, displacement and occupancy parameters for hydrated VPI-5 at 90°C ^a

Atom	x	y	z	PP	U(Å ²)
Al(1)	0.3837(1)	0	0.2394(2)	1.0	0.010(1) ^b
Al(2)	0.6507(1)	0.1709(1)	0.2063(2)	1.0	0.010(1) ^b
P(1)	0.5494(1)	0	0.3614(2)	1.0	0.018(2) ^c
P(2)	0.5025(1)	0.1858(1)	0.3192(2)	1.0	0.018(2) ^c
O(1)	0.4687(1)	0	0.3423(3)	1.0	0.040(2) ^d
O(2)	0.4280(2)	0	0.0422(3)	1.0	0.040(2) ^d
O(3)	0.4341(1)	0.1108(1)	0.2357(4)	1.0	0.040(2) ^d
O(4)	0.5835(1)	0.2056(1)	0.2419(3)	1.0	0.040(2) ^d
O(5)	0.7419(1)	0.2316(1)	0.3034(4)	1.0	0.040(2) ^d
O(6)	0.6180(1)	0.0744(1)	0.2785(3)	1.0	0.040(2) ^d
O(7)	0.5015(1)	0.1678(1)	0.5 ^f	1.0	0.040(2) ^d
H ₂ O(I)	0.3376(3)	0	0.4662(6)	1.0	0.030(2) ^e
H ₂ O(II)	0.2909(2)	0	0.1553(5)	1.0	0.030(2) ^e
H ₂ O(III)	0.1702(5)	0.3268(4)	0.550(1)	0.57(1)	0.13 ^f
H ₂ O(IV)	0.0830(7)	0.2934(6)	0.632(1)	0.39(1)	0.13 ^f
H ₂ O(V)	-.129(1)	0	0.101(2)	0.32(1)	0.13 ^f
H ₂ O(VI)	0	0.0767(6)	0.174(1)	0.49(1)	0.13 ^f
H ₂ O(VII)	0.219(1)	0.219(1)	0.060(3)	0.37(2)	0.13 ^f
H ₂ O(VIII)	0.0874(7)	0.1789(6)	0.240(1)	0.45(1)	0.13 ^f
H ₂ O(IX)	0.1144(5)	0.379(6)	0.901(1)	0.51(1)	0.13 ^f

^a Numbers in parentheses are the e.s.d.'s in the units of the least significant digit given

^{b, c, d, e} Displacement parameters with the same superscript were constrained to be equal

^f Kept fixed during least-squares refinement

Table 15: Interatomic distances (Å) and angles (deg.) in the structure of VPI-5 at 90°C

Al(1) - O1	1.820(4)	P(1) - O2	1.535(4)
Al(1) - O2	1.813(4)	P(1) - O3	1.526(5)
Al(1) - O3	1.816(5)	P(1) - O6	1.516(4)
Al(1) - H ₂ O(I)	2.04(4)	P(2) - O1	1.523(5)
Al(1) - H ₂ O(II)	1.89(4)	P(2) - O4	1.511(3)
Al(2) - O4	1.716(4)	P(2) - O5	1.521(3)
Al(2) - O5	1.725(4)	P(2) - O7	1.511(4)
Al(2) - O6	1.715(4)		
Al(2) - O7	1.713(5)		
O1 - Al1 - O1*A	174(3)	O6 - P1 - O2	108(2)
O2 - Al1 - O1	90(2)	O6 - P1 - O6	107(3)
O3 - Al1 - O1	93(2)	O3 - P1 - O2	111(3)
O8 - Al1 - O1	90(3)	O3 - P1 - O6	110(4)
O9 - Al1 - O1	88(3)	O5 - P2 - O4	109(3)
O3 - Al1 - O2	89(3)	O7 - P2 - O4	107(4)
O8 - Al1 - O2	178(2)	O7 - P2 - O5	110(4)
O9 - Al1 - O2	96(4)	O1 - P2 - O4	111(3)
O8 - Al1 - O3	88(3)	O1 - P2 - O5	109(2)
O9 - Al1 - O3	174(4)	O1 - P2 - O7	108(3)
O9 - Al1 - O8	86(4)		
O5 - Al2 - O4	110(4)		
O6 - Al2 - O4	105(3)		
O7 - Al2 - O4	110(2)		
O6 - Al2 - O5	114(7)		
O7 - Al2 - O5	110(3)		
O7 - Al2 - O6	106(4)		

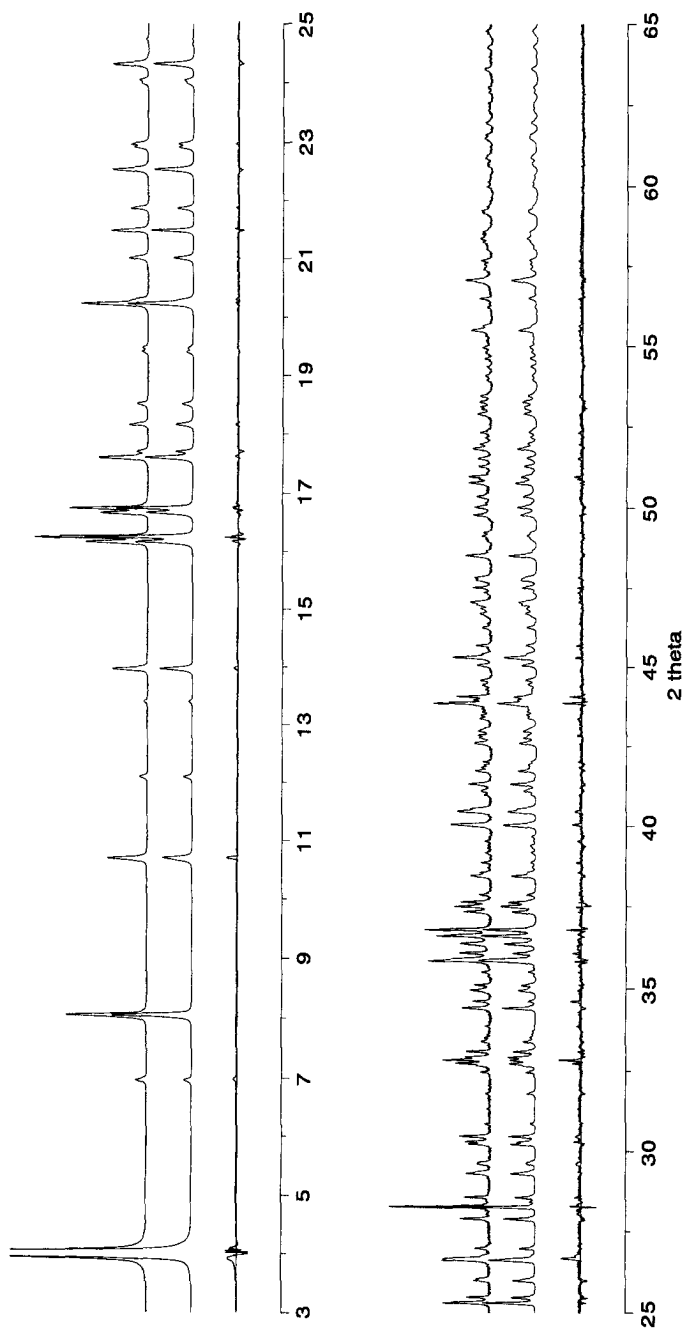


Fig. 15: Observed (top), calculated (middle) and difference (bottom) profiles for the Rietveld Refinement of as synthesized VPI-5 at 90°C in a closed system. To show more detail, the first peak has been cut to approximately 1/7 of its maximum. For the same reason, the second part of the profile has been scaled up by a factor of 7

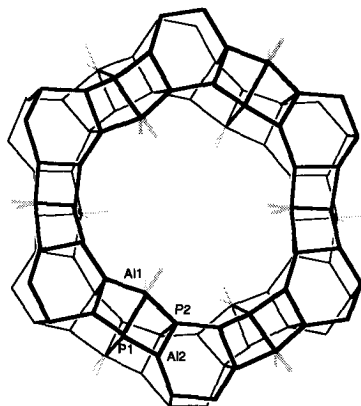


Fig. 16: The framework structure of VPI-5 at 90°C, showing the location of the octahedrally coordinated Al1. The oxygen bridges have been omitted for clarity

5.3. Discussion

The refined structure confirms that the symmetry of VPI-5 changes from $P6_3$ in the as synthesized form to $P6_3cm$ upon heating to 90°C in a closed container. This is the highest possible and topochemical symmetry. In this symmetry, there are only two crystallographically distinct P sites with the multiplicities 12 and 6, so the structure is fully consistent with the ^{31}P MAS NMR results. The Al atom located between the fused 4-rings is octahedrally coordinated to four framework oxygens and two water molecules. In contrast to the structure at room temperature, that at elevated temperature shows no evidence of deviation from the vertical mirror symmetry. Neither in the vicinity of the fused 4-rings, nor in the rest of the framework is any violation apparent.

The total amount of water located within the channels (42 molecules) is comparable to that found in the refinement of the hydrated form. However, the ordering observed in the latter does not exist at 90°C. The constraints imposed by the well defined water structure in as-synthesized VPI-5, may

explain the slight elongation of the a (0.1%) and contraction of the c (0.6%) lattice parameters upon heating.

It is interesting to note that after the 'symmetrization' of the structure at higher temperatures, the NMR parameters (i.e., the local structural environment) of both the new P2 and Al2 sites, are closer to the original P2 and Al2 than to those of the original P3 and Al3 sites in the low-temperature form (Table 12). Moreover, the significantly lower quadrupolar interaction of Al2 in comparison to Al3 indicates that the AlO_4 tetrahedra in the VPI-5 framework are less distorted at higher temperatures. The positions of the Al1 and P1 signals experience almost no changes. Apparently, the inclination of the octahedron around Al1 towards Al3 in the as-synthesized form, causes the slight distortion of the AlO_4 tetrahedron at Al3 observed by ^{27}Al MAS NMR. At 90°C this octahedron is no longer inclined, and the structure seems to be more relaxed.

A similar reversible symmetry change has been observed in ^{31}P MAS NMR experiments on VPI-5 from which all water molecules except those coordinated to Al had been removed [60]. The ^{31}P NMR spectra for that sample also showed three peaks at room temperature and two at ca. 80°C. Apparently, this material also adopts the lower symmetry at room temperature, even though there is no water structure in the channels. This fact indicates that the breakdown of the hydrogen-bonded water structure inside the pores of the fully hydrated material is not the primary cause of the symmetry change.

It has been suggested that water plays a key role in the crystallization of VPI-5 [40]. The results presented here show that the well-ordered water structure observed in as-synthesized VPI-5 does not exist at 90°C, which is well below the normal crystallization temperature. Thus, it is unlikely that the water structure itself is structure-directing during the synthesis of this aluminophosphate. However, it is possible that water has a stabilizing effect

on the triple crankshaft building unit of which VPI-5 (and also $\text{AlPO}_4\text{-H}_2$ [40]) is constructed, because, at least at 90°C and under closed conditions, the Al located between the fused 4-rings remains octahedrally coordinated.

6. Structure investigation of dehydrated VPI-5

It has been shown by ^{27}Al -MAS and DOR NMR measurements (see chapter 2), that all Al atoms in VPI-5 become tetrahedral upon dehydration [44,56-58]. The ^{31}P -MAS NMR spectrum also changes significantly [56,57], but its interpretation, as well as details of the structure of the dehydrated form of this aluminophosphate are still a subject of discussion.

6.1. Samples investigated

Table 16 summarizes the samples used for this study. Samples A to D were kindly provided by Piet Grobet, Centrum voor Oppervlaktechemie en Katalyse, K.U. Leuven. Sample E was prepared in our laboratory (see chapter 4).

Table 16: VPI-5 samples used for the dehydration investigations*

Sample	Comments
A	dipropylamine as organic additive, 3 year old sample
B	dipropylamine as organic additive, fresh sample
C	tetrabutylammonium hydroxide as organic additive
D	triisopropanolamine/ tetramethylammonium hydroxide (40:1) as organic additive (following M. Davis' procedure)
E	dipropylamine as organic additive, polyphosphoric acid as the source for P

*Samples A-D provided by Piet Grobet

The structural study was initiated with sample A, which was synthesized using di-n-propylamine as the organic species [129]. The other samples, B to D, showed a different behavior upon dehydration. This fact was the motivation for the synthesis of sample E, which was prepared according to

the procedure described in chapter 4 for the synthesis of a polycrystalline material.

All the as-synthesized samples have similar X-ray patterns. In Fig. 17, the powder diffraction patterns of samples A and E are shown. Sample E has a better crystallinity and therefore somewhat sharper peaks (better resolution). However, because of the morphology of the crystals (long needles aggregated into bundles), the powder diffraction pattern of this sample is affected by preferred orientation. These two facts could explain the small differences in the relative peak heights of these two materials. In the pattern of sample E, the peaks from AlPO_4 -11 have been marked with an asterisk.

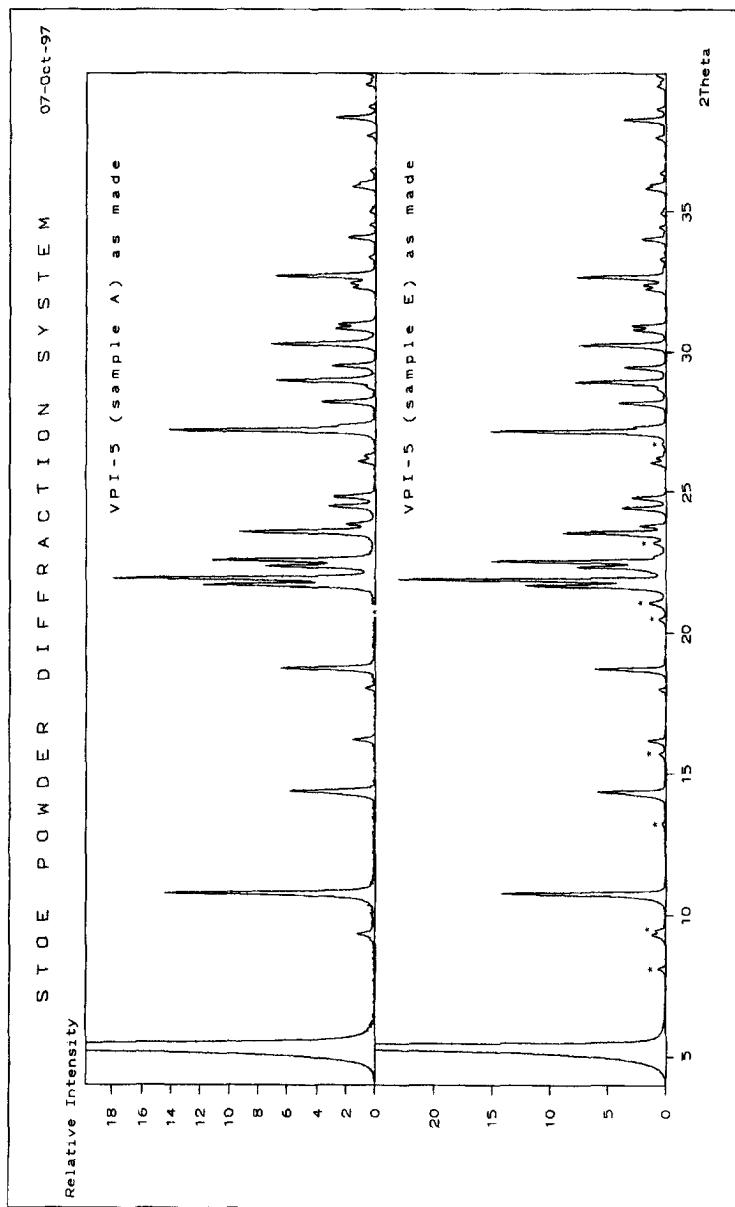


Fig. 17: Portion of the X-ray powder diffraction patterns of the as-synthesized samples A and E taken using $\text{CuK}\alpha_1$ radiation. Asterisks in the pattern of sample E denote AlPO_4 -11 peaks

6.2. Dehydration experiments

6.2.1. Experimental conditions

The thermal stability of the above VPI-5 samples was investigated in parallel experiments by means of thermogravimetric analysis (TGA) and X-ray powder diffraction (XRD).

For the dynamic and isothermic TGA investigations, the samples were heated in humid or dry air atmosphere using different temperature and time regimes. The dehydrated products were then quickly transferred to glass capillaries and examined by XRD on a STADI Stoe powder diffractometer. Further details on the dehydration experiments are presented in Table 17.

Table 17: Parameters varied during the dehydration experiments

Kind of experiment	isothermic (ISO) dynamic (DYN)
Atmosphere	humid air, flow of dry air, vacuum
Temperature ISO experiments (°C)	25, 35, 50, 60, 70, 100, 120
Heating rate DYN experiments (K/min)	1, 1.5, 3, 10, 20, 30
End-temperature DYN experiments (°C)	100, 120, 180, 250, 400, 500, 650

In addition, *in situ* dehydration experiments were carried out on a vacuum furnace mounted on the Scintag $\theta - \theta$ powder diffractometer, also using different time and temperature regimes.

6.2.2. Results and discussion

The results of the stability investigations on the as-synthesized samples A and E are summarized in Table 18. In the 'Results' column, a + or - superscript indicates a large quantity or only traces (close to the limits of detection by XRD) of the given phase, respectively.

Table 18a: Stability investigations carried out on sample A

Atmosphere	ISO/ DYN	Conditions	Results
humid air	ISO	60°C, 24 h	VFI, AET ⁺
	ISO	70°C, 24 h	VFI, AET ⁺
	DYN, ISO	RT - 120°C, 1.5 K/min	
		120°C, 3 h	VFI ⁺ , AET ⁺
	DYN, ISO	RT - 120°C, 1.5 K/min	
		120°C, 14 h	VFI ⁺ , AET ⁺
	DYN, ISO	RT - 50°C, 1.5 K/min	
		50°C, 12 h	VFI, AET
	ISO	RT, 11 days	VFI, AET
	ISO	35°C, 17 h	VFI, AET
dry air	ISO	35°C, 64 h	VFI, AET ⁺
	ISO	100°C, 30 min	VFI, AET ⁺
	ISO	100°C, 18 h	VFI ⁺ , AET ⁺
	DYN	35 - 100°C, 0.5 K/min	VFI ⁺ , AET ⁺
	DYN	35 - 100°C, 1.5 K/min	VFI, AET ⁺
	DYN	35 - 100°C, 10 K/min	VFI, AET ⁺
	DYN	35 - 250°C, 20 K/min	VFI, AET ⁺
	DYN	35 - 400°C, 25 K/min	VFI, AET
	DYN	35 - 500°C, 10 K/min	VFI, AET ⁺
	DYN	35 - 500°C, 30 K/min	VFI, AET
	DYN, ISO	35 - 120°C, 1.5 K/min	
		120°C, 3 h	VFI ⁺ , AET ⁺
	DYN, ISO	35 - 120°C, 10 K/min	
		120°C, 30 min	VFI, AET ⁺
	DYN, ISO	35 - 150°C, 20 K/min	
		150°C, 1 h	VFI, AET ⁺
	ISO, DYN	35°C, 17 h	
		35 - 100°C, 1 K/min	VFI ⁺ , AET ⁺
	ISO, DYN	RT, 72 h	
		RT - 150°C, 1.5 K/min	VFI, AET ⁺
vacuum	ISO	RT, 72 h	
		+ dry air	
		equilibrated in humid air	VFI
	DYN	RT - 150°C, 10 K/min	VFI, AET
		cooled RT, humid air ¹⁾	VFI, AET
	DYN, ISO	RT - 400°C, 25 K/min	VFI, AET
		cooled RT, humid air ¹⁾	VFI, AET ⁺
	DYN, ISO	RT - 500°C, 30 K/min	VFI, AET
		cooled RT, humid air ¹⁾	VFI, AET ⁺
	ISO, DYN	RT, 6 h	
		RT - 120°C, 1.5 K/min	
		120°C, 12 h	
		120°C - 500°C	VFI, AET
		cooled RT, humid air ¹⁾	VFI, AET
	ISO, DYN	RT, 48 h	
		RT - 120°C, 0.5 K/min	
		120°C, 12 h	
		120°C - 450°C, 0.5 K/min	
		450°C, 6 h	VFI
		cooled RT, humid air ¹⁾	VFI

¹⁾ cooled to RT, equilibrated in humid air

Table 18b: Stability investigations carried out on sample E

Atmosphere	ISO/ DYN	Conditions	Results
humid air	ISO	60°C, 24 h	VFI, AET
	ISO	70°C, 24 h	VFI, AET
	DYN, ISO	RT - 500°C, 1.5 K/min	VFI, AET*
		500°C, 24h	
	DYN, ISO	RT - 500°C, 10 K/min	VFI, AET
		500°C, 12 h	
vacuum	DYN, ISO	RT - 500°C, 30 K/min	VFI, AET
		500°C, 12 h	
	ISO, DYN	RT, 6 h	VFI
		RT - 120°C, 0.5 K/min	
		120°C, 12 h	
		120°C - 450°C	
		450°C, 6 h	
	ISO, DYN	cooled RT, humid air ¹⁾	VFI
		RT, 24 h	
		RT - 120°C, 0.5 K/min	
		120°C, 12 h	
		120°C - 700°C, 0.5 K/min	
	ISO, DYN	700°C, 12 h	VFI
		cooled RT, humid air ¹⁾	
		RT, 24 h	
		RT - 120°C, 0.5 K/min	
		120°C, 12 h	
	ISO, DYN	120°C - 650°C, 20 K/min	VFI
		650°C, 12 h	
		cooled RT, humid air ¹⁾	

¹⁾ cooled to RT, equilibrated in humid air

The TGA and DTG curves of the samples A to E taken in an open air atmosphere with a heating rate of 1.5 K/min, are shown in Fig. 18a to 18e, respectively.

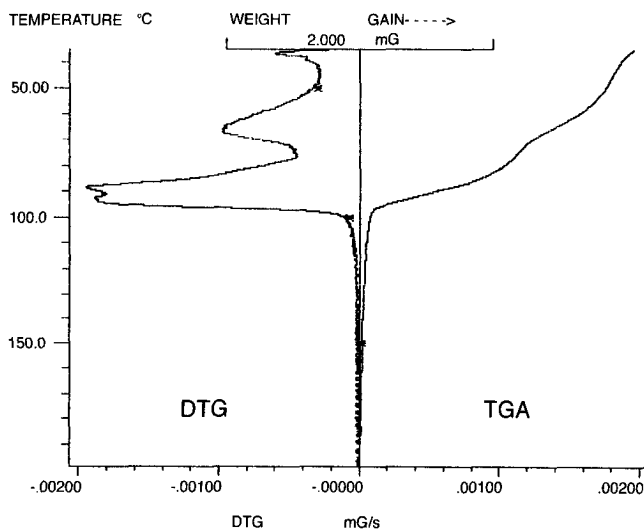


Fig. 18a: TGA and DTG curves of the VPI-5 sample A

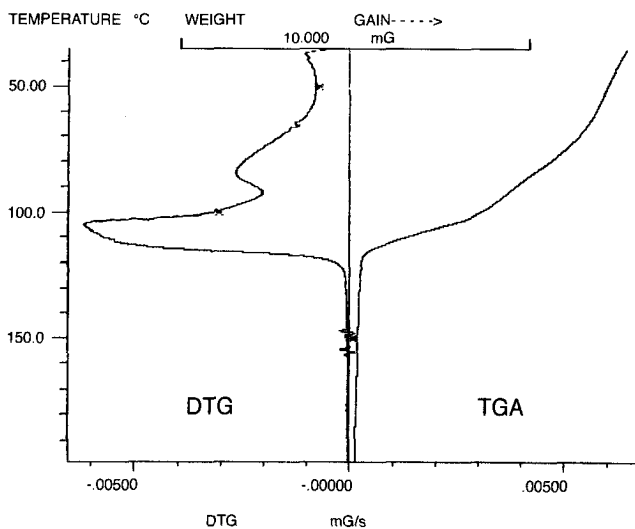


Fig. 18b: TGA and DTG curves of the VPI-5 sample B

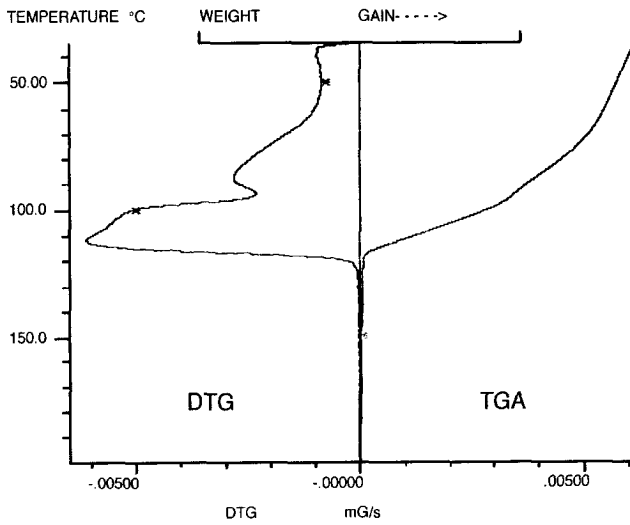


Fig. 18c: TGA and DTG curves of the VPI-5 sample C

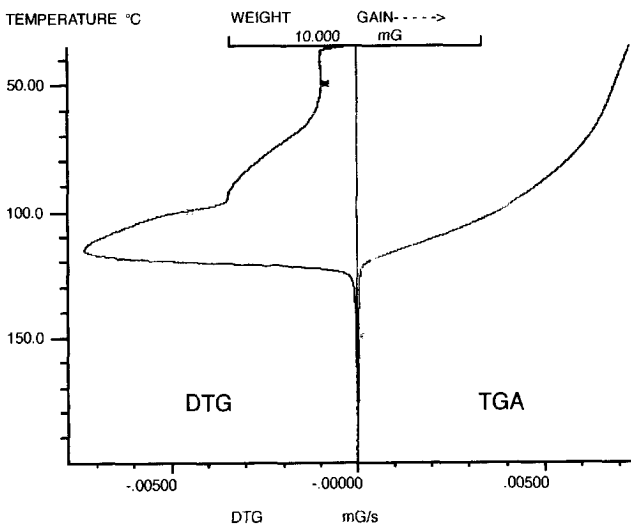


Fig. 18d: TGA and DTG curves of the VPI-5 sample D

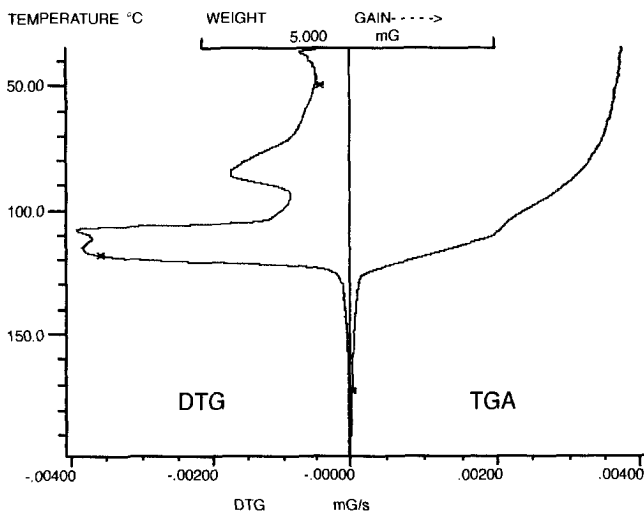


Fig. 18e: TGA and DTG curves of the VPI-5 sample E

In all samples, the total weight loss is caused by the removal of water up to ca. 24 wt% (verified by on-line mass spectrometry). No further weight losses were observed upon heating up to 650°C. The loss of water occurs in different stages, which is more evident for the samples synthesized with DPA, since their DTG curves (see, for instance, Fig. 18a and 18e) are better resolved. This behavior indicates that water is residing in several environments within the channels, in agreement with the reported structure of as-synthesized VPI-5 [38].

From these figures, it is also evident that the TGA curves are displaced towards higher temperatures, in the progression from sample A to E. This is indicative of an increase in the thermal stability, i.e. sample A is the least stable and sample E the most stable one.

The general tendencies are as follows: any attempt to dehydrate the samples under open or semi-open conditions, independent of the particular atmosphere, leads to a partial or total transformation to $\text{AlPO}_4\cdot 8$. The extent of the transformation is dependent on the sample

itself, the heating rate at which water is removed from the pores (dynamic experiments), the temperature and the time (isothermic experiments).

In the dynamic experiments, slower heating rates favor the phase transition, while higher temperatures and longer times in the isothermic experiments promotes it (see, for instance, Table 18b, experiments in humid air).

Once the samples have been evacuated at room temperature, they can be heated up to at least 650°C at practically any heating rate without conversion to $\text{AlPO}_4\text{-8}$ or loss of structural integrity. However, the duration of the outgassing is again dependent on the sample.

Under identical dehydration conditions, sample A is less stable than sample B. The reason for the different behavior of these two samples is not entirely clear. Sample A was three years old at the time of the experiment. It might be suspected that it has experienced a structural degradation with time, but its X-ray powder pattern does not differ from those of the other samples studied. Changes in the thermal stability with storage time have also been observed by Karlsson et al. [24].

Samples C and D, which were prepared with organic quaternary ions, showed a higher thermal stability (see Fig. 18) than those synthesized using the secondary amine DPA (samples A and B). These organic additives do not seem to act as templates (or space fillers) during the synthesis of VPI-5, but they do seem to influence the synthesis mechanism. Differences in the synthesis mechanisms of VPI-5 using tetrabutylammonium hydroxide and di-n-propylamine have been reported [22]. Apparently, different synthesis mechanisms produce samples with differing degrees of structural imperfections. These (e.g. P-OH defects) seem to facilitate the phase transformation. This might explain the different thermal behavior of the samples.

Although sample E was also prepared in the presence of di-n-propylamine, it showed the highest thermal stability. Apparently, the method reported in chapter 4 yields highly crystalline samples which contain fewer structural defects.

After careful dehydration, samples B to E showed very similar X-ray patterns (compare Fig. 19), which were different from that obtained for sample A. Therefore, the structural study was focused on two samples: A and E. The X-ray diffraction patterns of the samples A and E are compared in Fig. 20.

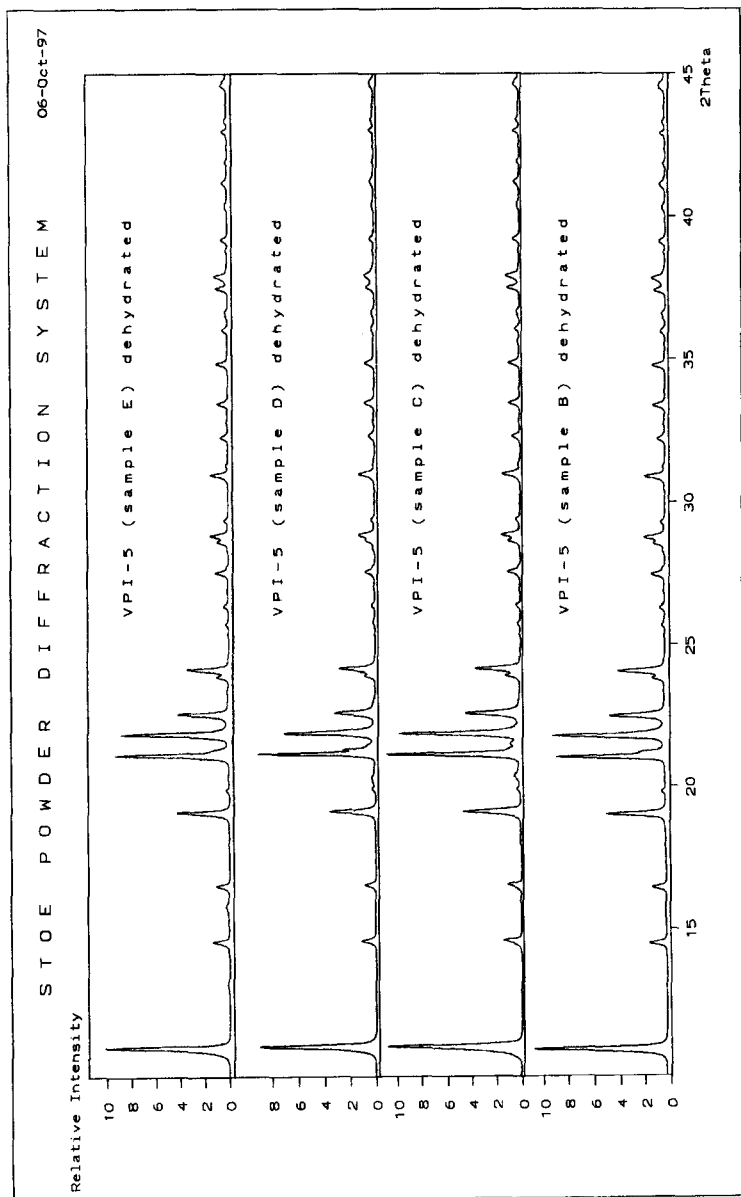


Fig. 19: Portion of the X-ray powder diffraction patterns of the dehydrated VPI-5 samples B to E taken using $\text{CuK}\alpha_1$ radiation

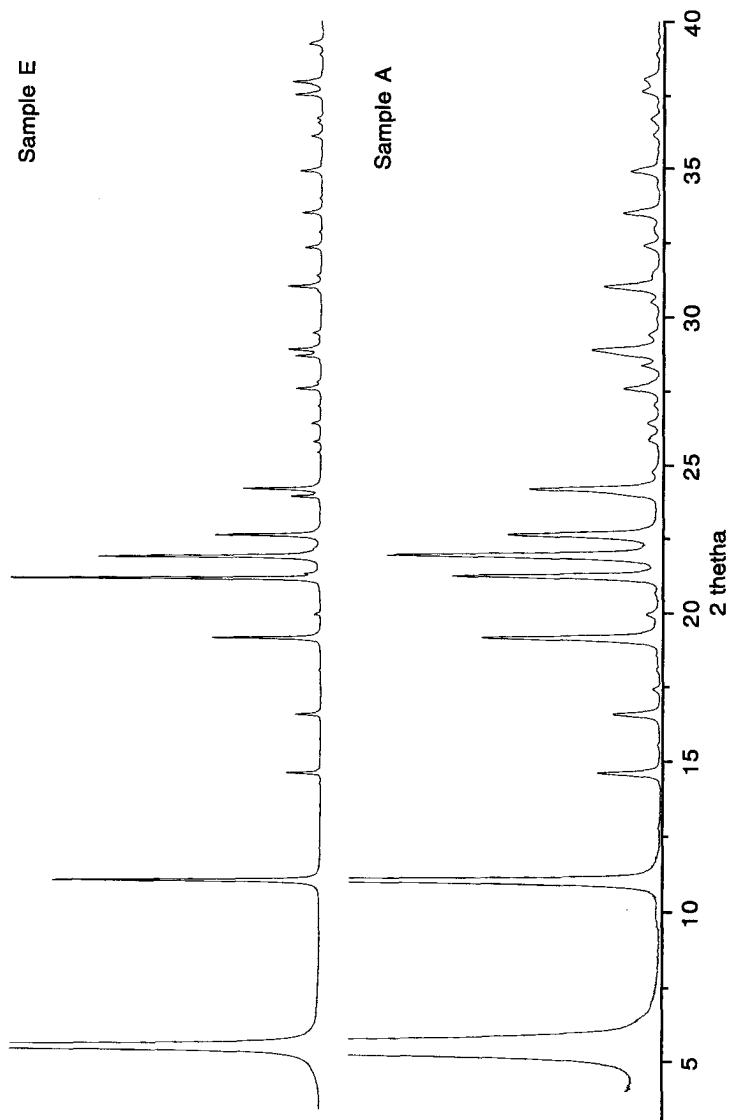


Fig. 20: Portion of the X-ray powder diffraction patterns of the dehydrated VPI-5 samples A and E (CuK α radiation)

6.3. Structural investigations

For the NMR investigations, the as-synthesized samples A and E were first put in a glass test tube which was then evacuated ($< 10^{-5}$ Pa) at room temperature for 48 hours. The sample, still under vacuum, was then heated slowly ($0.5^{\circ}\text{C}/\text{min}$) to 120°C , kept at that temperature overnight, heated to 450°C , and then kept at that temperature for another 6 hours. The dehydrated products were then allowed to cool while remaining under continuously pumped vacuum. The sealed glass tube was then transferred to a drybox ($p_{\text{H}_2\text{O}} < 4$ ppm) and the samples loaded in sealed zirconia rotors for the NMR experiments. For the powder diffraction experiments, sample E was loaded into a glass capillary (0.5 mm diameter) and sealed, while sample A was placed in a circular flat plate holder and dehydrated *in situ* in a furnace on a Scintag $\theta - \theta$ powder diffractometer.

6.3.1. Solid-state NMR

^{27}Al - and ^{31}P MAS NMR spectra were taken on a Bruker AMX 400 spectrometer. Table 19 summarizes further details of the data acquisition.

Table 19: Measuring conditions for the ^{27}Al - and ^{31}P - MAS NMR data acquisition

Parameter	^{27}Al MAS NMR	^{31}P MAS NMR
external standard	$(\text{NH}_4)\text{Al}(\text{SO}_4)_2 \cdot 12\text{H}_2\text{O}$	$\text{NH}_4\text{H}_2\text{PO}_4$
Frequency (MHz)	104.3	162.0
Pulse (μs)	1.5	2.0
Relaxation delay (s)	1.0	60.0
Rotor spinning speed (Hz)	8000-10000	10000

The ^{27}Al -MAS spectrum of both samples (Fig. 21) displays only one (slightly asymmetric) resonance line at ca. 36.2 ppm, confirming that in

the fully dehydrated form of VPI-5 all the Al atoms are tetrahedrally coordinated.

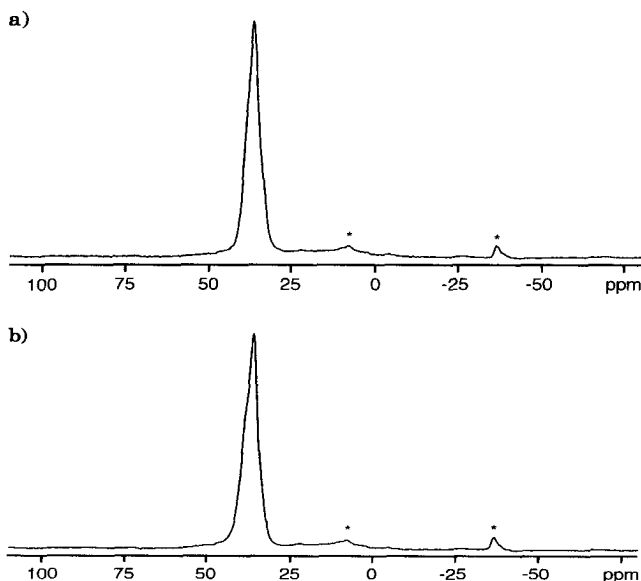


Fig. 21: ^{27}Al -MAS NMR spectrum of dehydrated VPI-5: (a) sample A and (b) sample E. Asterisks denote spinning side bands

The main feature of the ^{27}Al -DOR spectrum (104.3 Mhz) is a sharp, symmetric line at ca. 37 ppm for tetrahedral Al (see Fig. 22 for the spectrum of sample E).

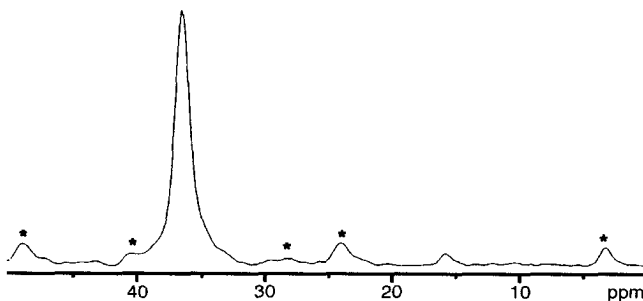


Fig. 22: ^{27}Al -DOR NMR spectrum of dehydrated VPI-5 (sample E). Asterisks denote spinning side bands

In the ^1H MAS spectra (MSL-400, 104.3 MHz) of the two samples, only one peak is observed at ca. 0 ppm. This is probably due to isolated Al-OH groups (see Fig. 23 for the ^1H MAS spectrum of sample E). There is no evidence for the existence of other signals, so the samples under study can be considered to be water free.

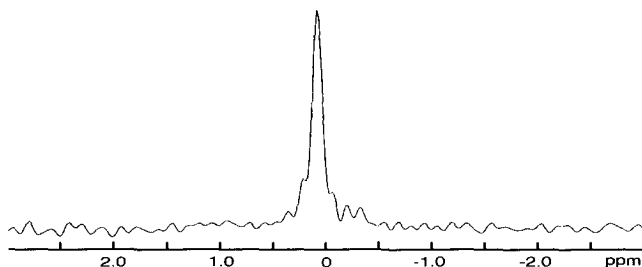


Fig. 23: ^1H MAS NMR spectrum of dehydrated VPI-5 (sample E)

For completely dehydrated VPI-5 two resonances with intensity ratios 2:1 would be expected in the ^{31}P -MAS spectrum, if the topochemical symmetry $P6_3cm$ is restored upon dehydration. However, the spectrum of both dehydrated samples clearly displays three prominent peaks at ca. -17.5, -27.1 and -32.4 ppm, a small spectral line at ca. -15.0 ppm, and a more diffuse peak near -22.3 ppm. The results of the spectrum deconvolution are presented in Table 20, the spectra in Fig. 24.

Table 20: Results of the simulation of the ^{31}P MAS NMR spectrum of dehydrated VPI-5

Signal	δ/ppm		Int. / %		n_p rel.*	
	sample A	sample E	sample A	sample E	sample A	sample E
1	-17.5	-17.5	12.8	13.1	1.0	1.0
2	-27.1	-27.2	41.9	42.7	3.3	3.3
3	-32.4	-32.4	25.0	26.0	2.0	2.0
6	-30.7	-30.5	13.1	13.2	1.0	1.0
7	-34.0	-34.1	4.7	3.9	0.4	0.3
4	-15.0	-15.1	0.9	0.8	0.1	0.1
5	-22.3	-22.3	1.6	1.1	0.1	0.1

*normalized to peak 1

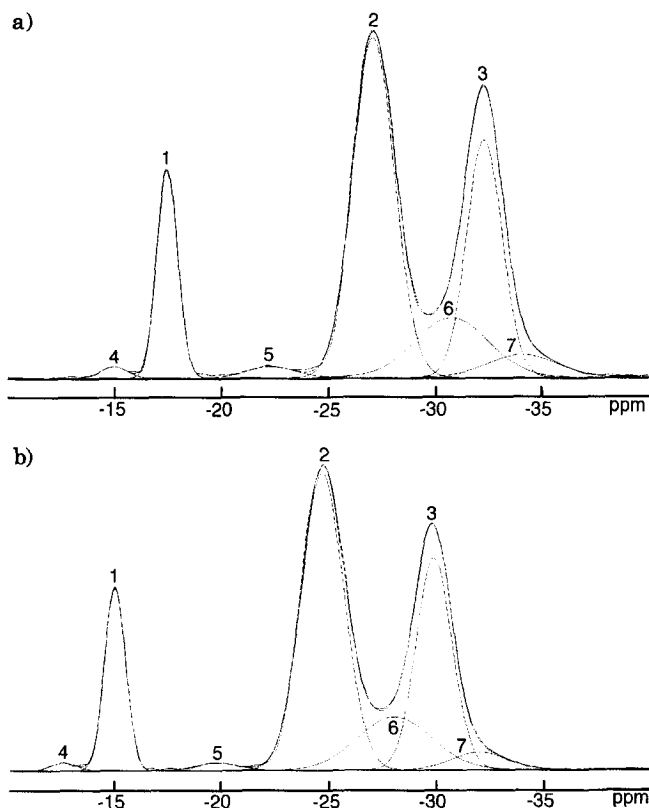


Fig. 24: Simulation of the ^{31}P MAS NMR spectra of dehydrated VPI-5: (a) sample A and (b) sample E

Taking into account just the strong signals 1, 2, 3 and 6, the relative intensities of 1:3:2:1 are obtained for both dehydrated VPI-5 samples. This is not fully consistent with the 1:5:3 intensity ratio found by Martens et al. [56]. There is, of course, the question as to whether the weak lines 4, 5 and 7 are from impurities of some kind or whether they also arise from P positions in the VPI-5 framework. These signals are observed with equal chemical shifts and intensities in samples that have been synthesized using different methods and structure-directing agents. Furthermore, given the relatively stringent conditions under which these samples were dehydrated and the results of the ^1H MAS NMR experiments, it is unlikely that water molecules are still residing in the channels. Thus, it must be

assumed that all observed resonances belong to the dehydrated structure, and that no partially dehydrated VPI-5 is present.

6.3.2. Rietveld refinement

6.3.2.1. Data collection

X-ray diffraction data on sample A were collected on a Scintag $\theta - \theta$ powder diffractometer. For sample E, the synchrotron powder diffraction pattern was collected at the European Synchrotron Radiation Facility (ESRF), in Grenoble, using a multi-analyzer-crystal detector system. The wavelength was calibrated with a standard silicon powder sample to be 0.92032 Å. Further details on the experimental conditions for data collection are given in Table 21.

Table 21: Experimental conditions for the powder diffraction data collection and crystallographic data for dehydrated VPI-5

Data Collection		Sample A	Sample E
Instrument		Scintag powder diffractometer	ESRF, BM 16, multiple analyzer Ge [111] Debye-Scherrer
Geometry		Bragg-Brentano	0.92032Å
Wavelength		1.54056Å	2 - 76° 2 θ
Range		4 - 70° 2 θ	continuous scan
Scan mode		step scan	2 - 40° 2 θ 0.1°/min
		0.02° 2 θ steps	40 - 70° 2 θ 0.05°/min
			binned in 0.008° 2 θ steps
Time		4 - 40° 2 θ 60s/step	
		40 - 70° 2 θ 120s/step	
Unit Cell		<i>Cm</i>	<i>Cm</i>
Space Group:		18.4680(5)Å	18.5218(1)Å
a		31.9703(4)Å	32.1247(2)Å
b		16.6759(2)Å	8.40026(2)Å
c		90.0°	90.0°
β			
Refinement			
Standard peak for peak shape function		(1) (220) 11.06° 2 θ	(1) (220) 6.58° 2 θ
		(2) (110) 5.52° 2 θ	(2) (020) 3.28° 2 θ
Peak range (number of FWHM)		15	12
No. of observations		3927	9076
No. of contributing reflections		3080	5746
No. of geometric 'observations'		452	226
No. of structural parameters		336	168
No. of profile parameters		9	9
$R_{\text{exp}} = [(N-P1-P2)/\sum w y^2(\text{obs})]^{1/2}$		0.067	0.047
$R_w = [\sum w(y(\text{obs}) - y(\text{cal}))^2 / \sum w y^2(\text{obs})]^{1/2}$		0.110	0.098
$R_F = \sum F(\text{obs}) - F(\text{cal}) / \sum F(\text{obs})$		0.054	0.062
Durbin-Watson d-statistic		1.89 (step size: 0.1)	1.93 (step size: 0.04)

6.3.2.2. X-ray Rietveld refinement of sample A

Although the NMR experiments suggested a lower symmetry, the Rietveld refinement using the XRS-82 package of programs [126] was initiated in the non-centrosymmetric space group $P6_3cm$. This is the highest possible symmetry allowing for the alternation of Al and P tetrahedra (topochemical symmetry). After the $\text{CuK}\alpha_2$ stripping has been performed, the data were scaled, the background estimated and subtracted, the 2 theta zero correction applied, and the whole pattern analyzed for changes in peak width and asymmetry. As suspected, the differences between the observed and the calculated patterns were very large, so the symmetry was reduced to $P6_3$. In both cases, however, attempts to refine the structure with geometric restraints, even with a high weight, led to a distorted geometry with unacceptable deviations in the bond distances and angles from ideal values. Furthermore, small but significant reflections requiring a doubling of the cell in the c direction were clearly apparent (see Fig. 25). In order to retain the VFI topology with a doubled unit cell, the space group had to be reduced to $P31m$ or lower. Distance Least-Squares (DLS) refinement [93] carried out in the small cell with $c = 8.3 \text{ \AA}$ showed a clear improvement in the geometry when the symmetry was changed from $P6_3cm$ or $P6_3$ to $P31m$. However, doubling the c axis brought no further improvement in either $P31m$ or $P3$.

A clear improvement in the geometry was apparent, however, when the symmetry was reduced still further to Cm , Cc or $C2_1$. Fig. 26 shows the tree of the space groups tested with DLS and the DLS-values obtained. Parallel Rietveld refinements in the monoclinic space groups resulted in a significantly better fit for Cm ($R_F = 0.054$, $R_{wp} = 0.110$) than for either Cc ($R_F = 0.112$, $R_{wp} = 0.250$) or $C2_1$ ($R_F = 0.145$, $R_{wp} = 0.267$). The symmetry constraints in Cc and $C2_1$ appear to be less compatible with ideal bond angles. In both space groups, the structure contains many extremely small P-O-Al angles and some unacceptably large ones. The refinement progressed well in the space group Cm , and the soft geometric restraints could be assigned less and less weight until they could be completely

removed without affecting the stability of the refinement. The relationship between the $P6_3cm$ and Cm unit cells is displayed in Fig. 27.

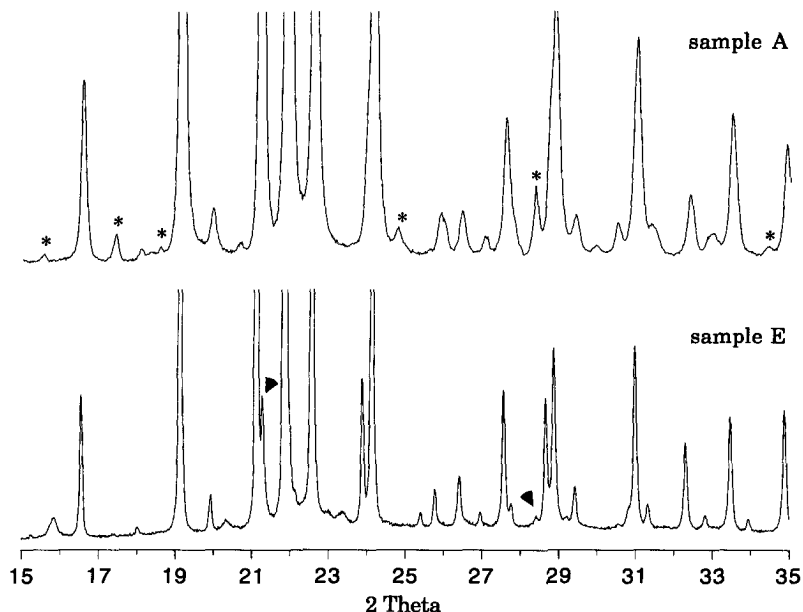


Fig. 25: Section of the X-ray powder patterns of samples A and E (in the latter case the 2θ scale has been changed to simulate a wavelength of 1.54056\AA). The peaks requiring a doubling of the cell are marked with asterisks in the pattern of sample A. Arrows in the pattern of sample E denote peaks not indexed in the space group Cm

To keep the number of variables as low as possible, only one displacement factor for each kind of atom was refined. For the calculations, scattering factors for neutral atoms were used in all cases.

Crystallographic data are summarized in Table 21 and the final positional and thermal parameters in Table 22a. The observed, calculated and difference profiles of the Rietveld refinement in the space group Cm are shown in Fig. 28.

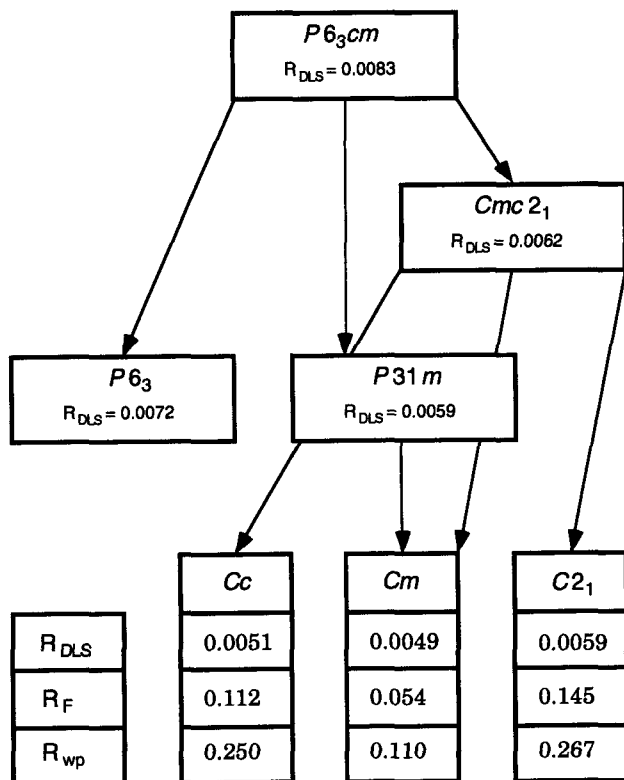


Fig. 26: Tree of space groups investigated during the course of the structure refinement of sample A. R_{DLS} denotes the R-value of the DLS refinement

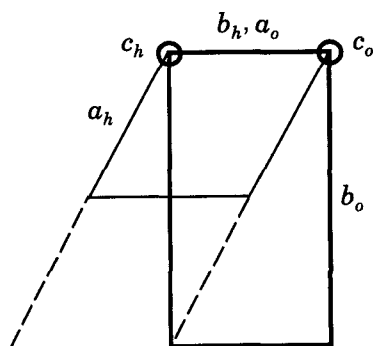


Fig. 27: Relationship between the $P6_3cm$ and Cm unit cells

Table 22a: Final positional and displacement parameters for dehydrated VPI-5, sample A^a

Atom	x	y	z	U(Å ²)
Al(1)	0.2106(3)	0.2137(1)	0.1293(4)	0.05(2) ^b
Al(2) ^c	0.06620	1/2	0.1313	0.05
Al(3)	0.1634(3)	0.3317(1)	0.0951(4)	0.05
Al(4)	0.2961(3)	0.2932(1)	0.3769(4)	0.05
Al(5)	0.0899(3)	0.2546(1)	0.3588(4)	0.05
Al(6)	0.0807(3)	0.41076(8)	0.3560(4)	0.05
Al(7)	0.1982(4)	0.2122(1)	0.5968(4)	0.05
Al(8)	0.0705(4)	1/2	0.5907(4)	0.05
Al(9)	0.1562(4)	0.33747(9)	0.6305(4)	0.05
Al(10)	0.2862(3)	0.2890(1)	0.8440(4)	0.05
Al(11)	0.0779(3)	0.2511(1)	0.8580(4)	0.05
Al(12)	0.0745(3)	0.41989(9)	0.8736(4)	0.05
Al(13)	0.4151(3)	0.2481(1)	0.1161(4)	0.05
Al(14)	0.4146(3)	0.08172(9)	0.1027(4)	0.05
Al(15)	0.3470(3)	0.16287(9)	0.3600(4)	0.05
Al(16)	0.4170(3)	0.2419(1)	0.6107(4)	0.05
Al(17)	0.4196(3)	0.08825(8)	0.6308(3)	0.05
Al(18)	0.3266(3)	0.16891(9)	0.8654(4)	0.05
Al(19)	0.4140(3)	0	0.3825(4)	0.05
Al(20)	0.4244(3)	0	0.8370(3)	0.05
P(1)	0.2893(3)	0.2931(1)	0.1879(4)	0.02(1) ^b
P(2)	0.0759(3)	0.2580(1)	0.1740(4)	0.02
P(3)	0.0787(3)	0.41076(8)	0.1646(3)	0.02
P(4)	0.1630(3)	0.33404(9)	0.4424(4)	0.02
P(5)	0.2142(3)	0.2063(1)	0.4074(4)	0.02
P(6)	0.0876(3)	0.5000	0.4044(4)	0.02
P(7)	0.2918(3)	0.28862(9)	0.6541(4)	0.02
P(8)	0.0746(4)	0.2529(1)	0.6749(4)	0.02
P(9)	0.0798(3)	0.41965(9)	0.6894(4)	0.02
P(10)	0.1584(3)	0.33445(9)	0.9026(4)	0.02
P(11)	0.2070(3)	0.2159(1)	0.9397(4)	0.02
P(12)	0.0667(3)	1/2	0.9480(3)	0.02
Atom	x	y	z	U(Å ²)
P(13)	0.3366(3)	0.16144(9)	0.1692(4)	0.02
P(14)	0.4287(3)	0.2460(1)	0.4210(4)	0.02
P(15)	0.4249(3)	0.08702(8)	0.4429(3)	0.02
P(16)	0.3167(4)	0.16552(8)	0.6704(4)	0.02
P(17)	0.4165(3)	0.2504(1)	0.9214(4)	0.02
P(18)	0.4080(3)	0.08418(9)	0.9108(4)	0.02
P(19)	0.4109(2)	0	0.1958(4)	0.02
P(20)	0.4180(3)	0	0.6522(3)	0.02
O(1)	0.1199(3)	0.2185(1)	0.1541(6)	0.04(2) ^b
O(2)	0.1112(2)	0.45443(6)	0.1550(3)	0.04
O(3)	0.2262(4)	0.2230(2)	0.0284(4)	0.04
O(4)	0.0365(3)	1/2	0.0333(2)	0.04
O(5)	0.2528(4)	0.2506(1)	0.1873(4)	0.04
O(6)	0.4931(2)	0	0.1950(3)	0.04
O(7)	0.2445(4)	0.3262(1)	0.1440(5)	0.04
O(8)	0.1006(4)	0.2938(2)	0.1205(5)	0.04
O(9)	0.0021(3)	0.4070(2)	0.1310(5)	0.04
O(10)	0.1292(4)	0.3791(1)	0.1257(5)	0.04
O(11)	-0.0040(3)	0.2477(2)	0.1654(5)	0.04
O(12)	0.1739(4)	0.3293(2)	-0.0074(4)	0.04
O(13)	0.2441(3)	0.3286(2)	0.4299(5)	0.04
O(14)	0.2953(4)	0.3063(2)	0.2762(4)	0.04
O(15)	0.2586(4)	0.2445(1)	0.3856(6)	0.04
O(16)	0.5067(3)	0	0.3876(6)	0.04
O(17)	0.1373(3)	0.2091(1)	0.3734(5)	0.04
O(18)	0.1190(3)	0.45946(6)	0.3699(4)	0.04
O(19)	0.1236(4)	0.2945(1)	0.4158(5)	0.04
O(20)	0.1333(4)	0.3712(1)	0.3946(4)	0.04
O(21)	0.0872(4)	0.2713(2)	0.2607(4)	0.04
O(22)	0.0718(4)	0.4027(2)	0.2544(3)	0.04
O(23)	0.1086(4)	0.2225(2)	0.6156(4)	0.04
O(24)	0.1033(4)	0.45518(7)	0.6345(4)	0.04

Table 22a: continued

Atom	x	y	z	U(Å ²)
O(25)	0.2048(4)	0.2003(2)	0.4973(4)	0.04
O(26)	0.1023(4)	1/2	0.4942(4)	0.04
O(27)	0.2502(4)	0.2559(1)	0.6078(4)	0.04
O(28)	0.2476(4)	0.3284(1)	0.6410(5)	0.04
O(29)	0.1040(5)	0.2974(1)	0.6660(5)	0.04
O(30)	-0.0002(4)	0.4061(2)	0.6820(4)	0.04
O(31)	0.1313(4)	0.3831(1)	0.6767(4)	0.04
O(32)	-0.0079(4)	0.2534(2)	0.6703(4)	0.04
O(33)	0.1412(4)	0.3411(2)	0.5294(4)	0.04
O(34)	0.2330(3)	0.3324(1)	0.8626(5)	0.04
O(35)	0.2956(4)	0.2796(2)	0.7436(4)	0.04
O(36)	0.2379(4)	0.2490(1)	0.8846(5)	0.04
O(37)	0.5061(4)	0	0.8862(3)	0.04
O(38)	0.1252(3)	0.2192(2)	0.9232(4)	0.04
O(39)	0.1101(3)	0.46054(7)	0.9288(4)	0.04
O(40)	0.1033(4)	0.3027(1)	0.8705(5)	0.04
O(41)	0.1278(4)	0.3782(1)	0.8964(5)	0.04
O(42)	0.0960(4)	0.2383(2)	0.7592(4)	0.04
O(43)	0.0898(4)	0.4339(2)	0.7755(4)	0.04
O(44)	0.2549(3)	0.1684(1)	0.1578(6)	0.04
O(45)	0.3632(3)	0.2895(1)	0.1473(5)	0.04
O(46)	0.3818(3)	0.03925(7)	0.1545(5)	0.04
O(47)	0.3773(4)	0.2000(1)	0.1390(5)	0.04
O(48)	0.3599(3)	0.1246(1)	0.1175(5)	0.04
O(49)	0.4259(4)	0.2512(2)	0.0132(4)	0.04
O(50)	0.4114(4)	0.0739(2)	0.0008(4)	0.04

^a Numbers in parentheses are the e.s.d.'s in the units of the least significant digit given

^b U of Al atoms were constrained to be equal U of Al1, U of P atoms were constrained to be equal U of P1, and U of O atoms were constrained to be equal U of O1

^c Al(2) was kept fixed during least-squares refinement

Atom	x	y	z	U(Å ²)
O(51)	0.3821(3)	0.2852(1)	0.4132(5)	0.04
O(52)	0.3847(4)	0.04591(7)	0.4272(5)	0.04
O(53)	0.2563(3)	0.1679(1)	0.3803(5)	0.04
O(54)	0.3938(4)	0.2082(1)	0.3806(5)	0.04
O(55)	0.4936(3)	0.0907(2)	0.3921(4)	0.04
O(56)	0.3745(4)	0.1228(1)	0.4208(4)	0.04
O(57)	0.5025(3)	0.2546(2)	0.3868(5)	0.04
O(58)	0.3524(4)	0.1530(2)	0.2583(4)	0.04
O(59)	0.2372(4)	0.1703(2)	0.6464(5)	0.04
O(60)	0.3698(4)	0.2881(2)	0.6236(5)	0.04
O(61)	0.3755(3)	0.04088(6)	0.6442(4)	0.04
O(62)	0.3675(4)	0.1978(1)	0.6325(5)	0.04
O(63)	0.3533(4)	0.1245(1)	0.6487(5)	0.04
O(64)	0.4381(4)	0.2373(2)	0.5106(4)	0.04
O(65)	0.4438(4)	0.0921(2)	0.5314(3)	0.04
O(66)	0.3672(3)	0.2866(1)	0.8954(5)	0.04
O(67)	0.3801(3)	0.04448(7)	0.8694(4)	0.04
O(68)	0.2403(3)	0.1760(1)	0.9037(5)	0.04
O(69)	0.3852(4)	0.2073(1)	0.8982(5)	0.04
O(70)	0.4855(3)	0.0948(1)	0.8857(6)	0.04
O(71)	0.3574(3)	0.1212(1)	0.8969(5)	0.04
O(72)	0.4872(3)	0.2562(2)	0.8759(4)	0.04
O(73)	0.3243(4)	0.1700(2)	0.7618(4)	0.04
O(74)	0.3869(3)	0	0.2834(4)	0.04
O(75)	0.4776(4)	0	0.5888(4)	0.04
O(76)	0.4478(4)	0	0.7371(3)	0.04

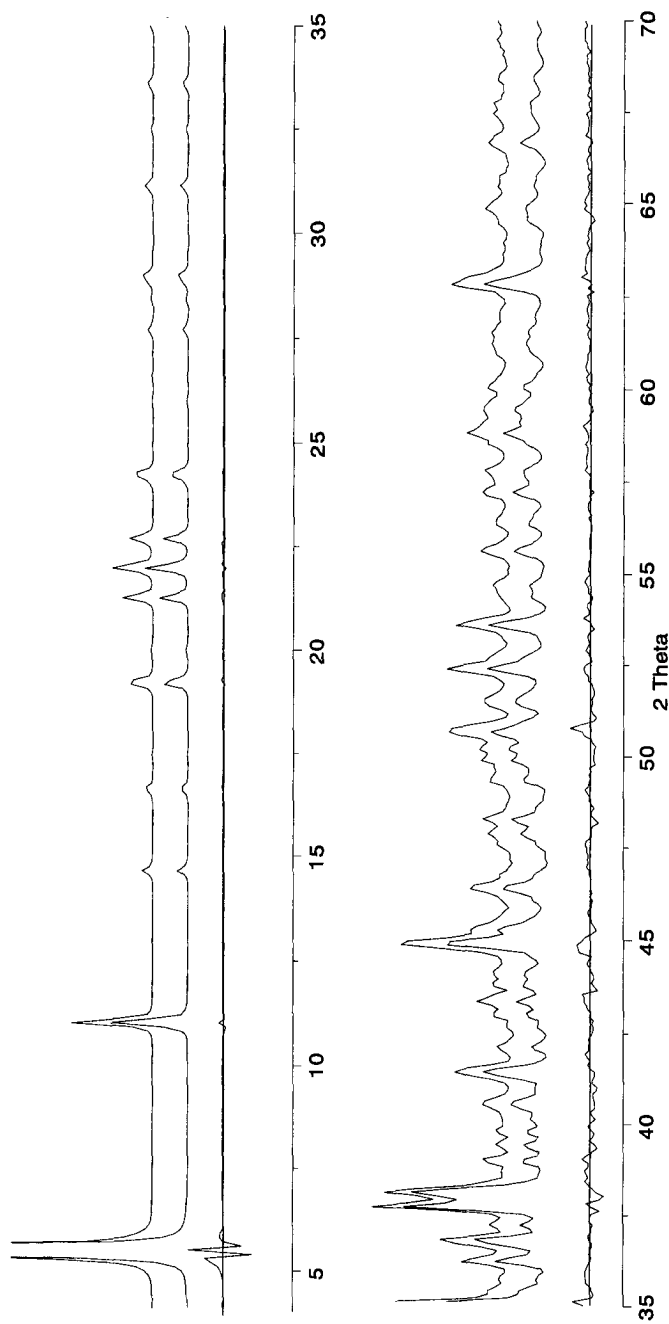


Fig. 28: Observed (top), calculated (middle) and difference (bottom) profiles for the Rietveld refinement of dehydrated VPI-5 (sample A). To show more detail, the first peak of the pattern has been cut at approximately $1/6$ of its maximum. For the same reason, the second half of the profile has been scaled up by a factor of 40

To check whether or not the disordered, two structure model of Poojary et al. [55] would be a viable alternative to the model described above, the X-ray powder pattern for that model was calculated and compared with the observed data (Fig. 29). However, it did not describe all the features in the pattern satisfactorily, even after the relative populations of the two models had been refined.

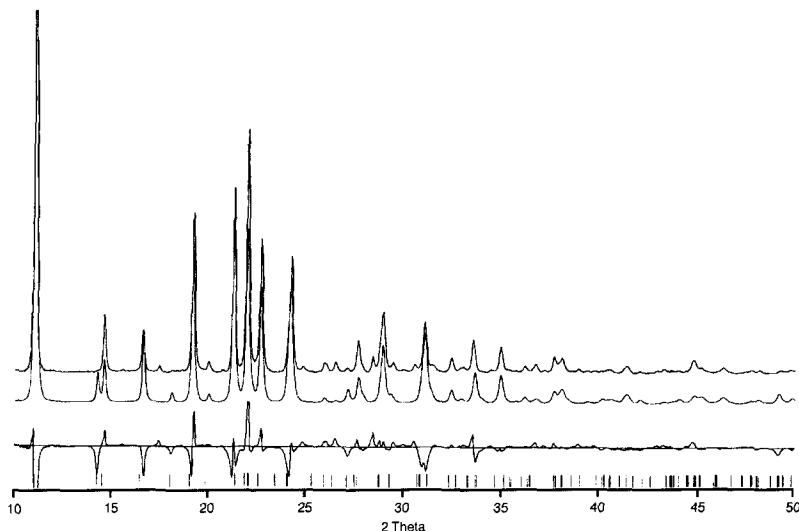


Fig. 29: Observed pattern from sample A dehydrated (top), powder pattern calculated with the atom positions from Ref. [55] (middle), difference profile (bottom)

6.3.2.3. Synchrotron Rietveld refinement of sample E

A close inspection of the powder diffraction patterns from the samples A and E (Fig. 25) reveals that there are significant differences, although the two dehydrated samples have identical solid-state NMR spectra.

The refinement of the structure of sample E was also initiated in the space group $P6_3cm$, using the synchrotron powder diffraction data and the atomic positions from the as-synthesized structure [38] as a starting model. However, the result was unsatisfactory. It was observed that some

peaks in the diffraction pattern remained unindexed, even after those belonging to the AlPO_4 -11 have been subtracted. Attempts to index the pattern in different unit cells while maintaining the hexagonal symmetry (i.e. $a' = 2a$, $c' = c$; $a' = \sqrt{3}a$, $c' = c$), did not lead to a better result. Similarly, a reduction of the symmetry to orthorhombic using different unit cells (i.e. $a' = a_h$, $b' = \sqrt{3}a_h$, $c' = c_h$; $a' = 2a_h$, $b' = \sqrt{3}a_h$, $c' = c_h$) proved to be insufficient. Thus, a symmetry reduction to monoclinic was again considered to be indispensable. Lattice parameter refinement in the space group Cm , however, did not suggest any significant deviation from the hexagonal metric. Therefore, the refinement was carried out in this monoclinic space group keeping the hexagonal metric ($a' = a_h$, $b' = \sqrt{3}a_h$, $c' = c_h$). Two peaks with d values 6.81 and 5.26 Å remained unindexed (see Fig. 25). Again, we have to assume that these two peaks belong to the structure, since they are observed, at the same position and with the same intensity, in all the dehydrated samples (B to E), although they have been synthesized using different methods. Moreover, they also appeared when the same samples were dehydrated under very different conditions (heating rate and time, dehydration temperature). Calcining the samples in air at much higher temperatures (up to 900°C) did not help, since it was not possible to assign these lines to any aluminophosphate-based condensed phase, such as AlPO_4 -tridymite.

A preferred orientation correction was applied assuming the c axis as the preferred axis, in accordance with the morphology of the crystals (long needles aggregated into long bundles) and the geometry of the experiment.

Only one displacement factor for each of the T-atoms and the oxygens was refined. For the calculations, scattering factors for neutral atoms were used in all cases.

Further details of the refinement are given in Table 21, final positional and thermal parameters in Table 22b, and the observed, calculated and difference profiles in Fig. 30.

Table 22b: Final positional and displacement parameters for dehydrated VPI-5, sample E^a

Atom	x	y	z	U(A ²)	Atom	x	y	z	U(A ²)
Al(1)	0.2035(2)	0.21402(8)	0.2593(6)	0.006	O(10)	0.3754(3)	0.2036(1)	0.3212(7)	0.01
Al(2) ^b	0.06620	1/2	0.2626	0.006	O(11)	0.3559(3)	0.2920(1)	0.3006(7)	0.01
Al(3)	0.1462(2)	0.33603(8)	0.2648(5)	0.006	O(12)	0.1157(3)	0.2146(1)	0.3313(7)	0.01
Al(4)	0.4134(2)	0.25040(9)	0.2711(5)	0.006	O(13)	0.1094(2)	0.45386(7)	0.3129(6)	0.01
Al(5)	0.4082(2)	0.08827(8)	0.2667(6)	0.006	O(14)	0.2509(3)	0.1691(1)	0.3115(8)	0.01
Al(6)	0.3256(3)	0.16745(8)	0.7676(6)	0.006	O(15)	0.2458(4)	0.2518(1)	0.3669(7)	0.01
Al(7)	0.4072(3)	0	0.7648(6)	0.006	O(16)	0.4889(2)	0	0.3755(6)	0.01
Al(8)	0.2861(2)	0.29093(8)	0.7701(6)	0.006	O(17)	0.3661(3)	0.1247(1)	0.3802(8)	0.01
Al(9)	0.0762(2)	0.25506(9)	0.7648(5)	0.006	O(18)	0.1130(3)	0.3747(1)	0.3833(7)	0.01
Al(10)	0.0679(3)	0.41623(8)	0.7623(6)	0.006	O(19)	0.9903(2)	0.2430(2)	0.3817(7)	0.01
P(1)	0.2838(2)	0.29353(7)	0.3913(5)	0.006(2) ^c	O(20)	0.0531(3)	0.4236(1)	0.5630(6)	0.01
P(2)	0.0728(2)	0.25311(9)	0.3885(5)	0.006	O(21)	0.0908(3)	0.2615(1)	0.5649(5)	0.01
P(3)	0.0692(2)	0.41570(8)	0.3848(6)	0.006	O(22)	0.3182(3)	0.1752(1)	0.5674(6)	0.01
P(4)	0.3282(3)	0.16797(7)	0.3867(6)	0.006	O(23)	0.3868(3)	0	0.5653(6)	0.01
P(5)	0.4064(2)	0	0.3875(6)	0.006	O(24)	0.2974(3)	0.3006(1)	0.5717(6)	0.01
P(6)	0.4168(2)	0.24474(8)	0.8959(5)	0.006	O(25)	0.4997(3)	0	0.7792(6)	0.01
P(7)	0.4085(2)	0.08860(7)	0.8893(6)	0.006	O(26)	0.2375(4)	0.2459(1)	0.7771(7)	0.01
P(8)	0.1540(3)	0.33748(7)	0.8889(5)	0.006	O(27)	0.1220(3)	0.3745(1)	0.7968(7)	0.01
P(9)	0.2021(2)	0.21338(8)	0.8824(6)	0.006	O(28)	0.4860(3)	0.2531(1)	0.8007(7)	0.01
P(10)	0.0656(3)	1/2	0.8870(4)	0.006	O(29)	0.3610(3)	0.1191(1)	0.7995(8)	0.01
O(1)	0.2124(3)	0.2255(1)	0.0601(6)	0.01(1) ^c	O(30)	0.2371(3)	0.1705(1)	0.8361(7)	0.01
O(2)	0.0425(3)	1/2	0.0636(3)	0.01	O(31)	0.1192(3)	0.2136(1)	0.8537(7)	0.01
O(3)	0.4359(3)	0.2442(1)	0.0758(5)	0.01	O(32)	0.1079(3)	0.45930(7)	0.8480(7)	0.01
O(4)	0.1473(3)	0.3504(1)	0.0674(5)	0.01	O(33)	0.3652(3)	0.2823(1)	0.8710(7)	0.01
O(5)	0.3987(3)	0.0977(1)	0.0683(6)	0.01	O(34)	0.4865(3)	0.0983(1)	0.8386(8)	0.01
O(6)	0.2340(3)	0.3292(1)	0.3326(7)	0.01	O(35)	0.2357(3)	0.3315(1)	0.8481(7)	0.01
O(7)	0.0948(3)	0.2917(1)	0.2909(6)	0.01	O(36)	0.3772(3)	0.04464(7)	0.8543(7)	0.01
O(8)	-0.0011(2)	0.4064(2)	0.2964(8)	0.01	O(37)	0.1051(3)	0.2986(1)	0.8632(6)	0.01
O(9)	0.3732(3)	0.04017(7)	0.3181(7)	0.01	O(38)	0.3839(3)	0.2021(1)	0.8541(7)	0.01

^a Numbers in parentheses are the e.s.d.'s in the units of the least significant digit given^b Al(2) was kept fixed during least-squares refinement^c U of tetrahedral atoms were constrained to be equal U of P1, and U of oxygen atoms were constrained to be equal U of O1

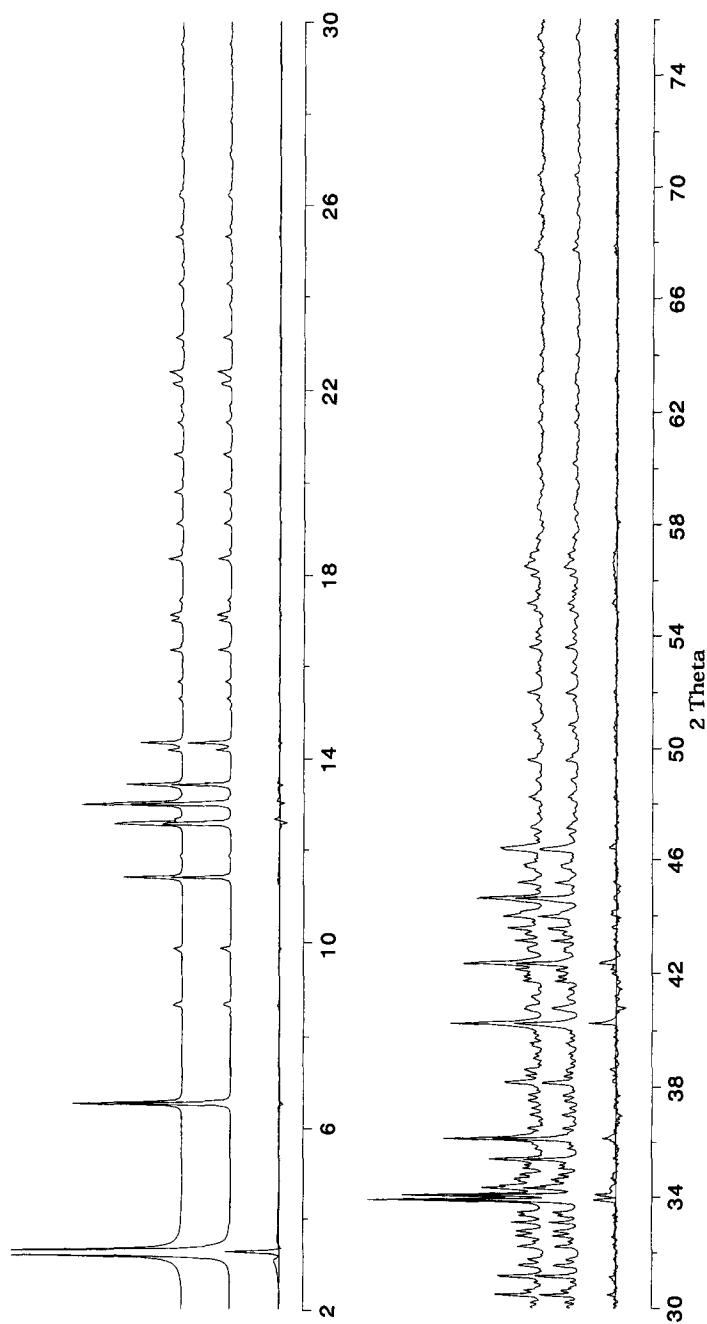


Fig. 30: Observed (top), calculated (middle) and difference (bottom) profiles for the Rietveld refinement of dehydrated VPI-5 (sample E). To show more detail, the first peak of the pattern has been cut at approximately 1/10 of its maximum. For the same reason, the second half of the profile has been scaled up by a factor of 14

Also in this case, calculated X-ray powder patterns based on Poojary's models [55] did not fit the observed diffraction pattern from sample E (Fig. 31), even after the relative populations of the two models had been refined.

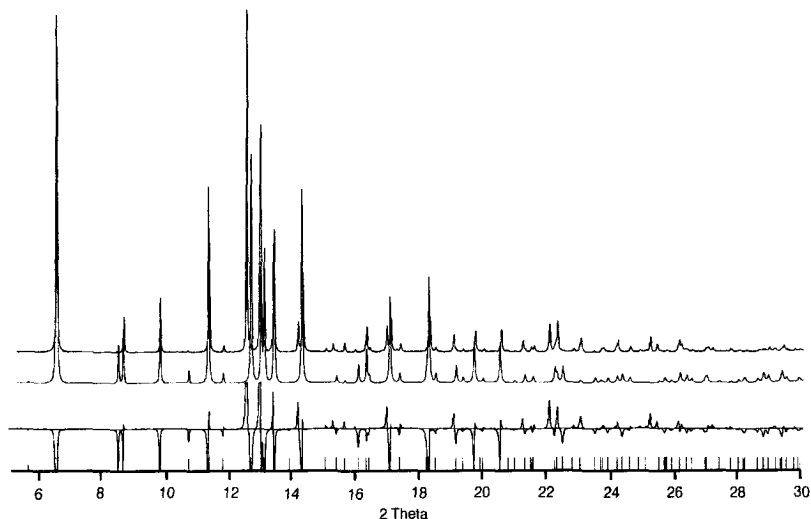


Fig. 31: Observed pattern from sample E dehydrated (top), powder pattern calculated with the atom positions from Ref. [55] (middle), difference profile (bottom)

6.3.3. Discussion

The Rietveld refinement carried out using the X-ray powder diffraction data of sample A showed that, in principal, it is possible to obtain a fully tetrahedral framework with the **VFI** topology. However, the structure contains some extremely small P-O-Al angles (see Table 23), which are located in the 18-rings associated with the fused 4-rings. This is displayed in Fig. 32, where for simplicity only one layer is drawn. In the next, symmetrically independent layer, these extremely small angles are located on the other side of the fused 4-rings. This distortion causes a symmetry reduction from $P6_3$ (in the as-synthesized form) to Cm . The central crankshaft chain running parallel to the c -axis is also distorted in such a manner (see Fig. 33) that the c -axis is doubled.

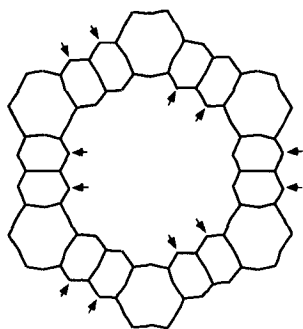


Fig. 32: Location of the extremely distorted P-O-Al angles in the dehydrated structures of samples A and E

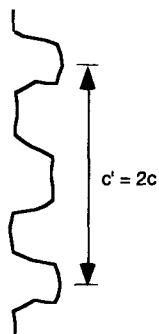


Fig. 33: Distortion of the crankshaft chain associated with fused 4 rings in the structure of sample A

The Rietveld refinement carried out using the synchrotron powder diffraction data of sample E, also indicated the existence of unusually small P-O-Al angles. In this case, a symmetry reduction to monoclinic (space group Cm) also proved to be indispensable. The deviation from the symmetrized positions (space group $P6_3cm$) is most pronounced (up to 0.6\AA) for the oxygen atoms located in the fused 4-rings, and for those located in the central chain of the triple crankshaft chain building unit (see Fig. 34).

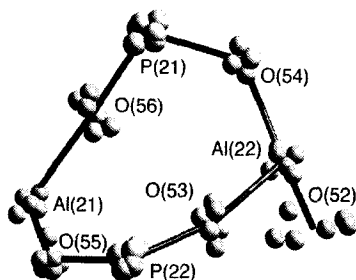


Fig. 34: Section of the dehydrated structure of sample E showing a 4-ring. The balls are generated by applying the symmetry operations of $P6_3cm$ to the positions of the monoclinic structure. The stick drawing and the labels represent the average symmetrized positions

In accordance with the solid state ^{27}Al NMR results, all the Al in both structures are tetrahedrally coordinated. Both structures also contain some extremely small P-O-Al angles (Table 23). For instance, in sample A

the average P-O-Al angles for P12 and P20 are 136° and 129° , respectively. For sample E, both P9 and P10 have an average P-O-Al angle of 136° . These small angles were obtained despite the fact that in the refinement soft restraints were used with a prescribed angle of $145^\circ \pm 8^\circ$. In both structures, all the oxygen atoms with these extremely small angles are in the 18-rings and associated with the fused 4-rings.

The existence of such small average angles is also indicated in the ^{31}P MAS NMR spectra, where an extreme chemical shift is observed for one of the peaks (compare Fig. 24 and Table 20). However, the results of the Rietveld refinements cannot explain the total number of crystallographic positions deduced from the ^{31}P MAS NMR spectra or their distribution. The multiplicity of the the space group is not compatible with the 1:5:3 ratio that was reported previously, or with the NMR results presented here. In sample A, P12 and P20 account for 4 of the 72 P's and in sample E, P9 and P10 for 6 of the 36 P's.

Considering the results of both Rietveld refinements, it could be speculated that the dehydration process of VPI-5 leads to a modulated structure. In the case of sample A, this modulation results in a simple doubling of the unit cell in the *c* direction. For sample E, the modulation could be incommensurate, and this might explain why every attempt to index the diffraction pattern failed. A series of electron diffraction experiments was carried out in the hope of finding evidence in this direction but, unfortunately, these experiments were unsuccessful because the many experimental difficulties inherent to the sample preparation (the sample cannot be dehydrated *in situ* without transformation to $\text{AlPO}_4\text{-8}$) and the fact that aluminophosphates are not very stable when exposed to an electron beam.

Table 23: P-O-Al angles distribution in the dehydrated structures of VPI-5

Sample A		
average P-O-Al angles [deg]	min.	129
P1-O-Al: 144(2)	max.	154
P2-O-Al: 142(2)	average	146
P3-O-Al: 149(3)		
P4-O-Al: 151(3)	selected single P-O-Al angles [deg]	
P5-O-Al: 145(2)	P2-O1-Al1:	128(2)
P6-O-Al: 144(2)	P3-O2-Al2:	126(2)
P7-O-Al: 141(3)	P5-O17-Al5:	128(2)
P8-O-Al: 146(2)	P6-O18-Al6:	129(3)
P9-O-Al: 147(3)	P7-O28-Al9:	129(2)
P10-O-Al: 151(3)	P8-O23-Al7:	127(2)
P11-O-Al: 142(2)	P10-O34-Al10:	126(2)
P12-O-Al: 136(2)	P12-O39-Al12:	122(2)
P13-O-Al: 150(3)	P13-O44-Al1:	126(2)
P14-O-Al: 150(3)	P14-O51-Al4:	127(3)
P15-O-Al: 153(3)	P16-O59-Al7:	126(2)
P16-O-Al: 154(3)	P18-O67-Al20:	128(3)
P17-O-Al: 150(2)	P20-O61-Al17:	122(2)
P18-O-Al: 147(2)		
P19-O-Al: 140(3)		
P20-O-Al: 129(2)		
Sample E		
average P-O-Al angles [deg]	min.	136
P1-O-Al: 145(2)	max.	151
P2-O-Al: 146(3)	average	145
P3-O-Al: 145(2)		
P4-O-Al: 149(2)	selected single P-O-Al angles [deg]	
P5-O-Al: 143(2)	P2-O12-Al1:	127(3)
P6-O-Al: 148(3)	P3-O13-Al2:	124(2)
P7-O-Al: 151(3)	P4-O14-Al1:	122(2)
P8-O-Al: 148(2)	P9-O30-Al6:	120(3)
P9-O-Al: 136(3)	P9-O31-Al9:	123(2)
P10-O-Al: 136(2)	P10-O32-Al10:	124(2)

VPI-5 undergoes a phase transition to $\text{AlPO}_4\text{-8}$ upon relatively mild thermal treatment. The results presented in chapter 4 and here show that only under very specific dehydration conditions is it possible to obtain a pure anhydrous phase of VPI-5. However, this material has an extremely distorted structure. This might be related to the strain inherent to the otherwise uncommon and apparently less stable *trans* conformation of the fused 4-rings. In the as-synthesized form of this aluminophosphate, the strain is reduced by the octahedral coordination of Al1, located between these rings. In the anhydrous structure, precisely this part of the framework is strongly stressed, making the structure less stable. Thus, it could be speculated that under normal dehydration conditions in an open atmosphere, VPI-5 readily converts to $\text{AlPO}_4\text{-8}$ in order to relieve the strain. In so doing, 2/3 of the strained triple crankshaft chain building units present in VPI-5 are eliminated.

A similar phase transition has been observed in the structurally related aluminophosphate $\text{AlPO}_4\text{-H2}$. The framework of this aluminophosphate also contains hydrated triple crankshaft chains that extend indefinitely along the *c* direction [40]. Interestingly, the structure of $\text{AlPO}_4\text{-H2}$ is also dramatically distorted when water is removed by evacuation, and upon heating irreversibly transforms to $\text{AlPO}_4\text{-tridymite}$ [40].

7. Structural investigations on $\text{AlPO}_4\text{-8}$

7.1. Brief literature overview

The aluminophosphate molecular sieve $\text{AlPO}_4\text{-8}$ is obtained via a solid-state transformation from VPI-5 by heating the latter in the presence of moisture. As described previously (chapter 2), this transformation is associated with a symmetry reduction from hexagonal to orthorhombic, and the material obtained is usually highly faulted.

The 'direct' hydrothermal synthesis of this aluminophosphate was first reported by Wilson et al. in 1982 [130], and later by Perez et al. [19]. However, in both cases, the preparation and drying procedures were appropriate for the synthesis and thermal transformation of VPI-5. Thus, there is no clear evidence to date that supports the direct synthesis of $\text{AlPO}_4\text{-8}$.

Structural models for $\text{AlPO}_4\text{-8}$ containing elliptical 14-ring pores were proposed independently by Vogt and Richardson [61] and Dessau et al. [131]. To this topology, the IUPAC code **AET** was assigned [4]. The former authors have also refined the structure of the dehydrated form by the Rietveld methods using neutron diffraction data [7]. However, they carried out their refinement in the centric space group $Cmcm$, which ignores the distinction between Al and P.

The crystal structures of the hydrated and dehydrated phases of this molecular sieve were also investigated by Poojary and Clearfield using X-ray powder data [132]. The dehydrated structure was refined in the space group $Cmc2_1$, that distinguishes between Al and P in the framework. They confirmed the framework structure proposed by Dessau [6] in the higher-symmetry space group. Attempts by these authors to refine the hydrated structure also in $Cmc2_1$, using the refined atom positions of the dehydrated form as starting model, failed. The authors observed that some of the diffraction peaks split or broadened upon rehydration and suggested

that the symmetry of this crystals is not ideally $Cmc2_1$, but rather monoclinic [132]. However, no attempt was made to refine the structure with this symmetry.

In Fig. 35 the ^{31}P - and ^{27}Al MAS NMR spectra of hydrated $\text{AlPO}_4\cdot 8$ are shown.

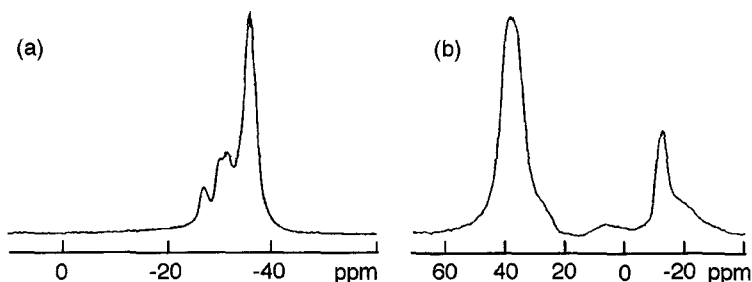


Fig. 35: (a) ^{31}P - and (b) ^{27}Al - MAS NMR spectra of hydrated $\text{AlPO}_4\cdot 8$ (from ref. 18)

The ^{31}P MAS spectrum reveals the existence of at least four signals, which have been assigned to different structural sites by different authors [e.g. 18,133]. The ^{27}Al MAS spectrum indicates that distinct hydration sites probably exist within the framework of this material, giving rise to different tetrahedral and octahedral ^{27}Al peaks. This has also been indicated by ^{27}Al quadrupolar nutation analysis combined with ^1H - ^{27}Al cross-polarization experiments [134].

7.2. Structural investigations

7.2.1. Sample preparation and data collection

The dehydrated $\text{AlPO}_4\cdot 8$ sample was prepared *in situ* by solid-state transformation from VPI-5. For the powder diffraction measurement, a glass capillary (0.5 mm diameter) was filled with VPI-5, and mounted on a STOE STADI powder diffractometer equipped with a high-temperature attachment. The capillary was slowly heated to 120°C (0.2 K/min) and kept at that temperature for 12 hours before heating to 450°C , where it was

again kept for another 12 hours. It was then quickly removed from the oven, sealed by melting and allowed to cool to RT. For the NMR investigations, the conversion took place under the same conditions in a quartz test tube which was then evacuated, closed and transferred to a drybox ($p_{\text{H}_2\text{O}} < 4$ ppm). In the drybox, the dehydrated product was transferred to a zirconia rotor of 4 mm diameter, which was then tightly closed with a boron nitride cap.

The procedure described above, produced a fairly crystalline material with a powder pattern having sharp lines, with a resolution that appears to surpass that of the powder patterns reported in the literature. It is generally assumed that this transformation starts simultaneously at many P-OH defect sites throughout the crystal, resulting in many domains of $\text{AlPO}_4\text{-8}$.

However, the fairly sharp peaks (e.g. 0.09° 2θ halfwidth at 12.97° 2θ) of its powder diffraction pattern, suggests the existence of relatively large coherently scattering domains in this specific sample. This might be an indication for a relatively low concentration of P-OH defects in the parent VPI-5 material, a fact that is further supported by its relatively high thermal stability (see chapter 4).

This comparatively good crystallinity of the material justified a further attempt to refine the dehydrated structure of $\text{AlPO}_4\text{-8}$. Therefore, synchrotron data were collected on the SNBL. Details of the experimental conditions for the synchrotron data collection are summarized in Table 24.

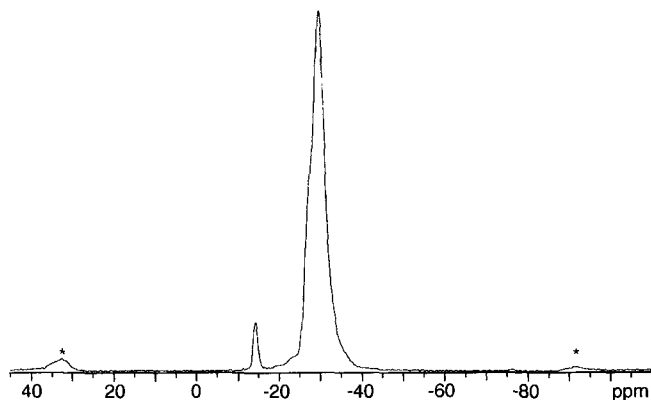
The ^{31}P - and ^{27}Al MAS NMR spectra were recorded on a Bruker AMX 400 spectrometer, with the conditions given in chapter 3.

Table 24: Experimental conditions for the powder diffraction data collection on dehydrated $\text{AlPO}_4\cdot 8$

Geometry	capillary mode	
Wavelength	1.09814Å	
Range	2.8 - 59.2° 2 θ	
Step size	0.01° 2 θ	
Measuring time	2.80 - 6.77° 2 θ	1s
	6.77 - 17.75° 2 θ	5s
	17.75 - 27.18° 2 θ	10s
	27.18 - 54.54° 2 θ	20s
	54.54 - 59.20° 2 θ	25s

7.2.2. Solid-state NMR

The ^{31}P - and ^{27}Al MAS NMR spectra of dehydrated $\text{AlPO}_4\cdot 8$ are shown in Fig. 36 and 37, respectively. The ^{31}P spectral pattern consists of a very broad line at ca. -30 ppm for tetrahedrally coordinated P, and a small signal at ca. -14 ppm. The latter could arise from P-OH terminal groups generated during the solid-state transformation, and/or from those that were already present in the as-synthesized VPI-5 sample.

**Fig. 36:** ^{31}P MAS NMR spectrum of dehydrated $\text{AlPO}_4\cdot 8$. Spinning sidebands are labeled with asterisks

The ^{27}Al spectrum (Fig. 37) has a resonance at ca. 37 ppm with a fairly large linewidth, indicating the presence of several non-equivalent tetrahedral Al sites in the framework. Since these overlapping signals could not be resolved with the DOR technique either [58], it might be assumed that the symmetry is rather low (resulting in a large number of crystallographically distinct Al sites), and/or that the stacking disorder produces a large distribution of Al environments that broaden the observed spectral lines. The small broad peak between 0 and 20 ppm (Fig. 37), may be the result of such stacking faults, or it could arise from an amorphous phase generated during the thermal treatment.

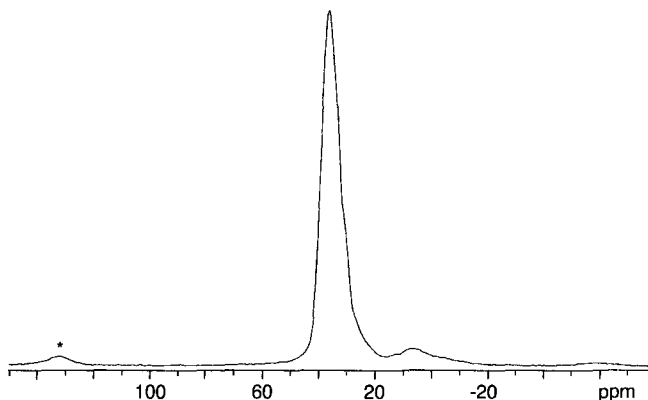


Fig. 37: ^{27}Al MAS NMR spectrum of dehydrated $\text{AlPO}_4\text{-8}$. Spinning sidebands are labeled with asterisks

7.2.3. Synchrotron powder diffraction

The high-quality data shown in Fig. 38 revealed the presence of small peaks that could not be indexed in the published orthorhombic cell with $a = 33.227$, $b = 14.745$ and $c = 8.3807\text{\AA}$ and the space group $Cmc2_1$ [132]. These peaks are present in all of the $\text{AlPO}_4\text{-8}$ samples that have been obtained by solid-state transformation from the VPI-5 samples A to E. These transformations took place under very different conditions (heating rate, final temperature, etc.). The unindexed peaks cannot be attributed to unreacted VPI-5, or to any known dense aluminophosphate phase.

Therefore, it must be assumed that they are part of the pattern of dehydrated $\text{AlPO}_4 \cdot 8$.

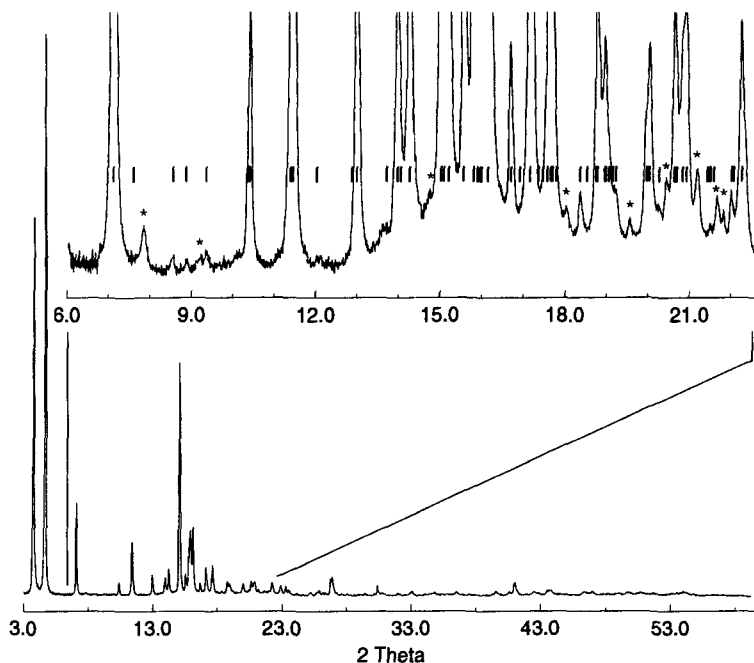


Fig. 38: Synchrotron powder pattern of dehydrated $\text{AlPO}_4 \cdot 8$. Ticks mark the position of reflections in the space group $Cmc2_1$. Asterisks mark unindexed peaks

Consequently, several attempts were made to index the whole pattern using the programs TREOR [135,136], DICVOL [137] and ITO [138], which work with different algorithms. Unfortunately, none of these programs found a satisfactory solution. All of the unit cells suggested by these programs have an unacceptably low figure of merit $M(20)$, although the quality of the data is very high and the input of the programs were checked. The solution with the highest figure of merit ($M(20) = 10.3$) was found with the program ITO. It is a triclinic cell with approximately the cell parameters reported by Poojary et. al [132]. But even with this cell not all the peaks of the diffraction pattern could be indexed.

Several attempts were also made to index the powder diagram by hand, using different unit cells derived from the original one by multiplying the cell parameters a , b and c with a factor of 2, 3 and combinations thereof, but retaining the orthorhombic symmetry. It was observed that some of the peaks were split and, consequently, the symmetry was also reduced to monoclinic and the monoclinic angle adjusted by hand. However, none of these attempts indexed the pattern satisfactorily. The indexing was normally checked by a 'Le-Bail-type' pattern fitting. This, together with the high resolution of the powder pattern allowed a very critical assessment of the various trials to index the pattern.

Since it must be assumed that the unindexed peaks do belong to the structure of the dehydrated material, there must be a reason, why it is not possible to assign indices to them. A plausible explanation is the following:

During the transformation to $\text{AlPO}_4\cdot 8$, only $2/3$ of the strained triple crankshaft chain building units that are present in VPI-5 are eliminated. Consequently, the **AET** framework still possesses 2 such units per unit cell. It has been shown (see chapter 6) that in the dehydrated framework of VPI-5, the central crankshaft chain is highly distorted and that the atoms of this chain might be modulated over several unit cells. It may be that a similar distortion is present in the dehydrated framework of $\text{AlPO}_4\cdot 8$, resulting in a modulated structure.

As for dehydrated VPI-5, attempts were made to gain some evidence supporting this hypothesis by means of electron diffraction. Unfortunately, there were also unsuccessful, because of experimental difficulties similar to those described in chapter 6.

Since a complete indexing of the experimental powder pattern was not possible, a conventional Rietveld refinement of the structure was not carried out. No attempt was made to simulate or refine a modulated

structure. The few additional reflections observed did not seem to justify such a project.

8. Conclusions

The aim of this project was the structural and thermal characterization of the aluminophosphate molecular sieve VPI-5 and of the structure-related $\text{AlPO}_4\text{-8}$. To gain some insight into the structure and the factors affecting the framework stability of the former, and the mechanism of its solid-state transformation to the latter, a series of powder diffraction and NMR experiments were performed.

Since the thermal stability of VPI-5 depends strongly on the synthesis and post-synthesis treatment conditions, a synthesis study was undertaken. The method first reported by E. Jahn was adapted for the reproducible production of highly crystalline samples with good thermal properties, and further modified for the production of relatively large single crystals ($250 \times 25 \times 25 \mu\text{m}^3$).

Comparison of the optimal conditions found for the synthesis of polycrystalline samples and those for single crystals, shows that the main differences between the two procedures are the time of the ultrasonic treatment, the amount of water and the crystallization temperature. It appears that a more diluted gel and a lower temperature allow for thicker and more perfect single crystals to be formed. The effect of the ultrasonic treatment is not yet well understood. This seems to be an important factor that needs to be investigated in more detail.

This method relies on the use of polyphosphoric acid with an average P chain length of 8 as the source for P. It is speculated that the concentration of the precursor species in the liquid phase would be reduced by using a polyphosphoric acid with a longer chain. This would reduce the supersaturation levels, and therefore the rate of nucleation and crystal growth would be lowered. In this way, a smaller number of viable nuclei with a more uniform outer surface would be produced, and this would be conducive to the growth of large single crystals. In this sense, it would be interesting to investigate the combined effect of prolonged

ultrasonic treatments with the use of polyphosphoric acids with longer P chains. Another aspect that would be interesting to investigate in conjunction with this, is the introduction of fluoride as a mineralizer during the synthesis process.

In contrast to other samples synthesized with DPA as the organic additive, the VPI-5 material obtained by this method showed good thermal stability. It would be interesting to investigate the combined effect of using polyphosphoric acids with longer chains with other organic additives (which normally produce more stable materials) on the thermal stability of VPI-5.

The role of water during the synthesis of VPI-5 is not obvious. However, according to the results of the Rietveld refinement carried out at 90°C in a closed system, the well defined water structure observed at RT does not exist at 90°C. Thus, it is unlikely that water itself is structure-directing. However, the Al located between the fused 4-rings remains octahedrally coordinated at 90°C, so it is possible that water has a stabilizing effect on the triple crankshaft building unit of which VPI-5 is constructed.

This structural study confirmed the symmetry change from $P6_3$ to $P6_3cm$ that had been suggested on the basis of solid-state NMR results. The NMR results presented here show that after the 'symmetrization' of the structure at higher temperatures, the NMR parameters (i.e. the local structural environment) of both the new P and Al sites located at the connection of 4- and 6-rings are closer to the original P2 and Al2, than to those of the original P3 and Al3 sites in the low temperature form. The significantly lower quadrupolar interaction of Al2 in comparison to Al3 indicates that the AlO_4 tetrahedra in the VPI-5 framework are less distorted at higher temperatures. Apparently, the inclination of the octahedron around Al1 (located at the center of the fused 4-rings) towards Al3 at RT, causes a slight distortion of the AlO_4 tetrahedron at Al3. At 90°C, this octahedron is not longer inclined, and the structure seems to be more relaxed.

Thermogravimetric experiments carried out to investigate the thermal stability of VPI-5 samples prepared using different procedures, show that once the samples have been evacuated at room temperature, they can be heated up to at least 650°C at practically any heating rate without conversion to $\text{AlPO}_4\text{-8}$ or loss of structural integrity. However, the duration of the outgassing is dependent on the sample. Although, in general, samples prepared with organic quaternary ions showed a higher thermal stability than those synthesized using di-*n*-propylamine, it was found that samples prepared with this amine but using polyphosphoric acid as the source of P showed the highest thermal stability. This might be explained by a lower concentration of P-OH defect sites.

The structures of two dehydrated samples prepared using different methods were investigated. The results of the Rietveld refinements carried out on both samples, led to the conclusion that it is possible to obtain a fully tetrahedral framework retaining the VFI topology, but only at the cost of extremely distorted fused 4-rings. These contain very small P-O-Al angles. This was also suggested by the ^{31}P MAS NMR investigations. This distortion causes a symmetry reduction from $P6_3$ to Cm . The deviation from the symmetrized positions is more pronounced (up to 0.6Å) for the oxygen atoms located in the fused 4-rings, and for those located in the central chain of the triple crankshaft chain building unit. In the structure of one of the samples studied (sample A), this central chain is also distorted in such a manner that the unit cell is doubled along the *c* direction. This does not apply for sample E, where two minor peaks in the powder pattern remained unindexed even after the unit cell was doubled. It is speculated that the dehydration process of VPI-5 leads to a modulated structure. Such a modulation could result in a simple doubling of the unit cell in the *c* direction for sample A, but be incommensurate in the case of sample E.

The high crystal quality of the parent material, allowed a good quality $\text{AlPO}_4\text{-8}$ powder to be obtained by solid-state transformation. The fairly sharp, well resolved peaks in the synchrotron powder diffraction pattern

of this material, is an indication for the existence of large coherently scattering domains.

The synchrotron powder diffraction pattern of this sample could not be completely indexed in the published orthorhombic cell. Some minor peaks are not accounted for. These could not be indexed in any other cell derived from the original one either. It is speculated that since the **AET** and **VFI** frameworks contain the same triple crankshaft building unit, a distortion similar to that observed in the VPI-5, may also be present in the dehydrated structure of $\text{AlPO}_4\text{-8}$, resulting in a modulated structure. This might explain why attempts to index the pattern failed.

The results presented in this work are another example of the complementary nature of diffraction and NMR techniques. Using a combination of the two allows a more detailed and, therefore, more complete picture of the structure of molecular sieves to be obtained.

References

- [1] F. d'Yvoire; *Bull. Chim. Soc. Fr.*, 1961, 1762
- [2] E.M. Flanigen, B.M. Lok, R.L. Patton, S.T. Wilson; *Pure Appl. Chem.*, 1986, **58**, 1351
- [3] E.M. Flanigen, R.L. Patton, S.T. Wilson; *Stud. Surf. Sci. Catal.*, 1988, **37**, 13
- [4] W.M. Meier, D.H. Olson, Ch. Baerlocher; *Atlas of Zeolite Structure Types*, Fourth Revised Edition, Elsevier, London, 1996
- [5] M.E. Davis, C. Saldariaga, C. Montes, J. Garces, C. Crowder; *Nature*, 1988, **331**, 698
- [6] R. Dessau, J.L. Schlenker, J.B. Higgins; *Zeolites*, 1990, **10**, 522
- [7] J.W. Richardson, Jr., E.T.C. Vogt; *Zeolites*, 1992, **12**, 13
- [8] E. Jahn, D. Mueller, J. Richter-Mendau in *Synthesis of Microporous Materials, Vol. I: Molecular Sieves*, M.L. Ocelli, H. Robson (Eds.), Van Nostrand-Reinhold, N. York, 1992, 248
- [9] G. Sumelius; Attempted translation of the original old-Swedish paper by Cronsted in *Synthesis of Microporous Materials, Vol. I: Molecular Sieves*, M.L. Ocelli and H. Robson (Eds.), Van Nostrand-Reinhold, N. York, 1992, 1
- [10] R.M. Barrer and H. Villiger; *Z. Kristall.* 1969, **128**, 352
- [11] J.V. Smith and W.J. Dytrych; *Nature*, 1984, **309**, 607
- [12] W.M. Meier in *New developments in Zeolite Science and Technology*, Y. Murakami, A. Iijima and J.W. Ward (Eds.), Elsevier, Amsterdam, 1986, 13
- [13] M.E. Davis, C. Saldariaga, C. Montes, J. Garces, C. Crowder; *Zeolites*, 1988, **8**, 362
- [14] M.E. Davis, C. Montes, J.M. Garces; in *ACS Symposium Series*, 1989, **398**, 291
- [15] E.G. Derouane, L. Maistriau, Z. Gabelica, A. Tuel, J.B. Nagy, R. von Ballmoos; *Appl. Catal.*, 1989, **51**, L13
- [16] P. Grobet, J. Martens, I. Balakrishnan, M. Mertens, P.A. Jacobs; *Appl. Catal.*, 1989, **56**, L21
- [17] B. Duncan, R. Szostak, K. Sorby, J.G. Ulan; *Catal. Lett.*, 1990, **7**, 367

- [18] L. Maistriau, Z. Gabelica, E.G. Derouane, E.T.C. Vogt, J. van Oene; *Zeolites*, 1991, **11**, 583
- [19] J.O. Perez, N.K. McGuire, A. Clearfield; *Catal. Lett.*, 1991, **8**, 145
- [20] D. Akporiaye, M. Stocker; *Zeolites*, 1992, **12**, 351
- [21] H. Cauffriez, L. Delmotte, J.L. Guth; *Zeolites*, 1992, **12**, 121
- [22] H. He, J. Klinowski; *J. Phys. Chem.*, 1994, **98**, 1192
- [23] J.R. Anderson, W.R. Jackson, D. Hay, Z. Yang, E. Campi; *Zeolites*, 1996, **16**, 15
- [24] A. Karlsson, D. Akporiaye, M. Stöcker; *Microporous Materials*, 1995, **4**, 31
- [25] M.E. Davis, C. Montes, P.E. Hathaway, J.P. Arhancet, D.L. Hasha, J.M. Garces; *J. Am. Chem. Soc.*, 1989, **111**, 3919
- [26] M.E. Davis, C. Montes, P.E. Hathaway, J.M. Garces; *Stud. Surf. Sci. Catal.*, 1989, **49**, 199
- [27] Z. Gabelica, L. Maistriau, A.G. Derouane in *Synthesis of Microporous Materials, Vol. I: Molecular Sieves*, M.L. Ocelli and H. Robson (Eds.), Van Nostrand-Reinhold, N. York, 1992, 289
- [28] M.E. Davis, D. Young; *Stud. Surf. Sci. Catal.*, 1991, **60**, 53
- [29] H.-X. Li, M.E. Davis; *Catalysis Today*, 1994, **19**, 61
- [30] J.A. Martens, I. Balakrishnan, P.J. Grobet, P.A. Jacobs; *Stud. Surf. Sci. Catal.*, 1991, **69**, 135
- [31] J.A. Martens, H. Geerts, L. Leplat, G. Vanbutsele, P.J. Grobet, P.A. Jacobs; *Catal. Lett.*, 1992, **12**, 367
- [32] M. Hartmann, L. Kevan; *J. Chem. Soc., Faraday Trans.*, 1996, **92**, 3661
- [33] P. Singh, R.A. Shaikh, R. Bandyopadhyay, B.S. Rao; *J. Chem. Soc., Chem. Commun.*, 1995, 2255
- [34] R.F. Shinde, I. Balakrishnan; *J. Phys. D.*, 1991, 1486
- [35] E.M. Flaniguen, R.L. Patton, S.T. Wilson; *Stud. Surf. Sci. Catal.*, 1988, **37**, 13
- [36] C.E. Crowder, J.M. Garces, M. Davis; *Adv. X-ray Anal.*, 1988, **32**, 507
- [37] P. Rudolf, C.E. Crowder; *Zeolites*, 1990, **10**, 163

- [38] L. B. McCusker, Ch. Baerlocher, E. Jahn, M. Bulow; *Zeolites*, 1991, **11**, 308
- [39] J.V. Smith; *Geometrical and Structural Crystallography*, John Wiley, N. York, 1982
- [40] H.-X. Li, M.E. Davis; *J. Chem. Soc. Faraday Trans.*, 1993, **89**, 951
- [41] G.O. Brunner; *Zeolites*, 1990, **10**, 612
- [42] D.M. Poojary, A. Clearfield; *Zeolites*, 1993, **13**, 542
- [43] G. Cheetham, M.M. Harding; *Zeolites*, 1996, **16**, 245
- [44] Y. Wu, B.F. Chmelka, A. Pines, M.E. Davis, P.J. Grobet, P.A. Jacobs; *Nature*, 1990, **346**, 550
- [45] J. Rocha, W. Kolodziejski, H. He, J. Klinowski; *J. Am. Chem. Soc.*, 1992, **114**, 4884
- [46] P.J. Grobet, A. Samoson, H. Geerts, J.A. Martens, P.A. Jacobs; *J. Phys. Chem.*, 1991, **95**, 9620
- [47] J.P. van Braam Houckgeest, B. Kraushaar-Czarnetzki, R.J. Dogterom, A. de Groot; *J. Chem. Soc., Chem. Commun.*, 1991, 666
- [48] L. Maistriau, Z. Gabelica, E.G. Derouane; *Appl. Catal.*, 1992, **81**, 67
- [49] G. Engelhardt, W. Veeman; *J. Chem. Soc., Chem. Commun.*, 1993, 662
- [50] E.R.H. van Eck, W. Veeman; *J. Am. Chem. Soc.*, 1993, **115**, 1168
- [51] C.A. Fyfe, K.T. Mueller, H. Grondey, K.C. Wong-Moon; *J. Phys. Chem.*, 1993, **97**, 13484
- [52] D. Goldfarb, H.-X. Li, M. Davis; *J. Am. Chem. Soc.*, 1992, **114**, 3690
- [53] M.J. Duer, H. He, W. Kolodziejski, J. Klinowski; *J. Phys. Chem.*, 1994, **98**, 1198
- [54] J.W. Richardson, Jr., J.V. Smith, J. Pluth; *J. Phys. Chem.*, 1989, **93**, 8212
- [55] J. Martens, E. Feijen, J.L. Lievens, P.J. Grobet, P.A. Jacobs; *J. Phys. Chem.*, 1991, **95**, 10025
- [56] D.M. Poojary, J. O. Perez, A. Clearfield; *J. Phys. Chem.*, 1992, **96**, 7709
- [57] J.O. Perez, P.J. Chu, A. Clearfield; *J. Phys. Chem.*, 1991, **95**, 9994

- [58] R. Jelinek, B.F. Chmelka, Y. Wu, M.E. Davis, J.G. Ulan, R. Gronsky, A. Pines; *Catal. Lett.*, 1992, **15**, 65
- [59] J. Rocha, A.P. Esculcas, Ch. Fernandez, J.P. Amoureux; *J. Phys. Chem.*, 1996, **100**, 17889
- [60] H. He, J. Klinowski; *Catal. Today*, 1996, **30**, 119
- [61] E.T.C. Vogt, J.W. Richardson; *J. Solid State Chem.*, 1990, **87**, 469
- [62] S. Prasad, I Balakrishnan; *Inorg. Chem.*, 1990, **29**, 4830
- [63] J.G. Ulan, R. Szostak, K. Sørby, R. Gronsky; *Mat. Res. Soc., Symp. Proc.*, 1990, **183**, 317
- [64] K. Sørby, R. Szostak, J.G. Ulan, R. Gronsky; *Catal. Lett.*, 1990, **6**, 209
- [65] M.W. Anderson, J. Shi, D.A. Leigh, A.E. Moody, F.W. Wade, B. Hamilton, S.W. Carr; *J. Chem. Soc., Chem. Commun.*, 1993, 533
- [66] Christian Lengauer, *personal communication*
- [67] K. Vinje, R. Szostak, K. Sorby, J.G. Ulan; *Catal. Lett.*, 1991, **72**, 361
- [68] C. Potvin, J.M. Manoli, M. Briend, D. Barthomeuf; *Catal. Lett.*, 1991, **8**, 145
- [69] M.J. Annen, D. Young, M.E. Davis, O.B. Cavin, C.R. Hubbard; *J. Phys. Chem.*, 1991, **95**, 1380
- [70] M.B. Kenny, K.S.W. Sing, C.R. Theocharis; *J. Chem. Soc., Faraday Trans.*, 1992, **88**, 3349
- [71] H. He, P. Barnes, J. Munn, X. Turrillas, J. Klinowski; *Chem. Phys. Lett.*, 1992, **196**, 267
- [72] X. Liu, H. He, J. Klinowski; *J. Phys. Chem.*, 1991, **95**, 9924
- [73] P.E. Hathaway, M.E. Davis; *Catal. Lett.*, 1990, **5**, 333
- [74] J. Jänchen, H. Stach, P.J. Grobet, J.A. Martens, P.A. Jacobs; *Zeolites*, 1992, **12**, 9
- [75] S.W. Webb, W.C. Conner; *Stud. Surf. Sci. Catal.*, 1991, **62**, 31
- [76] A. Saito, H.C. Foley; *AIChE Journal*, 1991, **37**, 429
- [77] M.B. Kenny, K.S.W. Sing, C.R. Theocharis; *J. Chem. Soc., Chem. Commun.*, 1991, 974
- [78] P.J.M. Carrot, M.B. Kenny, R.A. Roberts, K.S.W. Sing, C.R. Theocharis; *Stud. Surf. Sci. Catal.*, 1991, **62**, 685

- [79] J. Kärger, W. Keller, H. Pfeifer, S. Ernst, J. Weitkamp; *Microporous Materials*, 1995, **3**, 401
- [80] R.F. Parton, L. Uytterhoeven, P.A. Jacobs; *Stud. Surf. Sci. Catal.*, 1991, **53**, 395
- [81] S.B. Hong, E. Mielczarski, M. Davis; *J. Catal.*, 1992, **134**, 349
- [82] R. Mahrwald, U. Lohse, I. Girnus, J. Caro; *Zeolites*, 1994, **14**, 486
- [83] B. Hamilton, J.S. Rimmer, M. Anderson; *Adv. Mater.*, 1993, **5**, 583
- [84] J.I. Langford, D. Louër; *Rep. Prog. Phys.*, 1996, **59**, 131
- [85] Ch. Baerlocher, L. McCusker; *Stud. Surf. Catal.*, 1994, **85**, 391
- [86] H.M. Rietveld; *Acta Cryst.*; 1967, **22**, 151
- [87] H.M. Rietveld; *J. Appl. Cryst.*; 1969, **2**, 65
- [88] R.A. Young in *The Rietveld Method*, R.A. Young (Ed.), Oxford University Press, Oxford, 1993, 1
- [89] R.A. Young, D.B. Wiles; *J. Appl. Cryst.*, 1982, **15**, 430
- [90] M.M. Hall, V.G. Veeraraghavan, H. Rubin, P.G. Winchell; *J. Appl. Cryst.*, 1977, **10**, 66
- [91] J.I. Langford; *J. Appl. Cryst.*, 1978, **11**, 10
- [92] G.K. Wertheim, M.A. Butler, K.W. West, D.N.E. Buchanan; *Rev. Sci. Instrum.*, 1974, **11**, 1369
- [93] A. Hepp, Ch. Baerlocher; *Austral. J. Phys.*, 1988, **21**, 229
- [94] H. Toraya; *J. Appl. Cryst.*, 1990, **23**, 485
- [95] R.L. Snyder in *The Rietveld Method*, R.A. Young (Ed.), Oxford University Press, Oxford, 1993, 111
- [96] E. Prince in *The Rietveld Method*, R.A. Young (Ed.), Oxford University Press, Oxford, 1993, 44
- [97] R.A. Young, E. Prince; *J. Appl. Cryst.*, 1982, **12**, 357
- [98] Ch. Baerlocher; *Zeolites*, 1986, **6**, 325
- [99] R.J. Hill, R.X. Fischer; *J. Appl. Cryst.*, 1990, **23**, 462
- [100] R.J. Hill, H.D. Flack; *J. Appl. Cryst.*, 1987, **20**, 356
- [101] E. Prince; *J. Appl. Cryst.*, 1981, **14**, 157

- [102] L.B. McCusker in *Comprehensive Supramolecular Chemistry*, Vol. 7: *Solid-state Supramolecular Chemistry: Two- and Three-dimensional Inorganic Networks*, G. Alberti, T. Bein (Eds.), Pergamon, 1996
- [103] Ch. Baerlocher in *The Rietveld Method*, R.A. Young (Ed.), Oxford University Press, Oxford, 1993, 186
- [104] Ch. Baerlocher, A. Hepp, W.M. Meier; *Distance Least Squares Refinement Program DLS-76*, ETH Zurich, 1977
- [105] L.B. McCusker; *Acta Cryst.*, 1991, **A47**, 297
- [106] M. Stöcker; *Stud. Surf. Sci. Catal.*, 1996, **102**, 141
- [107] G.J. Kennedy, J.B. Higgings, C.F. Ridenour, H.-X. Li, M.E. Davis; *Solid State Nuclear Magnetic Resonance*, 1995, **4**, 173
- [108] J. Klinowski; *Anal. Chim. Acta*, 1993, **283**, 929
- [109] A Llor, J. Virlet; *J. Chem. Phys. Lett.*, 1988, **152**, 248
- [110] K.T. Mueller, B.Q. Sun, G.C. Chingas, J.W. Zwanziger, T. Terao, Pines, A; *J. Magn. Reson.*, 1990, **86**, 470
- [111] A. Samoson, E. Lippmaa, A. Pines; *Mol. Phys.*, 1988, **65**, 1013
- [112] H.W. Spiss in *NMR: Basic Principles and Progress*, P. Diehl, E. Fluck, R. Kosfeld (Eds.), Springer-Verlag, Berlin, 1978
- [113] Z. Luz, A.J. Vega; *J. Phys. Chem.*, 1986, **90**, 4903
- [114] A.J. Vega, Z. Luz; *Zeolites*, 1988, **8**, 19
- [115] M.E. Davis, R.I. Lobo; *Chem. Mater.*, 1992, **4**, 756
- [116] J.F. Charnell; *J. Cryst. Growth*, 1971, **8**, 291
- [117] V.N. Bogomolov, V.P. Petranovski; *Zeolites*, 1986, **4**, 121
- [118] H.K. Chae, W. Klemperer, D. Payne, C. Suchicital, D. Wake, S. Wilson; *Am. Chem. Soc. Symp. Ser.*, 1991, **455**, 528
- [123] J.L. Guth, H. Kessler, R. Wey; *Stud. Surf. Sci. Catal.*, 1986, **28**, 121
- [120] U. Müller, A. Brenner, A. Reich, K.K. Unger; *Am. Chem. Soc. Symp. Ser.*, 1989, **398**, 346
- [121] A. Kuperman, S. Nadimi, S. Oliver, G.A. Ozin, J.M. Garcés; *Nature*, 1993, **365**, 239

- [122] I. Girnus, M.M. Pohl, J. Richter-Mendau, M. Schneider, M. Noack, D. Venzke, J. Caro; *Adv. Mater.*, 1995, **7**, 711
- [123] S. Ernst in *Synthesis of porous materials: zeolites, clays and nanostructures*; M.L. Occelli, H. Kessler (Eds.), Marcel Dekker, Inc., N. York, 1997, 197
- [124] J. de Oñate Martínez, C. Falamaki, L.B. McCusker, Ch. Baerlocher; Synthesis of large syngle crystals of VPI-5 (in preparation)
- [125] H. Kessler, J. Patarin, C. Schott-Darie; *Stud. Surf. Sci., Catal.* 1994, **85**, 75
- [126] Ch. Baerlocher; *The X-ray Rietveld System XRS-82*, Institut für Kristallographie & Petrographie, ETH, Zurich, 1982
- [127] J. Pluth, J. Smith, W. Richardson; *J. Phys. Chem.*, 1988, **92**, 2734
- [128] *Xtal3.2 Reference Manual*; S.R. Hall, H.D. Flack, J.M. Steward (Eds.), Universities of Western Australia, Geneva and Maryland, 1992
- [129] Piet Grobet *private communication*
- [130] S.T. Wilson, B.M. Lock, E.M. Flaniguen; US Patent, 4 310 440, 1982
- [131] R.M. Dessau, J.L. Schenker, J.B. Higgings; *Zeolites*, 1990, **10**, 522
- [132] M.D. Poojary, A. Clearfield; *Mat. Chem. Phys.*, 1993, **35**, 301
- [133] D. Akporiaye, M. Stöcker; *Microporous Materials*, 1993, **1**, 423
- [134] J. Rocha, X. Liu, J. Klinowski; *Chem. Phys. Lett.*, 1992, **182**, 531
- [135] P.E. Werner, L. Eriksson, M. Westdahl; *J. Appl. Cryst.*, 1985, **18**, 367
- [136] J.W. Visser; *J. Appl. Cryst.*, 1969, **2**, 89
- [137] A. Boultif, D. Louër; *J. Appl. Cryst.*, 1991, **24**, 987
- [138] D. Taupin; *J. Appl. Cryst.*, 1989, **22**, 455

Appendix

Table A1: Results of the synthesis experiments using CATAPAL SB as the source of Al and the Esterline Angus ultrasonic bath

Table A2: Results of the synthesis experiments using CATAPAL SB as the source of Al and the ELMA ultrasonic bath

Table A1: Results of the synthesis experiments using CATAPAL SB as the source of Al and the Esterline Angus ultrasonic bath**Batch composition:** $\text{Al}_2\text{O}_3 \cdot \text{P}_2\text{O}_5 \cdot n\text{H}_2\text{O}$. DPA, t_m : 60 min, t_r : 30 min, T_r : 130°C

t_{ES} [min]	n [mol]*	t_r [h]	pH	Results
15	50	16	6	VFI (bundles), gel
		24	7	VFI (bundles)
		48	7	VFI (bundles), AEL ⁻
	70	16	6	VFI (bundles, thin needles), gel
		24	7	VFI (bundles, thin needles), AEL ⁻
		48	7	VFI (bundles, thin needles), AEL ⁻
30	60	16	7	VFI (small bundles), gel
		24	7	VFI (small bundles)
		48	7	VFI (small bundles), AEL
		64	7	VFI (small bundles), AEL ⁺
	70	16	6	VFI (small bundles), gel
		24	6	VFI (small bundles), AEL ⁻
		48	6	VFI (small bundles), AEL ⁺
		90	6	VFI (small bundles), AEL ⁺
	80	16	6	VFI (bundles, thin needles), gel
		24	6	VFI (bundles, thin needles), gel
		48	6	VFI (bundles, thin needles), AEL, gel
		90	6	VFI (bundles, thin needles), AEL ⁺ , gel
	90	16	6	AEL, gel
		24	6	VFI (some bundles), AEL ⁺
		48	6	VFI (some bundles), AEL ⁺
		64	6	VFI (some bundles), AEL ⁺
	120	16	6	AEL, gel
		24	6	VFI (some bundles), AEL ⁺
	150	16	6	AEL, gel
		24	6	AEL ⁺
		36	6	AEL ⁺
	200	16	5	AEL, gel
		24	5-6	AEL ⁺
		36	6	AEL ⁺
45	50	24	7	VFI (some bundles), AEL, gel
		48	7	VFI (some bundles), AEL ⁺ , gel
	70	24	6	VFI (some bundles), AEL ⁺ , gel
		48	7	VFI (some bundles), AEL ⁺ , gel

* n represents the total amount of water. From this quantity, 30 moles were used for the gel preparation

Table A2: Results of the synthesis experiments using CATAPAL SB as the source of Al and the ELMA ultrasonic bathBatch composition: $\text{Al}_2\text{O}_3 \cdot \text{P}_2\text{O}_5 \cdot \text{nH}_2\text{O} \cdot \text{DPA}$, t_m : 60 min, t_r : 30 min, T_r : 130°C

t_B [min]	n [mol] [*]	t_c [h]	pH	Results
15	50	24	6-7	VFI (bundles), gel
		48	7	VFI (bundles), gel
		64	7	VFI (bundles, some degradation)
	70	24	6-7	VFI (smaller bundles), gel
		48	6-7	VFI (as above)
		64	7	VFI (as above, some degradation),
	80	24	6-7	VFI (smaller bundles), gel
		48	6-7	VFI (as above)
		64	7	VFI (as above, some degradation),
22	50	16	7	VFI (bundles), gel
		24	7	VFI (bundles)
		48	7	VFI (bundles)
	70	16	6-7	VFI (bundles), gel
		24	7	VFI (bundles)
		48	7	VFI (bundles),
	80	16	6-7	VFI (small bundles), gel
		24	7	VFI (small bundles), gel
		48	7	VFI (small bundles)
30	50	16	6	VFI (bundles), gel
		24	6	VFI (bundles)
		48	6	VFI (some bundles), AEL
	70	16	6	VFI (bundles), gel
		24	6	VFI (bundles)
		48	6	VFI (some bundles), AEL
	80	16	6	VFI (smaller bundles), gel
		24	6	VFI (as above), AEL
		48	7	VFI (as above), AEL ⁺

* n represents the total amount of water. From this quantity, 30 moles were used for the gel preparation

List of abbreviations and symbols

1D	1-dimensional
2D	2-dimensional
3Q	triple-quantum
δ_{iso}	isotropic chemical shift
η	asymmetry parameter of the electric field gradient
a, b, c	cell parameters
A	absorption factor
Al^{oct}	octahedrally coordinated Al
Al^{tet}	tetrahedrally coordinated Al
b_i	background count at the i th step in the diffraction pattern
BL	beamline
Bo	magnetic field strength
CP	cross-polarization
d_{PW}	Durbin-Watson statistic factor
DLS	distance least-squares
DOR	double-rotation
DPA	di-n-propylamine
DTG	differential thermogravimetric analysis
ESRF	European Synchrotron Radiation Facility
$ F_{hkl} $	structure factor
FWHM	full-width at half-maximum
(hkl)	Miller indices
IUPAC	International Union of Pure and Applied Chemistry
L_{hkl}	Lorentz-polarization factor
MAS	magic-angle spinning
M_{hkl}	multiplicity factor of the hkl reflection
M(20)	figure of merit in the indexing programs
n	total amount of water used in the synthesis experiments
N	number of observations
n_{av}	average P chain length in polyphosphoric acid
NMR	nuclear magnetic resonance

O_{hkl}	preferred orientation correction function
pH	pH value
P_{hkl}	peak profile function
PSD	position sensitive detector
QCC	quadrupole coupling constant
R_{exp}	statistical expected R-value
RT	room temperature
R_F	structural R-value
R_{wp}	weighted R-value
s	scale factor
SNBL	Swiss Norwegian Beam Line
S_y	residual function to be minimized in a Rietveld refinement
t_c	crystallization (reaction) time
T_c	crystallization (reaction) temperature
TEDOR	transferred-echo double resonance
TGA	thermogravimetric analysis
t_m	milling time
t_s	stirring time
t_{US}	ultrasonic treatment time
U	temperature factor
VT	variable-temperature
w_i	weight assigned to an individual intensity in a powder pattern
XRD	X-ray diffraction (in this work: X-ray powder diffraction)
y_{ci}	calculated intensity at the i th step of the diffraction pattern
y_i	observed intensity at the i th step of the diffraction pattern

Acknowledgments

I wish to express my sincere gratitude to...

...Prof. Walter Meier, for accepting me coming to work in his institute as an exchange student,

...Prof. Reinhard Nesper, for kindly agreeing to supervise this project, and for the freedom granted during all these years,

...Prof. Walter Steurer, for his willingness to become a referee of this thesis,

...Dr. Lynne B. McCusker and Dr. Christian Bärlocher, who shared all my (not only scientific) troubles and always helped me out with their advises. Only their infinite patience and wholeheartedly support made this work possible. My warmest thanks to you. This is your work!

...my colleagues from the zeolite group, for the wonderful and inspiring atmosphere, and also for their patience... Thanks to Dr. Ralf Grosse Kunstleve, Simon Brenner, Thomas Wessels, Prof. Tone Meden, Dr. Christian Lengauer, Dr. Cavus Falamaki,

...all my colleagues from the Laboratory of Crystallography, especially to Mrs. Erika Spengler for her always opportune advises, and Roman Gubser and Monika Krichel for his irreplaceable technical assistance,

...Mrs. Elke Jahn for guiding my first steps in the synthesis of VPI-5,

...Dr. Holger Meyer zu Altenschildesche, Dr. Gillian Harvey-Estermann, Petra Bitterli-Stoschitzky, Marcia Müller and Dr. Günter Engelhardt for their assistance during the many NMR experiments, and also for uncountable fruitful discussions,

...Dr. Michael Wörle for his willingness to help with X-ray measurements or whatever, always with a smile in his face, and Samir Al-Wakeel for his assistance with the electron micrographs,

...my excellent friends in Zurich and abroad, which have shared with me not only the good times. I am deeply indebted to Dally Moya, Carlos Cuéllar, Maureen Ferry, Philip Moscoso, Silvia Villodres, Paul Kühne, Alfredo Cuéllar, Alejandro Keller, César Fernández, Detlef and Bärbel Melcher, Ernesto and Ines López, Felipe Domínguez, Tomas Lang, Daniel Buhl, and last but not least, Jacques Lange. Thank you for your friendship and love!

...the Swiss Federal Commission for Scholarships to Foreign Students for the financial assistance, and especially Prof. Hans W. Tobler and Mrs. Elisabeth Schniederlin for their understanding and support.

I would really like to extend my deepest gratitude to my family and friends in Havana. They cannot share this moment with me, but they have been always present. I want to hope that I will be able to hug and thank them personally in the near future.

Curriculum Vitae

Date and place of birth

June 4, 1962 in Havana, Cuba

Citizenship

Cuban

Marital Status

Unmarried

Education

- 1968 - 1975 Primary School, Havana
- 1975 - 1978 Secondary School, Havana
- 1978 - 1981 High School, Havana
- 1981 - 1983 Student of Physics
University of Havana
- 1983 - 1988 Student of Physics
Dresden University of Technology
- 1988 Diploma in Physics
- 1988 - 1991 Research Associate
National Center for Scientific Research, Havana
- 1991 - 1992 Exchange Student
Laboratory of Crystallography and
Mathematics and Physics Department
Swiss Federal Institute of Technology Zurich

Scholarship holder
Swiss Federal Commission for Scholarships
- 1992 - 1997 Ph.D. Student
Laboratory of Crystallography and
Department of Chemistry
Swiss Federal Institute of Technology Zurich

Scholarship holder
Swiss Federal Commission for Scholarships

Assistantships

- 1991 - 1992 Crystallography I and II
- 1992 - 1995 Analysis for Engineers
- 1995 - 1997 Differential Equations and System Analysis